FOR FURTHER TRAN

A021 780

ade000168

NRL Memorandum Report 3753

AD A055912

AD No. ___

DDC FILE COPY

⑥

DARPA—NRL Laser Program Semiannual Technical Report to Defense Advanced Research Projects Agency 1 April 1977-30 September 1977.

⑨ Interim rept.,

Laser Physics Branch
Optical Sciences Division

⑫

⑩ W. S. Watt

⑪ April 1978

⑫ 146p.

⑭ NRL-MR-3753

⑮ DARPA Order-2062

DDC
RECEIVED
JUL 5 1978
B

⑱ SBIE

⑲ AD-E000 168

NAVAL RESEARCH LABORATORY
Washington, D.C.

251 950

Approved for public release; distribution unlimited.

78 06 16 008

SECURITY CLASSIFICATION OF THIS PAGE (When Data Entered)

REPORT DOCUMENTATION PAGE

READ INSTRUCTIONS BEFORE COMPLETING FORM

1. REPORT NUMBER
NRL Memorandum Report 3753

2. GOVT ACCESSION NO.

3. RECIPIENT'S CATALOG NUMBER

4. TITLE (and Subtitle)
DARPA-NRL LASER PROGRAM — SEMIANNUAL TECHNICAL REPORT TO DEFENSE ADVANCE RESEARCH PROJECTS AGENCY — 1 April 1977 - 30 September 1977

5. TYPE OF REPORT & PERIOD COVERED
Interim report on a continuing NRL problem.

6. PERFORMING ORG. REPORT NUMBER

7. AUTHOR(s)
Laser Physics Branch
Optical Sciences Division

8. CONTRACT OR GRANT NUMBER(s)

9. PERFORMING ORGANIZATION NAME AND ADDRESS
Naval Research Laboratory
Washington, D.C. 20375

10. PROGRAM ELEMENT, PROJECT, TASK AREA & WORK UNIT NUMBERS
NRL Problem K03-53
Project 7E20

11. CONTROLLING OFFICE NAME AND ADDRESS
Defense Advanced Research Projects Agency
Arlington, Virginia 22209

12. REPORT DATE
April 1978

13. NUMBER OF PAGES
145

14. MONITORING AGENCY NAME & ADDRESS (if different from Controlling Office)

15. SECURITY CLASS. (of this report)
UNCLASSIFIED

15a. DECLASSIFICATION/DOWNGRADING SCHEDULE

16. DISTRIBUTION STATEMENT (of this Report)
Approved for public release; distribution unlimited.

17. DISTRIBUTION STATEMENT (of the abstract entered in Block 20, if different from Report)

18. SUPPLEMENTARY NOTES

19. KEY WORDS (Continue on reverse side if necessary and identify by block number)

Lasers
Electrical lasers
Laser diagnostics
Electronic state lasers
Chemical kinetics
Electronic state lifetimes
Energy transfer
Chemiluminescence

20. ABSTRACT (Continue on reverse side if necessary and identify by block number)

The DARPA-NRL Laser Program is concerned with the development of laser technology of electronic state lasers and associated physics. In particular the development of the XeF laser has been emphasized. Experimental and theoretical efforts were made to understand and improve laser performance. The radiative lifetimes of XeF and KrF were measured by the photolytic dissociation of XeF_2 and KrF_2 respectively. In addition quenching rate constants and radiative lifetimes are used in a code to predict laser performance of both XeF and KrF. A description of the code is given.

(Continues)

next page

DD FORM 1 JAN 73 1473 EDITION OF 1 NOV 65 IS OBSOLETE
S/N 0102-014-6601

78 06 16 008

SECURITY CLASSIFICATION OF THIS PAGE (When Data Entered)

20. Abstract (Continued)

Experimentally further efforts have been made to measure optical absorption in the XeF laser and to improve performance by investigating the role of the diluent gas.

In other work, an excited metal-rare gas mixture was investigated to evaluate them as laser candidates. Finally quenching measurements of Ba were begun. If high values are obtained for the quenching measurements, there is a possibility that a Ba-N_2O electronic state chemical laser can be made.

TABLE OF CONTENTS

SEMIANNUAL TECHNICAL REPORT

REPORTING PERIOD

1 April 1977 - 30 Sept. 1977

1.	DARPA Order	2062, Amendments 12 & 15
2.	Program Code Number	7E20
3.	Name of Contractor	Naval Research Laboratory
4.	Effective Date of Contract	1 July 1972
5.	Contract Expiration Date	30 September 1977
6.	Amount of Contract	$440,000
7.	Contract Number	62301E
8.	Principal Investigator	W. S. Watt
9.	Telephone Number	(202) 767-3217
10.	Project Scientist	S. K. Searles
11.	Telephone Number	(202) 767-2255
12.	Title of Work	DARPA/NRL Laser Technology Program

SPONSORED BY

DEFENSE ADVANCED RESEARCH PROJECTS AGENCY

DARPA Order No. 2062

XeF^* AND KrF^* KINETICS

The near completion of a fast-pulsed, electron-beam-driven kinetics experiment was reported in March. Since then final assembly of the experimental apparatus and several experiments have been completed. The purpose of these studies was to measure rate constants that are critical to the performance of the XeF and KrF excimer laser systems.

XeF^* Quenching

The first experiments were directed toward measurement of the rates of quenching of the XeF(B) state by gases commonly used in e-beam and discharge pumped XeF lasers. These rates are important in accessing the possibility of scaling the volume and power output of XeF to larger systems.

The experimental system used to measure XeF quenching rates is shown in Fig. A. $ArCl^*$ radiation at 175 nm was produced by irradiating Ar/Cl_2 mixtures with a 600 keV electron beam from a Febetron 706. The 175 nm ArCl photons penetrated a Suprasil absorption tube containing XeF_2 and the quenching gas. The XeF_2 was photodissociated by the 175 nm radiation creating XeF(B) state molecules. The subsequent radiative decay of these molecules was monitored as a function of the pressure of the quenching gas.

Data analysis was accomplished by monitoring the 351 nm XeF^*

Note: Manuscript submitted February 27, 1978.

fluorescence decay waveforms with a 351 nm bandpass filter and an S-5 photodiode. These waveforms were recorded by a fast oscilloscope, digitized, and plotted on a semi-log scale. From these plots exponential decay times were measured.

Typical data are shown in Figs. B and C where the decay constant, Σ, is plotted as a function of Xe and NF_3 pressure, respectively. Least squares fitting of the data points is denoted by the solid line. Linear and quadratic coefficients for the least squares fitting yield the XeF^* two and three body quenching rates, respectively. Tables I - III summarize the experimental results. The value of the XeF(B - X) radiative lifetime is in agreement with previous work in dissociating XeF_2 either with direct electron beam pumping or photodissociation with an ArF laser.

Table II summarizes the quenching rates of $XeF^*(B)$ by Ne and Ar. This is the first measurement of the Ne Quenching rate. It is important because Champagne and Harris[1] recently have shown that Ne is superior to Ar as a diluent in e-beam pumped XeF laser mixtures.

Finally, Table III presents the results for quenching by He, Xe, NF_3 and F_2. The NF_3 and F_2 rates are in good agreement with those reported by Setser,[2] but the strong three body quenching of XeF^* by Xe has not been previously observed. It seems to support the existence of the Xe_2F^* trimer.

The accompanying manuscripts, soon to be published in Optics Letters and the Journal of Chemical Physics, discuss more fully the experimental technique and the interpretation of the data.

KrF^* Quenching

Similar experiments in which KrF_2 is photolyzed can yield lifetimes and quenching rates for KrF^*. Until recently, the one obstacle to these experiments was synthesis of the KrF_2. We have successfully generated sufficient quantities of KrF_2 that lifetime and quenching experiments are in progress. Figures D and E present the data obtained for quenching of $KrF^*(B)$ by KrF_2 and Xe, respectively. The zero pressure intercept of Fig.D defines the KrF(B→X) radiative lifetime of 6.9 ns. Finally, the slopes of the lines shown in Fig.D and E yield the following rates:

$$KrF^*(B) + KrF_2 \rightarrow \text{Products:}\quad K_1 = 1.6\cdot 10^{-10}\ cm^3\text{-sec}^{-1} \qquad (1)$$

$$KrF^*(B) + Xe \rightarrow \text{Products:}\quad K_2 = 4.3\cdot 10^{-9}\ cm^3\text{-sec.}^{-1} \qquad (2)$$

<u>$KrF^*(B) \rightarrow XeF^*(B)$ Energy Transfer</u>

The very large rate given in the last section for the rate of quenching of $KrF^*(B)$ by xenon raises the question: what are the products of reaction (2)? A rate of that magnitude suggests an efficient collisional mecahnism.

Preliminary experiments have been conducted to study the products of reaction (2). In these studies, spontaneous emission spectra of $Ar/Kr/F_2$ mixtures (KrF laser composition) were recorded with and without xenon doping. Figure F gives the results. The top trace corresponds to a gas mixture of 2000 torr Ar/100 Kr/3 torr F_2 and the prominent features are the B→X and C→A bands of KrF centered at 248 and 270 nm, respectively. Spectrum (b) represents the addition of <u>1 torr Xe</u> to mixture (a) and the appearance of the XeF(B→X) and C→X (260 nm) bands is evident. With the addition of 20 torr Xe (spectrum (c)) to the KrF mixture, the XeF 351 nm band clearly dominates the spectrum. Also the strength of the XeF(C→X) band in these high pressure e-beam pumped mixtures is unusual.

The rapid growth of the XeF fluorescence with the addition of such low Xe concentrations suggest that XeF(B,C) states are the primary products of reaction (2). That is:

$$KrF^{*}(B) + Xe \rightarrow XeF^{*}(B) + Kr. \qquad (3)$$

By integrating the KrF^{*} and XeF^{*} spectra of Figure F, the branching ratio for the formation of $XeF^{*}(B)$ from reaction (2) is estimated to be ~ 0.9. The significance of this result is the possibility of using (3) as an alternative pumping scheme for the XeF. Alternative, since the present method of forming XeF^{*} relies on a 2-body collision between Xe^{M} and F_2 or NF_3 or $Xe^{+} - F^{-}$ ion-ion recombination. The large amounts of xenon currently used in XeF laser system limits the efficiency to $\lesssim$ 3%, probably due to Xe_2^{+} absorption. The KrF laser on the other hand is ~ 7% efficient and so using $KrF^{*}(B)$ as a precursor to $XeF^{*}(B)$ may prove to be an efficient way of producing XeF B state molecules. In preliminary experiments using the 50 ns gun, strong XeF lasing occurred when just 1 torr xenon was added to a KrF laser mixture and lasing on KrF or both XeF and KrF simultaneously could be obtained by simply varying the Xe partial pressure.

In summary, by photolyzing XeF_2 or KrF_2 in the presence of a background gas, the rates of quenching of XeF(B) and KrF(B) by various molecules and the rare gases have been determined. Also, the rate of transfer of energy from KrF^{*} to XeF^{*} has been shown to be large.

References

1. L. F. Champagne and N. W. Harris, Appl. Phys. Lett. 31, 513 (1977).
2. H. C. Brashears, Jr., D. W. Setser and D. DesMarteau, Chem. Phys. Lett. 48, 84 (1977).

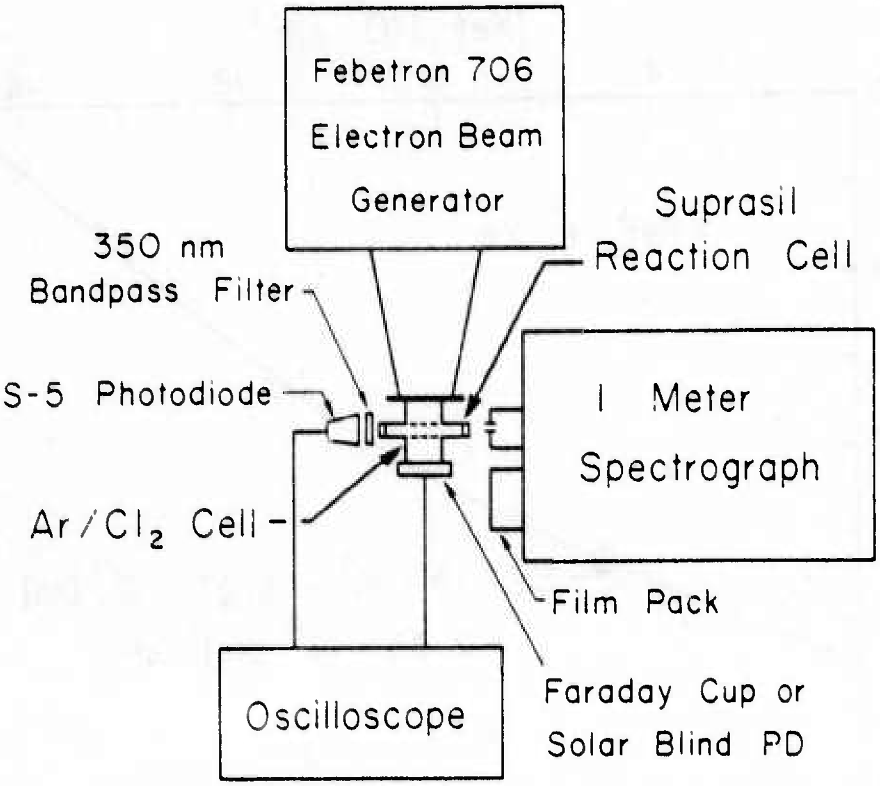

Fig. A. Partial schematic diagram of the experimental apparatus used to measure the rates of quenching of XeF^* and KrF^* by various gases.

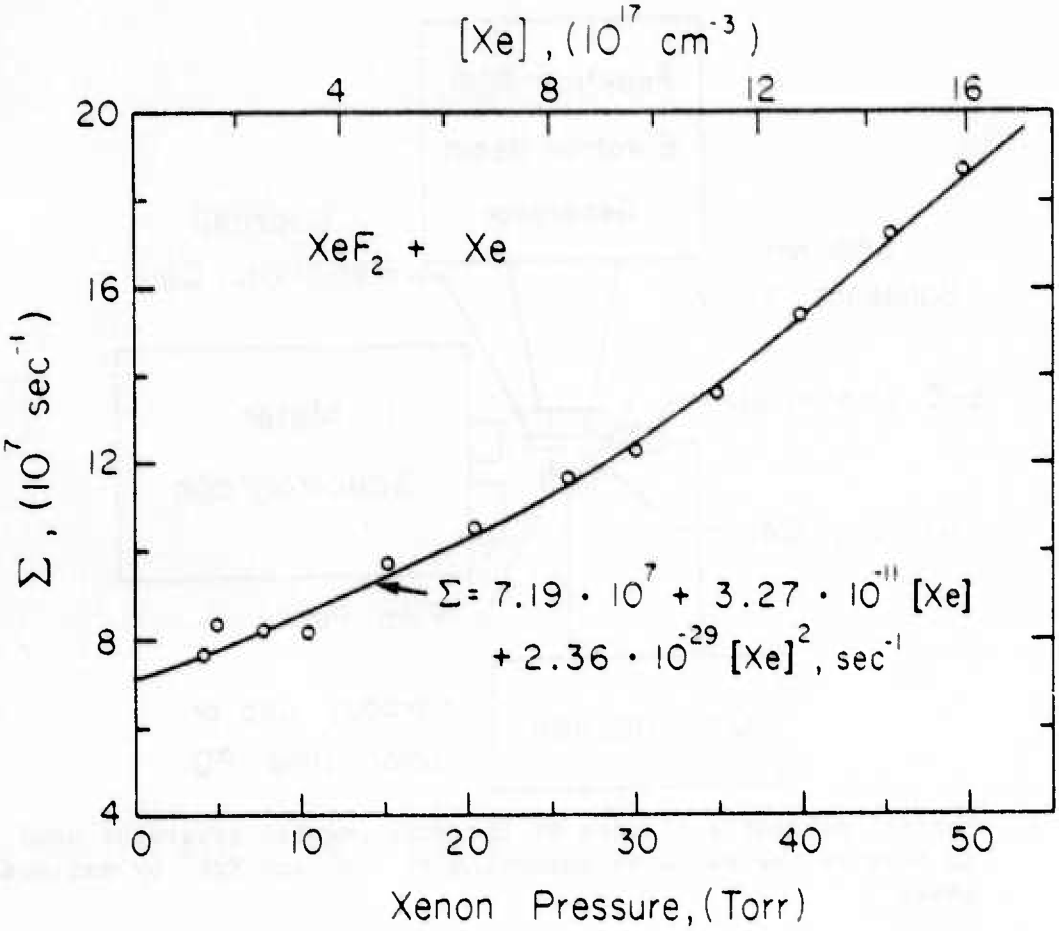

Fig. B. Rate of Decay of XeF(B) emission versus xenon pressure.

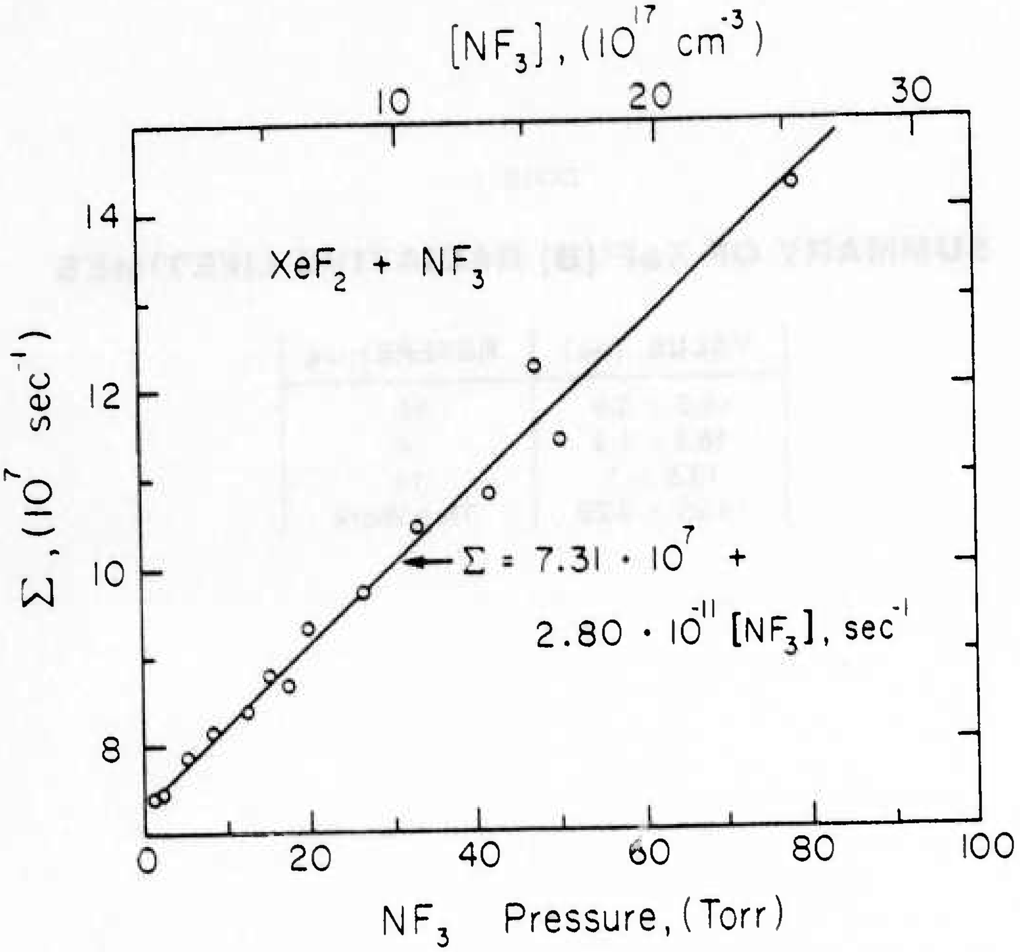

Fig. C. Variation of decay constant, Σ, with NF_3 pressure.

TABLE I

SUMMARY OF XeF*(B) RADIATIVE LIFETIMES

VALUE, (ns)	REFERENCE
16.5 ± 5.0	10
18.8 ± 1.3	4
13.5 ± 1	11
14.25 ± 0.20	This Work

TABLE II

$XeF^*(B)$ QUENCHING BY Ne, Ar AND XeF_2

QUENCHER	RATE CONSTANT[a]	REFERENCE
Ne	$(7.68 \pm 1.6) \cdot 10^{-13}$	This Work
Ar	$(8 \pm 4) \cdot 10^{-13}$ $(2.88 \pm 0.5) \cdot 10^{-12}$ $(4.92 \pm 1.56) \cdot 10^{-12}$	14 9 This Work
2 Ar (Three body process)	$(1.5 \pm 0.5) \cdot 10^{-32b}$ $(7.23 \pm 2.30) \cdot 10^{-32}$	14 This Work
XeF_2	$3.5 \cdot 10^{-10}$ $1.97 \cdot 10^{-10}$ $(2.56 \pm 0.32) \cdot 10^{-10}$	4 11 This Work

a. units: cm^3-sec^{-1}
b. units: cm^6-sec^{-1}

TABLE III

XeF*(B) COLLISIONAL QUENCHING RATES

QUENCHER	RATE CONSTANT[a]	REFERENCE
He	$(4.07 \pm 1.46) \cdot 10^{-13}$	This Work
Xe	$(3.9 \pm 0.8) \cdot 10^{-11}$	7
	$(3.27 \pm 0.74) \cdot 10^{-11}$	This Work
2Xe (Three body process)	$(2.36 \pm 0.53) \cdot 10^{-29}$[b]	This Work
NF_3	$(2.0 \pm 0.1) \cdot 10^{-11}$	7
	$(2.80 \pm 0.15) \cdot 10^{-11}$	This Work
F_2	$(3.36 \pm 0.3) \cdot 10^{-10}$	7
	$(3.80 \pm 0.13) \cdot 10^{-10}$	This Work

a. units: cm^3-sec^{-1}
b. units: cm^6-sec^{-1}

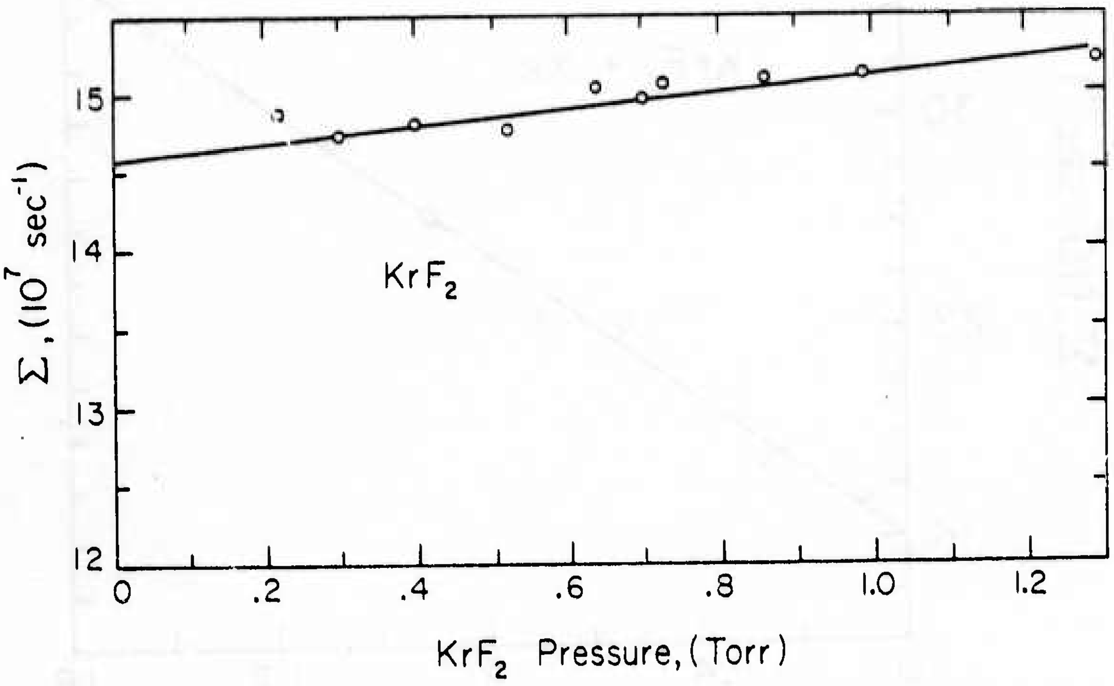

Fig. D. Quenching of KrF(B) by KrF_2. Zero pressure intercept yields the inverse of the KrF(B→X) radiative lifetime, 6.9 ns.

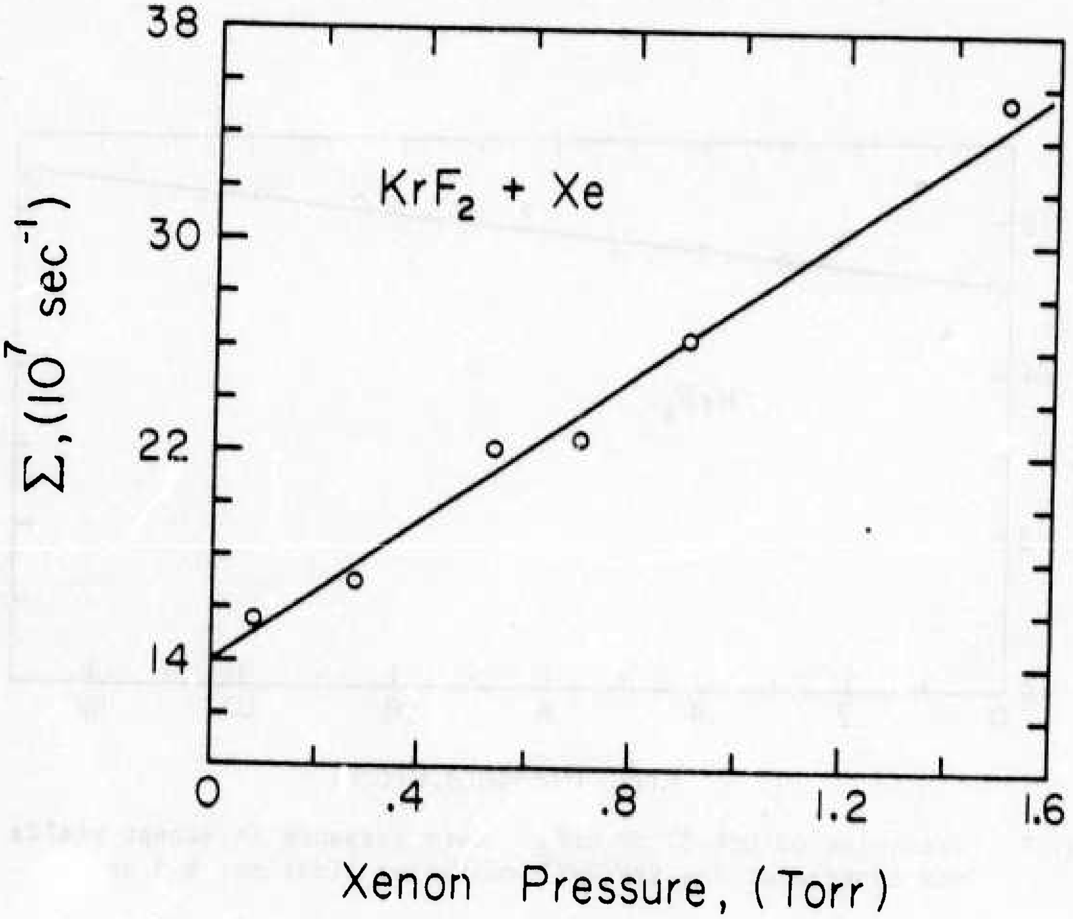

Fig. E. Decay constant, Σ, versus Xe pressure.

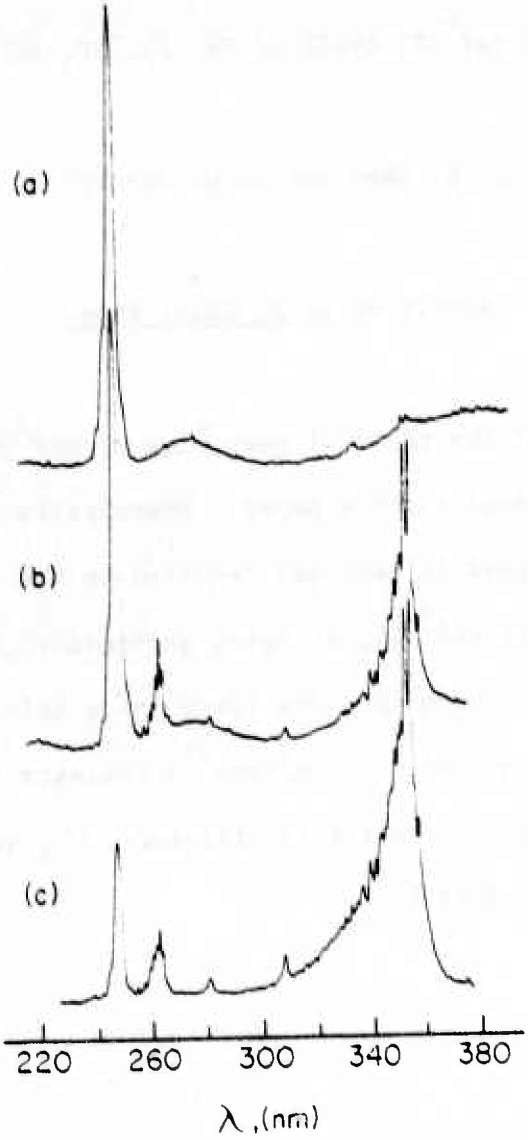

Fig. F. Electron beam pumped 2000 torr Ar/100 torr Kr/3 torr F_2 mixtures for various Xe additive pressures: (a) no xenon added, (b) 1 torr Xe and (c) 20 torr Xe.

COLLISIONAL DEACTIVATION STUDIES OF THE $XeF^*(B)$ STATE BY He, Xe, NF_3 AND F_2

J. G. Eden and R. W. Waynant

Submitted to *J. Chem. Phys.*

Measurements of the rates of quenching of $XeF^*(B)$ by He, Xe, NF_3 and F_2 are reported in this paper. Photolyzing XeF_2 in the presence of the desired diluent gas resulted in the single-step, collisionless formation of $XeF^*(B)$, allowing exponential decay studies of the B state population to be made. The large three body quenching rate measured for xenon ($\sim 2.4 \cdot 10^{-29}$ cm^6-sec^{-1}) suggests the existence of the trimer Xe_2F^*. Also, for a given pressure, NF_3 quenches XeF(B) $\sim$ 13 times slower than does F_2.

I. Introduction

Since the discovery of the XeF excimer laser in early 1975,[1] tremendous progress in the improvement of its output power and electrical efficiency has been realized.[2,3] Still, the lack of knowledge of critical kinetic rate constants has impeded efforts to obtain the highest efficiencies expected for this system.

Recently, however, the measurement of key $XeF^{*}(B)$ optical and collisional rates has accelerated. Eden and Searles[4] utilized electron impact dissociative excitation of XeF_2 to determine the B→X band lifetime as 16.5 ± 5.0 ns. Subsequently, Ewing[5] refined the experimental technique using a low intensity, repetitively pulsed electron beam and deduced a spontaneous lifetime of 13.5 ± 1 ns. By pumping in the red wing of the XeF_2 VUV absorption spectrum using an ArF laser, Burnham and Harris[6] were able to photolytically populate the XeF(B) state. Monitoring the radiative decay of the excited state manifold, they measured a radiative lifetime of 19.8 ± 1.3 ns. To measure the quenching of $XeF^{*}(B)$ by various gases, Brashears, Setser and DesMarteau[7] (BSD) photolyzed XeF_2 in the steady state with VUV radiation. Using a different approach, Rokni and co-workers[8] employed a kinetic analysis of the XeF^{*} emission from e-beam excited $Ar/Xe/F_2$ gas mixtures.

Previous experimental measurements of the radiative lifetime or deactivation rates for XeF were forced to rely upon excitation pulses (optical or electron) longer than xenon fluoride's radiative lifetime. In this paper, photolytic production of $XeF^{*}(B)$ by irradiating XeF_2 and diluent gas mixtures with a 5 ns FWHM pulse of incoherent ArCl (B→X: 175 nm) radiation has been used to measure the rates of quenching of the $XeF^*(B)$ state by He, Xe, NF_3 and F_2. With this same technique, the quenching rates for Ne, Ar and XeF_2 and the radiative lifetime of the XeF(B→X) band have already been reported.[9] The use of narrow photolyzing pulses permits the accurate measurement of these collisional rates by simply monitoring the time evolution of the 350 nm XeF(B→X) emission as a function of the desired diluent pressure. Also, several of these rates have not been reported before and are important for numerical modeling studies of the XeF laser. The experimental apparatus used in this investigation is described in detail in Section II. Section III presents the theory and data analysis while Section IV discusses and evaluates the experimental results. Finally, Section V presents the conclusions of this study.

II. Experimental Apparatus

A schematic diagram of the experimental apparatus used in this study is shown in Fig. 1. A 600 keV, 3 ns FWHM beam of electrons from a Febetron 706 generator penetrated a Teflon coated, 25 μm thick titanium foil and excited a high pressure Ar/Cl_2 gas mixture contained in a cylindrical stainless steel cell. The $ArCl^*$ (175 nm) optical excitation pulse created by the beam had a ~ 5 ns FWHM and was characterized by a decay time of ~ 2.5 ns. Mounted transverse to the electron beam was a UV grade (Suprasil) quartz reaction cell where the photolytic pumping and collisional quenching of $XeF^*(B)$ occurred. The resultant 350 nm radiation was monitored by a bandpass filter (λ_0 + 348 nm, $\Delta\lambda$ = 9.4 nm) and a fast S-5 photodiode (ITT F4018). A one meter Minuteman spectrograph/monochromator equipped with Polaroid film was also available. The spectrograph resolution was ≃ 0.1 nm and the photographic negatives were scanned by a Joyce-Loebl microdensitometer. Wavelength calibration was accomplished using a Hg lamp.

A Faraday cup or solar blind photodiode and 171.5 nm bandpass filter were used interchangeably at the end of the Ar/Cl_2 cell to study the electron gun current or the $ArCl^*(B)$ state spontaneous emission, respectively. To record the $XeF(B \rightarrow X)$ fluorescence waveforms, a Tektronix 7904 oscilloscope, triggered by a capacitive voltage divider on the Febetron, was used. Analysis of the oscilloscope traces was facilitated by a digitizer and a CDC 3800 computer. Recently, a Tektronix 7912 transient digitizer and an on-line mini-computer have provided considerably faster data acquisition and analysis.

Both the Ar/Cl_2 and quartz reaction cells were evacuated to $p \leq 10^{-5}$ torr by an oil diffusion pump and were thoroughly outgassed. The helium and xenon used in these experiments were research grade and the F_2, NF_3 and Cl_2 were of technical grade purity. All gases were used without further purification. To insure repeatability of the data, it was found necessary to thoroughly passivate the Ar/Cl_2 cell by allowing 20-50 torr of pure Cl_2 to stand in the cell for one-half hour before experiments could be performed. Gas mixtures of 99.5% Ar/0.5% Cl_2 (p_{total} = 2050 torr) were admitted to the cell and the mixture was used for ~ 3 hours before replacement became necessary. The XeF_2 (obtained from PCR, Inc.) was degassed using a dry ice cooled reservoir under continuous pumping.

The quenching data were acquired and analyzed in the following way. Roughly 0.3 torr XeF_2 and the desired pressure of background gas were admitted to the Suprasil cell. After firing the electron beam, the 350 nm fluorescence waveforms were photographed on the oscilloscope, digitized and plotted on a semilog scale by a computer. These plots were observed to be linear over several e-foldings and their exponential decay constants were then plotted as a function of the diluent gas pressure. As a result of this procedure, the primary experimental errors are statistical and arose from noise on the oscilloscope traces and manual errors incurred during the digitizing process.

III. Theory and Typical Data

A. VUV Photolysis of XeF_2

The absorption spectrum of XeF_2 in the vacuum ultraviolet has been reported by Jortner et al.[10] A strong absorption band peaked at $\lambda \sim 158$ nm corresponds to the allowed transition $10\,\sigma_g \rightarrow 7\,\sigma_u$.[11] The upper state of this continuum is expected to be dissociative[10,11] with the XeF(B,D) + F levels as product channels. The threshold wavelength for photodissociative production of $XeF^*(B)$ is 202 nm. That is, the dissociation energy of XeF_2 is $\simeq 2.6$ eV[12] and the $XeF(B,v'=0)$ state lies ~ 3.53 eV above the $XeF(X,v''=0) + F$ dissociation limit.[13]

Several VUV fluorescence sources were tried in an effort to efficiently photolyze XeF_2. The Xe_2^* excimer radiation at 172 nm[14] was observed to produce strong XeF(B→X) 350 nm fluorescence, but the 172 radiation decayed slowly due to collisional coupling between the Xe_2 (1_u and 0_u) states.[15] Rare gas-halide emission has been shown previously to be useful as an incoherent pump for various applications,[6,16] but for these experiments, ArF(B→X) emission at 193 nm gave extremely weak XeF fluorescence.[6] Fortunately, the photolytic yield of XeF(B) using ArCl(B→X) fluorescence as a pump is high.

Aside from the high fluorescence yield of XeF(B), the ArCl band at 175 nm[17-19] is an attractive source for other reasons. First, as discussed in the Appendix, e-beam excited Ar/Cl_2 mixtures produce Cl^* (4p) and Cl_2^*(E) exicted species as well as $ArCl^*$(B). Although the Cl^* (4p) atoms radiate in the VUV ($135 \leq \lambda \leq 139$ nm), this is well below the cutoff wavelength for Suprasil quartz. Also, the XeF_2 vapor is transparent to the 258 nm E→B band of Cl_2. Therefore, only the $ArCl^*$(B→X) radiation is transmitted into the quartz cell and interacts with the XeF_2, creating XeF(B):

$$XeF_2 + h\nu\ (175\ \mathrm{nm}) \rightarrow XeF_2^*\ (10\ \sigma_g \rightarrow 7\ \sigma_u) \rightarrow XeF^*(B) + F. \qquad (1)$$

The pumping process represented by (1) is depicted in Fig. 2.

Secondly, the ArCl photon energy of roughly 7.1 eV is insufficient to excite the XeF(D) + F state (cf. Fig. 2). Consequently, spectra of 175 nm excited, low pressure XeF_2 vapor using a 1.0 m monochromator and high speed film revealed no 260 nm D→X emission.[7,11] In fact, as shown in Fig. 3, the only fluorescence observed was that due to transitions from low lying B vibrational levels to the X ground state. For pure XeF_2 vapor, only the $v' = 1$ and 2 levels of XeF(B) are excited, suggesting that the fluorine fragment of Eqn. (1) absorbs the excess photon energy of ~ 0.95 eV. With the addition of diluent gas to the XeF_2 vapor, vibrational relaxation occurs (cf. Fig. 3) and the appearance of the $v' = 0$ level becomes noticeable. BSD[7] have noticed similar effects when irradiating XeF_2 with CW radiation from CO(160-180 nm), Hg(185 nm) or Kr(123.6 nm) lamps.

Another attractive feature of ArCl(B→X) radiation for these experiments is shown in Fig. 4. On this graph, the ArCl 175 nm fluorescence and e-beam gun current are plotted versus time. After the electron beam is extinguished, the ArCl radiation falls rapidly ($\tau \leq 3$ ns). Also shown in the figure is the XeF(B→X) fluorescence due to 0.3 torr XeF_2 and 5.38 torr NF_3. The XeF emission decays exponentially for several e-foldings with a decay constant of 12.9 ns which is substantially longer than that of the pump pulse.

B. Rate Equations and Data Analysis

Since the ArCl(B→X) fluorescence pulse width and decay times are much shorter than the XeF(B→X) spontaneous radiative lifetime,[9] then the 175 nm optical pump pulse may be considered (to a first approximation) to be a δ-function on the time scale of these experiments. Thus, XeF(B) molecules are created (by the pump pulse) at t=0 and are destroyed through radiation and collisions according to the equation:

$$[XeF(B)] = [XeF(B)]_{t=0}\, e^{-\Sigma t} \tag{2}$$

where

$$\Sigma = \tau_r^{-1} + k_1\,[Q] + k_2\,[Q]^2, \tag{3}$$

τ_r is the B state radiative lifetime (14.25 ns),[9] the brackets represent particle densities, and k_1 and k_2 are the two and three-body quenching rates of $XeF^*(B)$ by the atomic or molecular species, Q. The simplicity of this analysis hinges on the single-step, collisionless formation of $XeF^*(B)$ by photolysis of XeF_2. If a collisional process were also involved in the formation of XeF^*, such as $Xe^M + F_2$ "harpoon" collisions which occur in excited $Ar/Xe/F_2$ mixtures, the data interpretation would be severely complicated.

As mentioned in Section II, the XeF(B→X) waveforms were recorded by either a Tektronix 7904 oscilloscope of Tektronix 7912 digitizer used with an on-line minicomputer. After being digitized, the fluorescence traces were plotted on a semilog, amplitude versus time scale as shown in Fig. 4. From this plot (for a given diluent pressure), the decay constant Σ was determined from a linear fit of the falling portion of the waveform. Subsequently, Σ was plotted as a function of diluent pressure and a least squares fit of the data points made it possible to determine the coefficients k_1 and k_2 from Eqn. (3). This analysis, which is the same as that used previously,[9] was employed to measure the rates of quenching of XeF(B) by He, Xe, NF_3 and F_2, gases frequently used in electron beam or discharge excited XeF lasers.

IV. Experimental Results and Discussion

Plots of the decay constant, Σ as a function of He, Xe, NF_3 and F_2 pressure are shown in Figs. 5-8, respectively. The least squares fitting of the data (denoted by the solid line) is also given for each diluent gas. A comparison of the results reported here with the rates measured by previous investigators is presented in Table I. To convert the half-quenching pressures given by ref. 7 to collisional rates, the XeF(B→X) radiative lifetime of 14.25 ns was used.

The two body quenching rates of XeF(B) by Xe, NF_3 and F_2 are in good agreement with those measured by BSD[7] using steady state, VUV absorption techniques. In line with their results, we find NF_3 to be a poor quencher of XeF^* compared to F_2. Keeping in mind that the branching ratio for XeF^*(B) formation is higher for NF_3 than F_2[20], it appears that NF_3 is more attractive than F_2 as a fluorine donor in e-beam pumped systems. The rate of collisional destruction of B state molecules by helium has not been previously measured, but it may be significant since He densities of 10^{19} - 10^{20} cm^{-3} are commonly used in discharge-excited XeF lasers.[21]

The existence of three body quenching for Xe, which is evident from the data of Fig. 6, is in contrast to the findings of BSD who were unable to observe a three body contribution to Xe quenching for pressures up to 700 torr Xe. Higher pressure data points taken at 79 and 117 torr xenon are not shown in Fig. 6 and yet lie within 10% of the least squares fitting line shown on the graph. Also, we recently measured the quenching rate of $XeF^*(B)$ by 2 Kr to be $8.6 \cdot 10^{-31}$ cm^3-sec^{-1}. Therefore, the three body quenching rate for xenon presented in Table I is consistent with similar rate constants measured previously for 2 Ar[8, 9] and 2 Kr. Finally, the xenon rate constant is ~ 27 times that for Kr and ~ 328 times the Ar rate indicating that polarizability of the rare gas diluent is not the sole factor in determining the excimer quenching rate.[22]

The fact that the three body rate dominates Σ (cf. Fig. 6) for $[Xe] > 1.174 \cdot 10^{18}$ $cm^{-3} \simeq 54$ torr strongly suggests the rapid formation of an intermediate complex, such as Xe_2F^*, by the kinetic sequence:

$$XeF^*(B) + 2Xe \rightarrow Xe_2F^* + Xe \rightarrow 3Xe + F. \qquad (4)$$

The intense blue emission band (λ_{max} ~ 420 nm) that has been observed in high pressure, e-beam or discharge pumped $Ar/Xe/F_2$ or Xe/F_2 gas mixtures[23,24] is possibly due to the radiative decay of this trimer. Broad band continuum fluorescence from the analogous molecule, Kr_2F^*, has also been observed and identified.[25]

V. Conclusions

Measurements of the rate of quenching of $XeF^*(B)$ molecules by He, Xe, NF_3 and F_2 have been reported. By photolyzing XeF_2 (in the presence of the desired diluent gas) with short pulse (5 ns) VUV radiation, single step collisionless formation of $XeF^*(B)$ resulted, allowing simple exponential quenching studies to be made. The measured rates are in good agreement with previous work and show that: 1) for even low xenon partial pressures ($\leq$ 100 torr), formation of Xe_2F^* by three body quenching of $XeF^*(B)$ is a significant loss mechanism, and 2) NF_3 is superior to F_2 as a fluorine donor. Finally, since neon has recently been shown to have some distinct advantages over argon as the major constituent in electron beam-pumped or discharge sustained XeF laser mixtures, it appears that the best performance of these lasers will be obtained for $Ne/Xe/NF_3$ mixtures.

The authors gratefully acknowledge many useful dicussions with S. K. Searles and R. Burnham and thank C. Mullins for technical assistance.

APPENDIX

In the experiments reported here, electron beam pumped Ar/Cl_2 mixtures have been used to photolytically dissociate XeF_2, creating $XeF^*(B)$. Therefore, the radiative products formed in such excited mixtures, and their relative concentrations, are vital to interpretation of the experimental data.

For the mixture compositions used in these experiments (99.5% Ar, 0.5% Cl_2), the bulk of the beam energy is absorbed by the argon, creating primarily $Ar^*(3P)$ and Ar^+.[26] Gundel and co-workers[27] have carefully studied the products of the $Ar^*(3P) - Cl_2$ collision. The major products are $Cl^*(4p)$, $Cl_2^*(E)$ and $ArCl^*(B)$ which were found to be formed in 16%, 3% and 49% of the collisions, respectively.

Due to dissociative attachment of Cl_2 with low energy electrons ($Cl_2 + e^- \rightarrow Cl^- + Cl$), ArCl(B) molecules are also created by ion-ion recombination:[8]

$$Ar^+ + Cl^- + Ar \rightarrow ArCl(B) + Ar. \qquad (5)$$

References

1. C. A. Brau and J. J. Ewing, Appl. Phys. Lett. 27, 435 (1975).
2. L. F. Champagne, J. G. Eden, N. W. Harris, N. Djeu and S. K. Searles, Appl. Phys. Lett. 30, 160 (1977).
3. L. F. Champagne and N. W. Harris, Appl. Phys. Lett. 31, 513 (1977).
4. J. G. Eden and S. K. Searles, Appl. Phys. Lett. 30, 287 (1977).
5. J. J. Ewing, 7th Winter Colloquium on Quantum Electronics, Park City Utah(1977), unpublished.
6. R. Burnham and N. W. Harris, J. Chem Phys. 66, 2742 (1977).
7. H. C. Brashears, Jr., D. W. Setser and D. DesMarteau, Chem. Phys. Lett. 48, 84 (1977).
8. M. Rokni, J. H. Jacob, J. A. Mangano and R. Brochu, Appl. Phys. Lett. 30, 458 (1977).
9. J. G. Eden and R. W. Waynant, Opt. Lett. (to be published).
10. J. Jortner, E. G. Wilson and S. A. Rice in Noble Gas Compounds, edited by H. H. Hyman (U. of Chicago Press, Chicago, 1963), p. 358.
11. J. E. Velazco, J. H. Kolts, D. W. Setser and J. A. Coxon, Chem. Phys. Lett. 46, 99 (1977).
12. J. Berkowitz, W. A. Chupka, P. M. Guyon, J. H. Holloway and R. Spohr, J. Phys. Chem. 75, 1461 (1971).
13. J. Tellinghuisen, G. C. Tisone, J. M. Hoffman and A. K. Hays, J. Chem. Phys. 64, 4796 (1976).

14. J. B. Gerardo and A. W. Johnson, IEEE JQE QE-9, 748 (1973).

15. J. W. Keto, R. E. Gleason, Jr. and G. K. Walters, Phys. Rev. Lett. 33, 1365 (1974).

16. J. C. Swingle, C. E. Turner, Jr., J. R. Murray, E. V. George and W. F. Krupke, Appl. Phys. Lett. 28, 387 (1976).

17. M. F. Golde and B. A. Thrush, Chem. Phys. Lett. 29, 486 (1974).

18. M. F. Golde, J. Mol. Spectroscopy 58, 261 (1975).

19. R. W. Waynant, Appl. Phys. Lett. 30, 234 (1977).

20. J. E. Velazco, J. H. Kolts and D. W. Setser, J. Chem. Phys. 65, 3468 (1976).

21. R. Burnham and N. Djeu, Appl. Phys. Lett. 29, 707 (1976).

22. The intermediate excited species, ($XeRF^*$, R=Ar, Kr or Xe), is presumably formed in 3 body collisional quenching of XeF(B) by the rare gases, (see eqn. 4). The radiative lifetime of these excited molecules is possibly responsible for the large 3 body rates observed in this work.

23. J. G. Eden, Naval Research Laboratory Memorandum 3356; September, 1976.

24. C. A. Brau and J. J. Ewing, J. Chem. Phys. 63, 4640 (1975).

25. J. A. Mangano, J. H. Jacob, M. Rokni and A. Hawryluk, Appl. Phys. Lett. 31, 26 (1977).

26. L. R. Peterson and J. E. Allen, Jr., J. Chem. Phys. 56, 6068 (1972).

27. L. A. Gundel, D. W. Setser, M. A. A. Clyne, J. A. Coxon and W. Nip, J. Chem. Phys. 64, 4390 (1976).

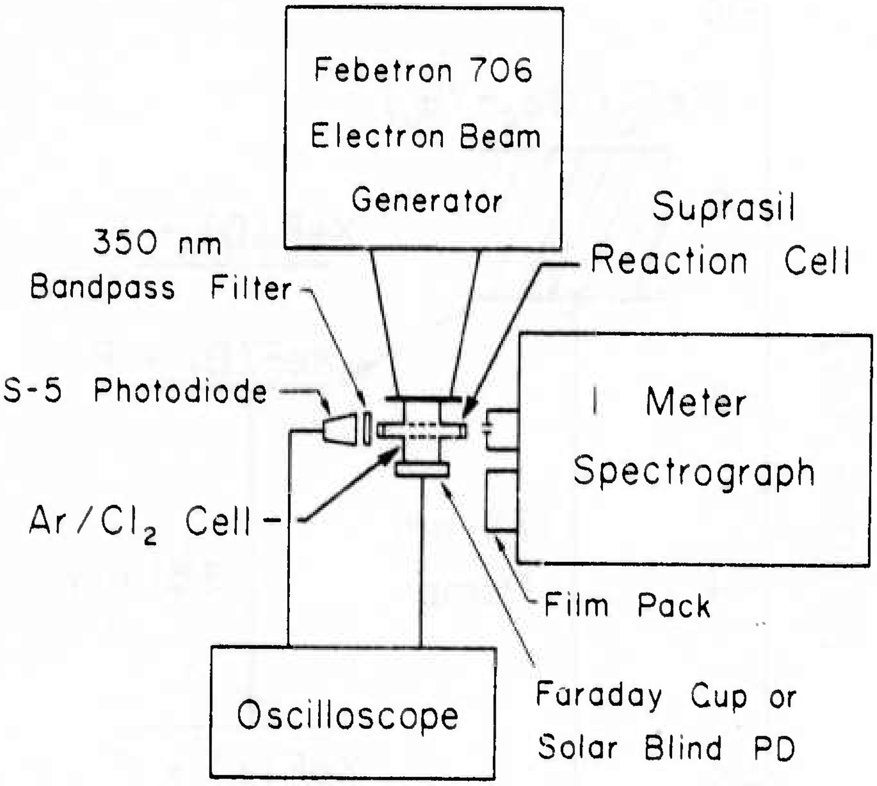

Fig. 1. Schematic diagram of the experimental apparatus.

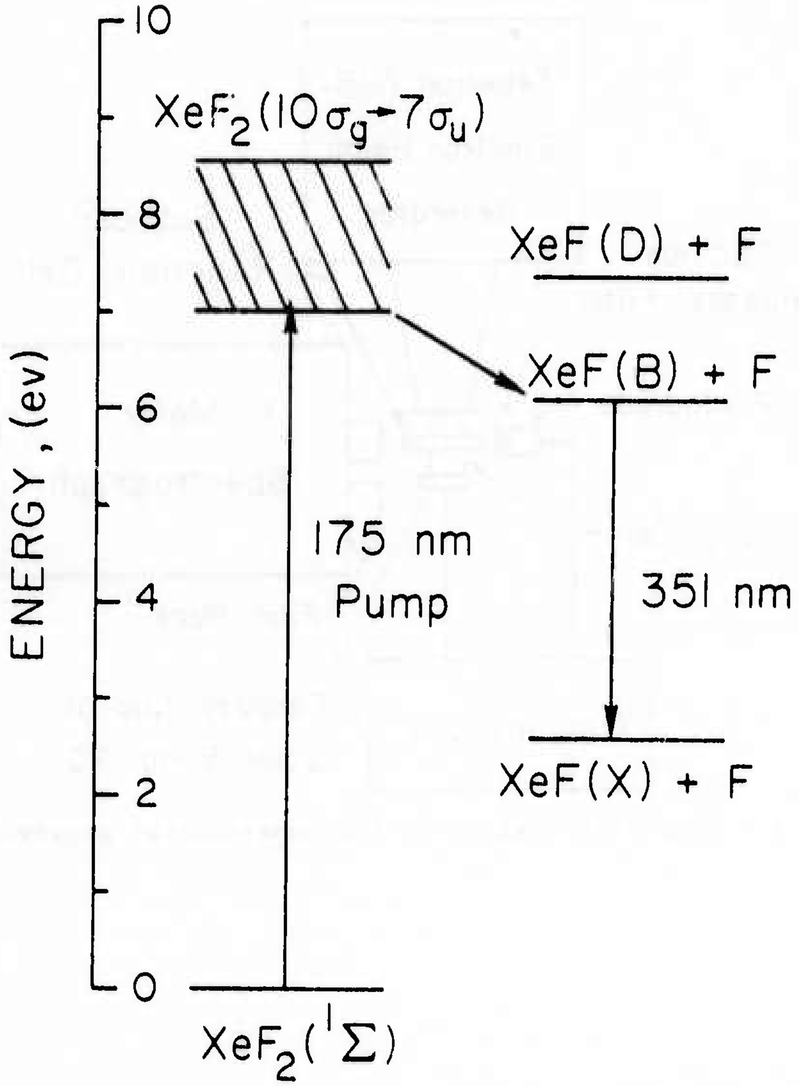

Fig. 2. Energy level diagram of XeF_2 (Ref. 11) and XeF schematically portraying photodissociation of XeF_2 by ArCl 175 nm emission.

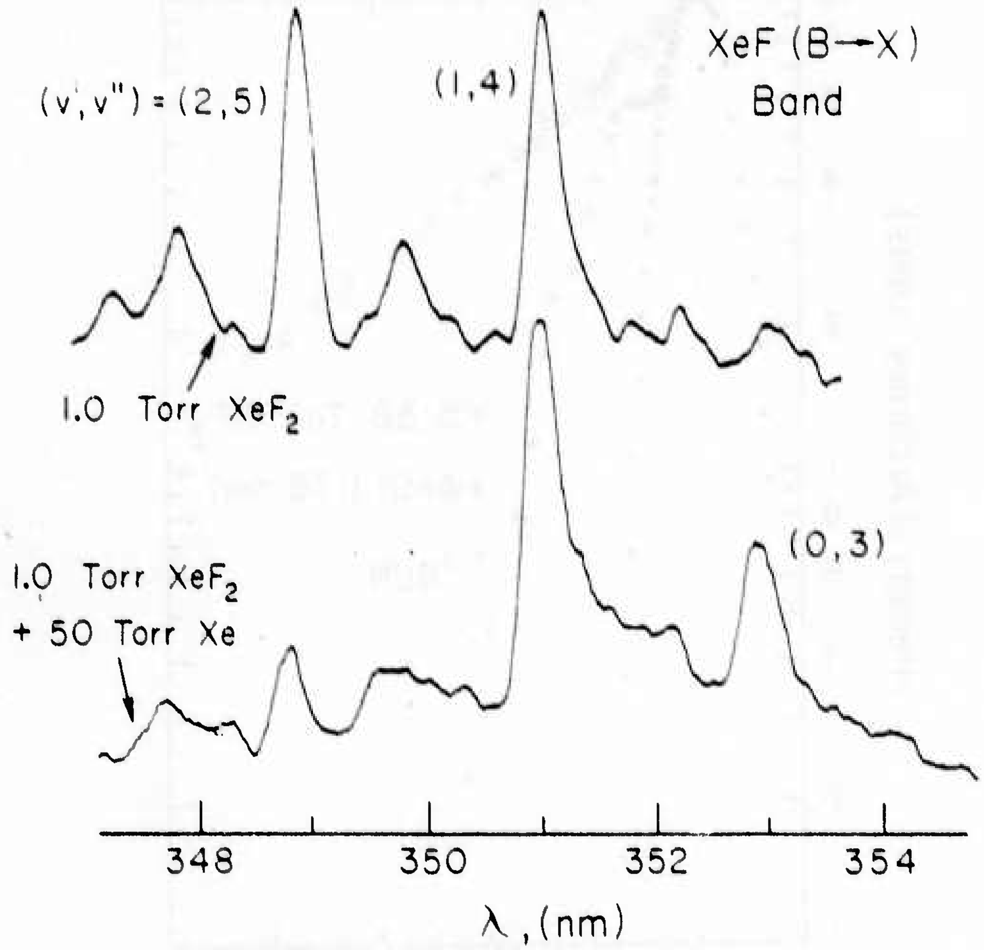

Fig. 3. XeF(B→X) emission spectra of 175 nm photolyzed, low pressure XeF_2 vapor: Top--1.0 torr XeF_2; Bottom--1.0 torr XeF_2 plus 50 torr xenon. The vibrational assignments for the various transitions are those given by Ref. 13.

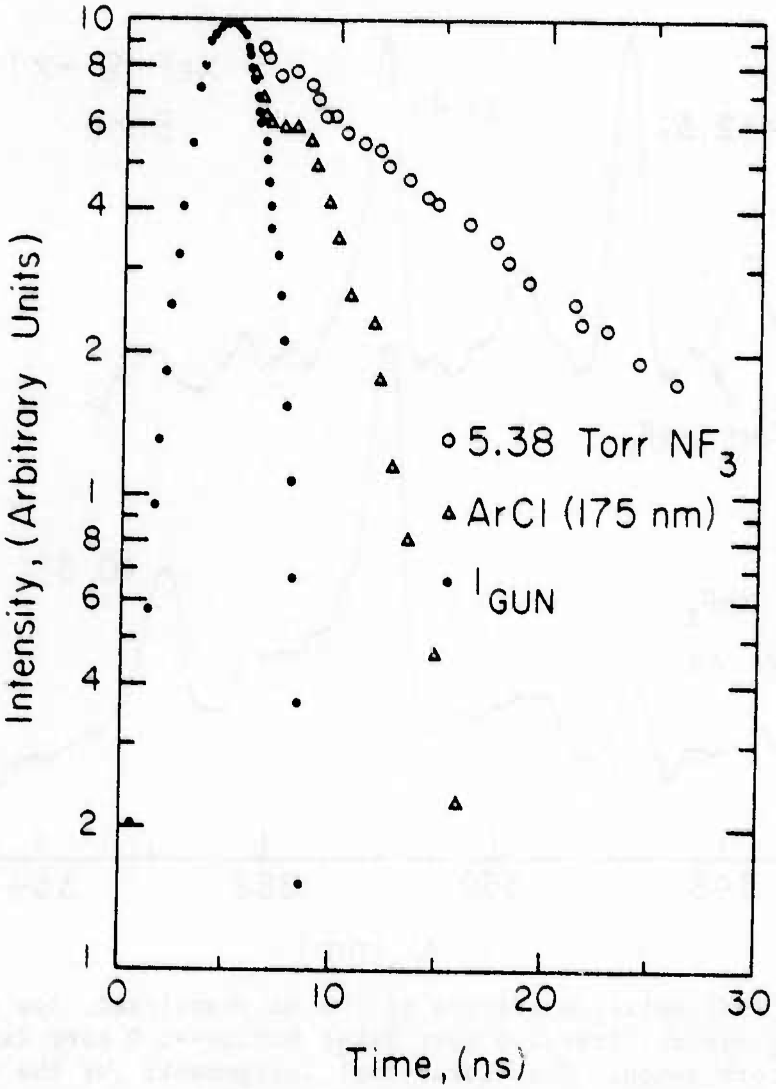

Fig. 4. Typical electron beam current waveform (•) and ArCl 175 nm (Δ) and XeF(B→X) fluorescence (o) traces, the 351 nm XeF emission data points shown correspond to the gas mixture: ~ 0.3 torr XeF_2 + 5.38 torr NF_3. T = 0 represents initiation of the e-beam pulse.

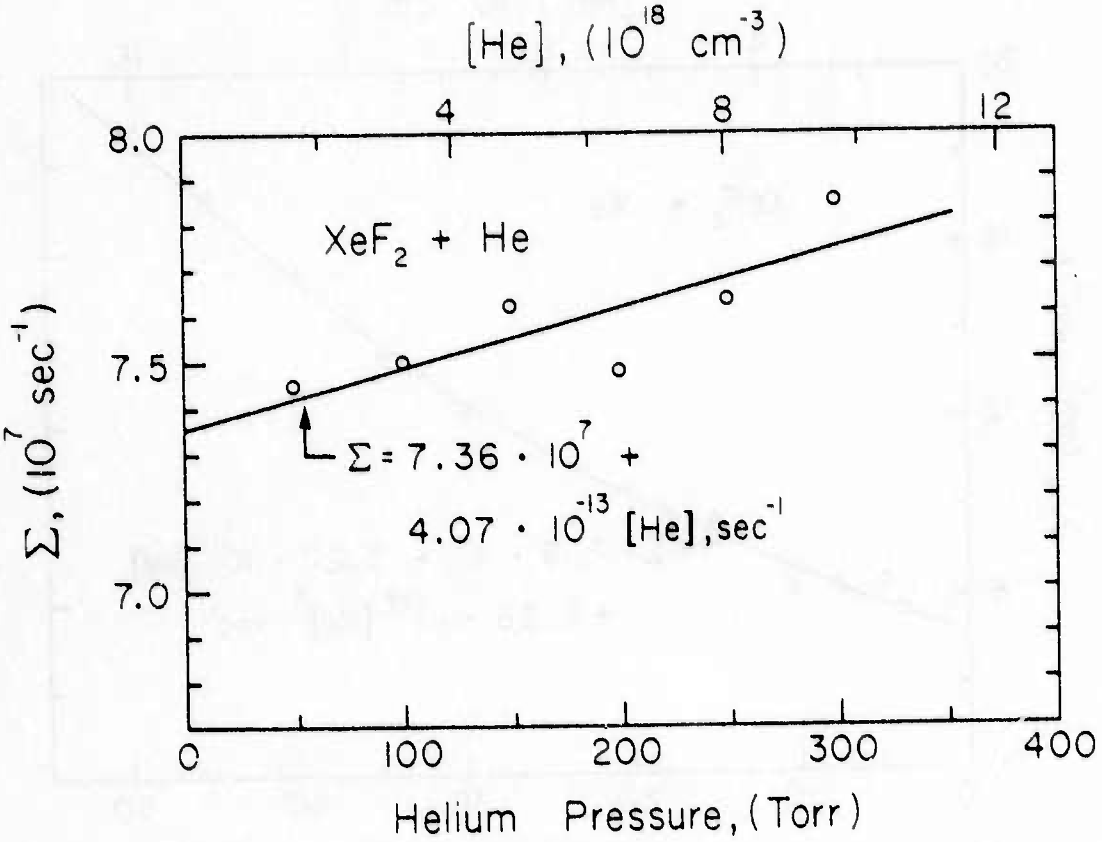

Fig. 5. Decay constant, Σ, as a function of helium pressure. The solid line represents the least squares fitting of Eqn. (3) to the data points. The experimental errors for the data points shown are $\lesssim$ 7%.

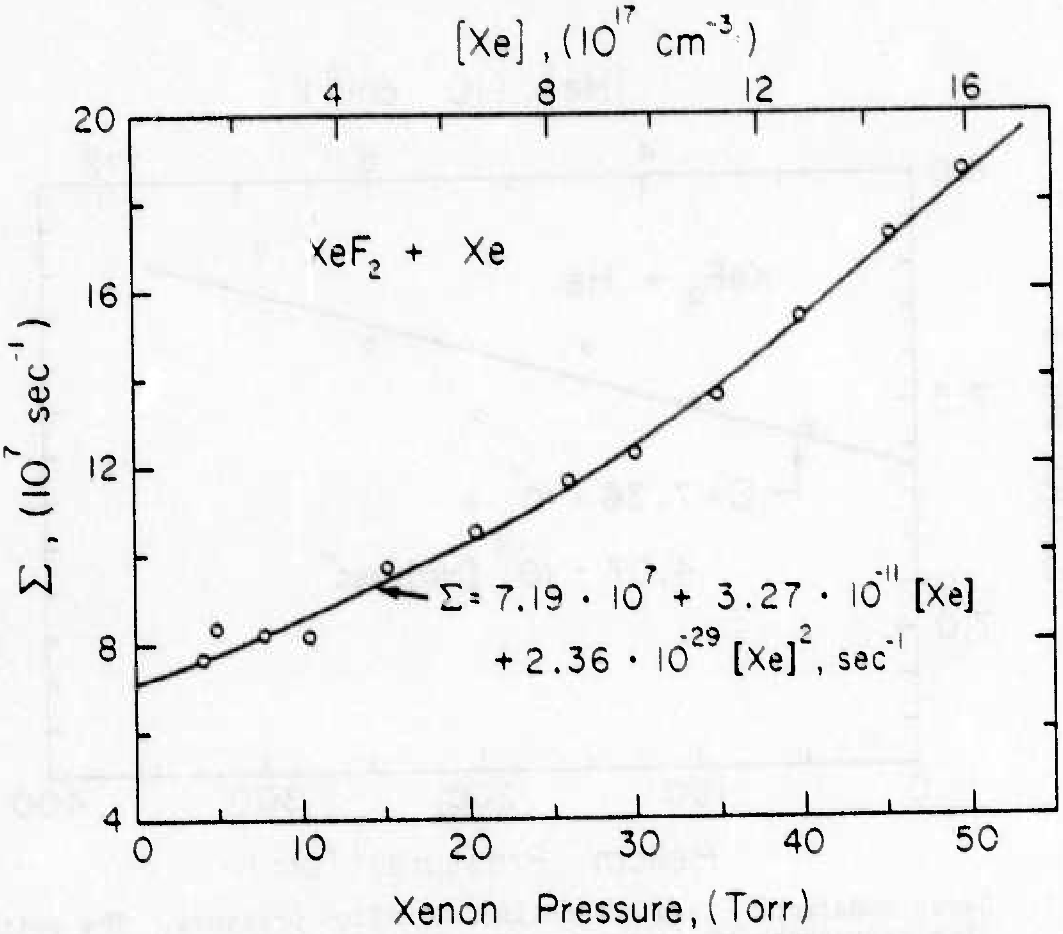

Fig. 6. Decay constant, Σ, versus xenon pressure exhibiting strong three body quenching of the XeF*(B) state. Data points at 79 and 117 torr xenon are not shown. Uncertainty in the experimental points is ≈ 5%.

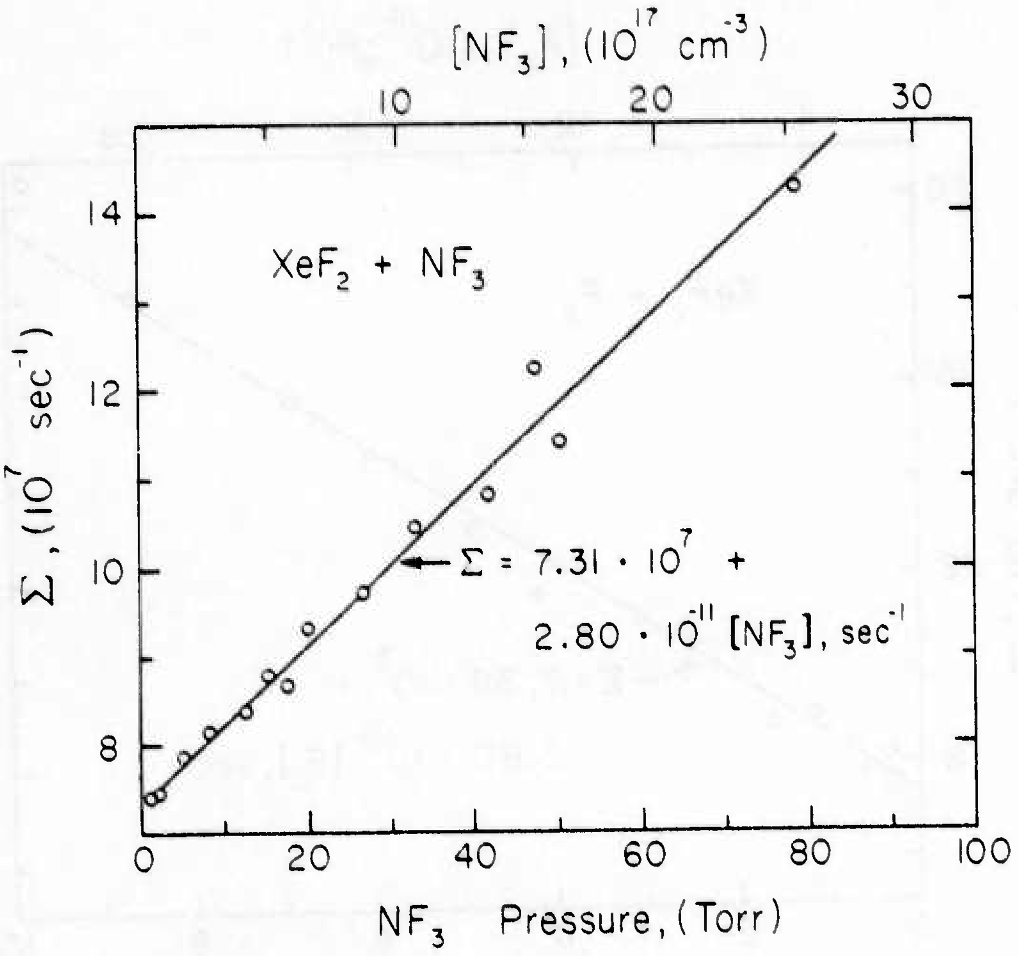

Fig. 7. Decay of XeF(B→X) emission as a function of [NF_3]. The data uncertainty is ≤ 8%.

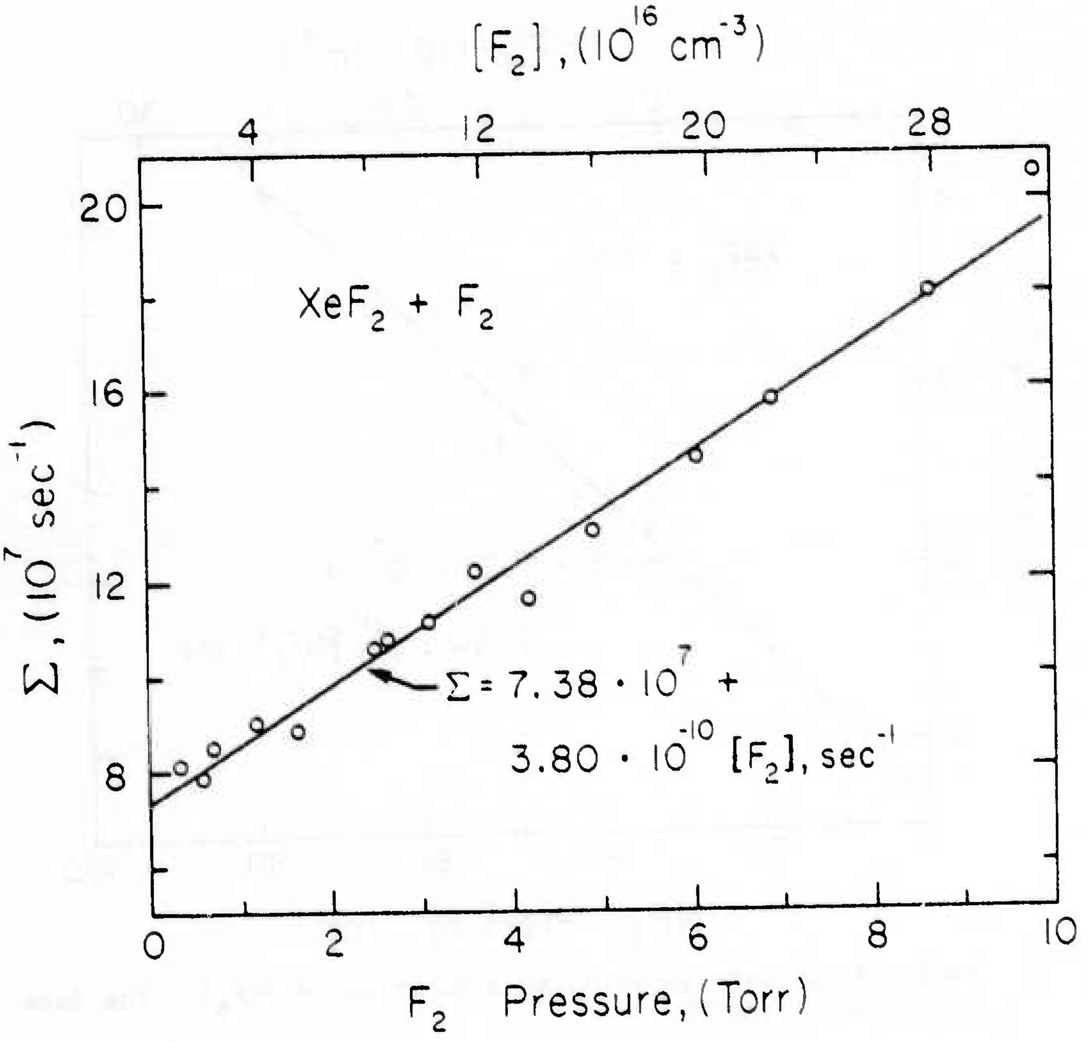

Fig. 8. F_2 pressure dependence of the decay constant, Σ. The data exhibits a linear dependence on $[F_2]$ and the error per experimental point is ≤ 8%.

Table I.

Summary of $XeF^*(B)$ collisional deactivation rates as determined by several investigators. Estimated uncertainties in the rates are also shown in the parentheses.

$XeF^*(B)$ COLLISIONAL QUENCHING RATES

QUENCHER	RATE CONSTANT [a]	REFERENCE
He	$(4.07 \pm 1.46) \cdot 10^{-13}$	This Work
Xe	$(3.9 \pm 0.8) \cdot 10^{-11}$ $(3.27 \pm 0.74) \cdot 10^{-11}$	7 This Work
2Xe (Three body process)	$(2.36 \pm 0.53) \cdot 10^{-29}$ [b]	This Work
NF_3	$(2.0 \pm 0.1) \cdot 10^{-11}$ $(2.80 \pm 0.15) \cdot 10^{-11}$	7 This Work
F_2	$(3.36 \pm 0.3) \cdot 10^{-10}$ $(3.80 \pm 0.13) \cdot 10^{-10}$	7 This Work

a. units: cm^3-sec^{-1}
b. units: cm^6-sec^{-1}

LIFETIME AND COLLISIONAL QUENCHING MEASUREMENTS OF $XeF^*(B)$ BY PHOTOLYSIS OF XeF_2

J. G. Eden and R. W. Waynant
Naval Research Laboratory
Washington, D. C. 20375

To be Published in Optics Letters

Abstract

By photolyzing XeF_2 using $ArCl^*$ 175 nm radiation, the spontaneous radiative lifetime of the XeF(B→X) band has been measured to be 14.25 ± 0.2 ns. Also, the rates of two body collisional deactivation of the XeF(B) state by Ne, Ar and XeF_2 have been determined to be 7.7×10^{-13} cm^3-sec^{-1}, 4.9×10^{-12} cm^3-sec^{-1} and 2.6×10^{-10} cm^3-sec^{-1}, respectively. A three body quenching rate of 7.2×10^{-32} cm^6-sec^{-1} was found for Ar. The large two and three body quenching rates of XeF^* by Ar suggest that Ne may be preferable to Ar as a diluent in high pressure XeF (350 nm) laser mixtures.

To better understand the physical properties of electron beam or discharge excited XeF lasers, it is desirable to know the emitting state's radiative and collisional lifetimes. Specifically, the resistance of $XeF^*(B)$ to quenching by background gases in the laser mixture is crucial to attempts to scale the output power of this laser system.

The radiative lifetime of $XeF^*(B)$ and the quenching rates of this state by Ne, Ar and XeF_2 have been measured and are reported here. In this experiment, ArCl excimer radiation at 175 nm[1,2] was used to create $XeF^*(B)$ molecules by photolytically dissociating XeF_2. That is, the absorption of a 175 nm photon by XeF_2 results in the formation of the XeF_2^* results in the formation of the XeF_2^* $(10\,\sigma_g \rightarrow 7\,\sigma_u)$ state[3] which immediately dissociates, directly creating $XeF^*(B)$. The resulting time-dependent $XeF(B \rightarrow X)$ emission at $\lambda \sim 350$ nm was monitored for various diluent pressures, from which the quenching rates were determined.

The threshold wavelength for photodissociative production of $XeF^*(B)$ is ≈ 202 nm.[3,4] Experimentally, it was found that the photolytic yield of $XeF^*(B)$ is much greater (> 10X) for 175 nm than 193 nm (ArF $[B \rightarrow X]$ radiation,[4] despite only a factor of ~ 2 difference in the absorption coefficient of XeF_2 at these wavelengths.[5] The Xe_2^* excimer (172 nm) produces strong $XeF(B \rightarrow X)$ fluorescence but the Xe_2^* (1_u and 0_u^+) states are collisionally coupled[6] and so the 172 nm emission decays too slowly ($\tau \sim$ 22 ns) at reasonable pressures (3-5 atm) to be useful in these experiments. Therefore, ArCl $(B \rightarrow X)$ radiation, due to its short decay time (~ 2.5 ns for mixtures used in this work) and 175 nm wavelength, was an ideal optical source for the experiments described below.

The $ArCl^*$ optical excitation pulse was created by irradiating 99.5%

Ar/0.5% Cl_2 gas mixtures (p_{total} = 2050 torr) with a 3 ns FWHM beam of 600 keV electrons from a Febetron 706 accelerator. A Suprasil quartz absorption tube (1.22 cm. o.d., 3.36 cm excitation length), which contained the XeF_2 and diluent gas, was mounted transverse to the electron beam and coaxial with the ArCl photolytic cell. The rare gases used in these experiments were research grade and the XeF_2 was degassed in a dry ice-cooled quartz reservoir prior to its use.

Electron beam excitation of Ar/Cl_2 gas mixtures produces $Cl^*(4P)$, $Cl_2^*(E)$ and $ArCl^*(B)$ excited species[7] which subsequently radiate at 133-139 nm, 258 nm and 175 nm, respectively. The VUV Cl^* radiation emitted by the e-beam irradiated mixtures is rejected by the Suprasil quartz tube whereas the XeF_2 is transparent to the weak Cl_2^* (E→B) emission produced at 258 nm. The 175 nm fluorescence emitted by the $ArCl^*(B)$ molecules, however, penetrates the quartz absorption tube, exciting a XeF_2 ground state molecule:

$$XeF_2 + h\nu\ (175\ \text{nm}) \rightarrow XeF_2^*\ (10\,\sigma_g \rightarrow 7\,\sigma_u) \rightarrow XeF^*(B) + F. \qquad (1)$$

XeF^*(B→X) emission spectra of low pressure, $ArCl^*$ photolyzed XeF_2 vapor were recorded on Polaroid Type 57 film using a 1.0 m spectrograph (dispersion = 0.81 nm/mm; resolution ≈ 0.1 nm) and a 10 cm focal length lens. Only low vibrational levels of $XeF^*(B)$ were observed ($v \leq 2$, corresponding to the 348, 351 and 353 nm B→X transitions),[8,9] even at XeF_2 pressures of $\lesssim 0.3$ torr, indicating that the excess photon energy (≈ 0.95 eV) of Eqn. (1) appears as translational energy of the fluorine fragment. The D→X band of XeF at 265 nm was not observed since this state is energetically inaccessible. Photoelectric monitoring of the XeF(B→X) emission was accomplished using a S-5 photodiode and bandpass filter (λ_o = 348 nm, $\Delta\lambda$ = 9.4 nm) for spectral selectivity. After the termination of the 175 nm excitation pulse, which was observed by a solar blind photodiode and a 171.5 ± 20 nm bandpass filter, the XeF^* radiation decayed exponentially over several time constants.

To a first approximation, the 175 nm excitation pulse can be considered a δ-function compared to the B state radiative lifetime. Therefore, the B state population is essentially formed by dissociation at t = 0 and decays according to the relation:

$$[XeF^*(B)] = [XeF^*]_{t=0}\, e^{-\Sigma t} \qquad (2)$$

where

$$\Sigma = \tau_r^{-1} + k_1[Q] + k_2[Q]^2, \qquad (3)$$

τ_r = $XeF^*(B)$ state radiative lifetime, indicate particle densities and k_1 and k_2 represent the two and three body destruction rates of $XeF^*(B)$ by the atomic or molecular species, Q. Thus, by monitoring the exponential decay rate of the XeF(B→X) emission as a function of the diluent concentration, Q, the rates of collisional quenching of $XeF^*(B)$ by Ne, Ar and XeF_2 were determined.

Fig. 1 is a plot of the decay constant, Σ, of the B→X radiation as a function of XeF_2 pressure. The least-squares fitting of the data points is denoted by the solid line and the zero-pressure intercept yields the $XeF^*(B\rightarrow X)$ radiative lifetime of 14.25 ns. This result compares favorably with the results of experiments involving direct e-beam dissociation of XeF_2[10,11] or photolytic pumping of $XeF^*(B)$ utilizing a 16 ns FWHM ArF laser pulse.[4] A summary of measurements of the radiative lifetime for the B→X band is presented in Table I. From the slope of the line in Fig. 1, $k_1(XeF_2) = 2.56 \cdot 10^{-10}\, cm^3\text{-}sec^{-1}$, which is also in agreement with previous studies.[4,10,11]

Experimental results for quenching of $XeF^*(B)$ by Ne and Ar are shown in Figs. 2 and 3, respectively. For these measurements, $\lesssim 0.3$ torr XeF_2 and the desired pressure of rare gas were admitted to the absorption cell. To vary the diluent pressure and avoid XeF_2 decomposition, a fresh mix was prepared for each electron beam shot. Although fluctuations of the neon data and experimental difficulties encountered for diluent pressures in excess of 1 atm prevented the determination of the neon three-body collisional quenching rate, $k_2(Ne)$, an upper limit for k_2 of 10^{-32} cm^6-sec^{-1} was estimated. In general, it was found that the uncertainty in the deactivation rates increased for the lighter quenchers. A comparison of the quenching rates presented here with previously reported measurements is given in Table II. Although it has not been measured previously, the rate of quenching of $XeF^*(B)$ by Ne is an important parameter since the recent observed improvement of neon on XeF laser performance.[12]

For Ar, although the 2-body quenching rate measured in this investigation is in good agreement with Ref. 9,[13] both 2- and 3-body rates are larger than previously reported values.[14] This discrepancy may, however, be partially accounted for by noting that the results of Ref. 14 relied on a complex kinetic analysis of XeF^* emission from e-beam excited Ar/Xe/F_2 mixtures to measure quenching by Ar and Xe. In those experiments, it was not possible to resolve XeF excimer formation processes from destruction mechanisms and the reported rates depended on accurately knowing other kinetic rates.

The large 2 and 3-body quenching rates for Ar indicate their adverse effect on energetic XeF laser development. The two-body quenching rate of neon is almost an order of magnitude smaller than that for argon. Since the use of neon rather than argon also reduces 351 nm optical losses in the XeF laser medium[12], then Ne appears to be superior to Ar as a diluent for high power, electron beam pumped XeF laser systems.

A possible product of the Ar quenching reaction is the $ArXeF^*$ molecule:

$$XeF^* + Ar \text{ (or 2 Ar)} \rightarrow ArXeF^* \text{ (+ Ar)}. \qquad (4)$$

The creation of $ArF^*(B)$ (by a substitution reaction)[15] or Xe_2F^* are clearly not allowed by (4). A mechanism analogous to (4) has been postulated for the KrF system[16] where the trimer formation rate is expected to be significant (10^8 - 10^9 sec^{-1}) for the Ar densities encountered in high pressure e-beam mixtures. Therefore, the two and three-body destruction rates of $XeF^*(B)$ by Ar are likely to be important in high energy XeF laser modeling

In summary, short pulse photolysis of XeF_2 in the presence of a background rare gas has been employed to measure the rate of quenching of XeF(B) by Ne and Ar. These rates are valuable in predicting gas mixture compositions and excitation conditions for optimum XeF laser performance. Measurements of the quenching of $XeF^*(B)$ by other gases (Xe, F_2, NF_3) are continuing and the results will be reported in the future.

The authors wish to thank C. Mullins for excellent technical assistance and R. Burnham and S. Searles for many helpful suggestions.

References

1. M. F. Golde and B. A. Thrush, "Vacuum UV emission from reactions of metastable inert gas atoms: chemiluminescence of ArO and ArCl," Chem. Phys. Lett. 29, 486 (1974).
2. R. W. Waynant, "A discharge-pumped ArCl superfluorescent laser at 175.0 nm," Appl. Phys. Lett. 30, 234 (1977).
3. J. E. Velazco, J. H. Kolts, D. W. Setser and J. A. Coxon, "Excitation of XeF^* by reactions of XeF_2 with Ar ($^3P_{0,2}$), Kr ($^3P_2$) and Xe ($^3P_2$)," Chem. Phys. Lett. 46, 99 (1977).
4. R. Burnham and N. W. Harris, "Radiative lifetime of the C state of XeF," J. Chem. Phys. 66, 2742 (1977). The XeF excited state responsible for the 350 nm band is now denoted as the B state--see J. Tellinghuisen, A. K. Hays, J. M. Hoffman and G. C. Tisone, J. Chem. Phys. 65, 4473 (1976).
5. J. Jortner, E. G. Wilson and S. A. Rice in Noble Gas Compounds, edited by H. H. Hyman (U. of Chicago Press, Chicago, 1963), p. 358.
6. J. W. Keto, R. E. Gleason, Jr. and G. K. Walters, "Production mechanisms and radiative lifetimes of argon and xenon molecules emitting in the ultraviolet," Phys. Rev. Lett. 33, 1365 (1974).
7. L. A. Gundel, D. W. Setser, M. A. A. Clyne, J. A. Coxon and W. Nip, "Rate constants for specific product channels from metastable Ar ($^3P_{2,0}$) reactions and spectrometer calibration in the vacuum ultraviolet," J. Chem. Phys. 64, 4390 (1976).
8. J. Goldhar, J. Dickie, L. P. Bradley and L. D. Pleasance, "Injection locking of a xenon fluoride laser," Appl. Phys. Lett. (to be published) and references cited.

9. H. C. Brashears, Jr., D. W. Setser and D. DesMarteau, "Vacuum-ultraviolet photolysis of XeF_2: XeF(B) fluorescence and quenching," Chem. Phys. Lett. 48, 84 (1977).

10. J. G. Eden and S. K. Searles, "XeF(C½) radiative lifetime measurement," Appl. Phys. Lett. 30, 287 (1977).

11. J. J. Ewing, 7th Winter Colloquium on Quantum Electronics, Park City, Utah (1977), unpublished.

12. L. F. Champagne and N. W. Harris, "The influence of diluent gas on the XeF laser," Appl. Phys. Lett. 31, 513 (1977).

13. The 2-body argon quenching rate ascribed in Table II to Ref. 12 has been calculated using Brashears et. al's half-quenching pressure and the 14.25 ns XeF radiative lifetime presented earlier.

14. M. Rokni, J. H. Jacob, J. A. Mangano and R. Brochu, "Two and three body quenching of XeF^* by Ar and Xe," Appl. Phys. Lett. 30, 458 (1977).

15. J. A. Mangano, J. H. Jacob and J. B. Dodge, "Electron-beam controlled discharge pumping of the XeF laser," Appl. Phys. Lett. 29, 426 (1976).

16. J. A. Mangano, J. H. Jacob, M. Rokni and A. Hawryluk, "Three-body quenching of KrF^* by Ar and broad-band emission at 415 nm," Appl. Phys. Lett. 31, 26 (1977).

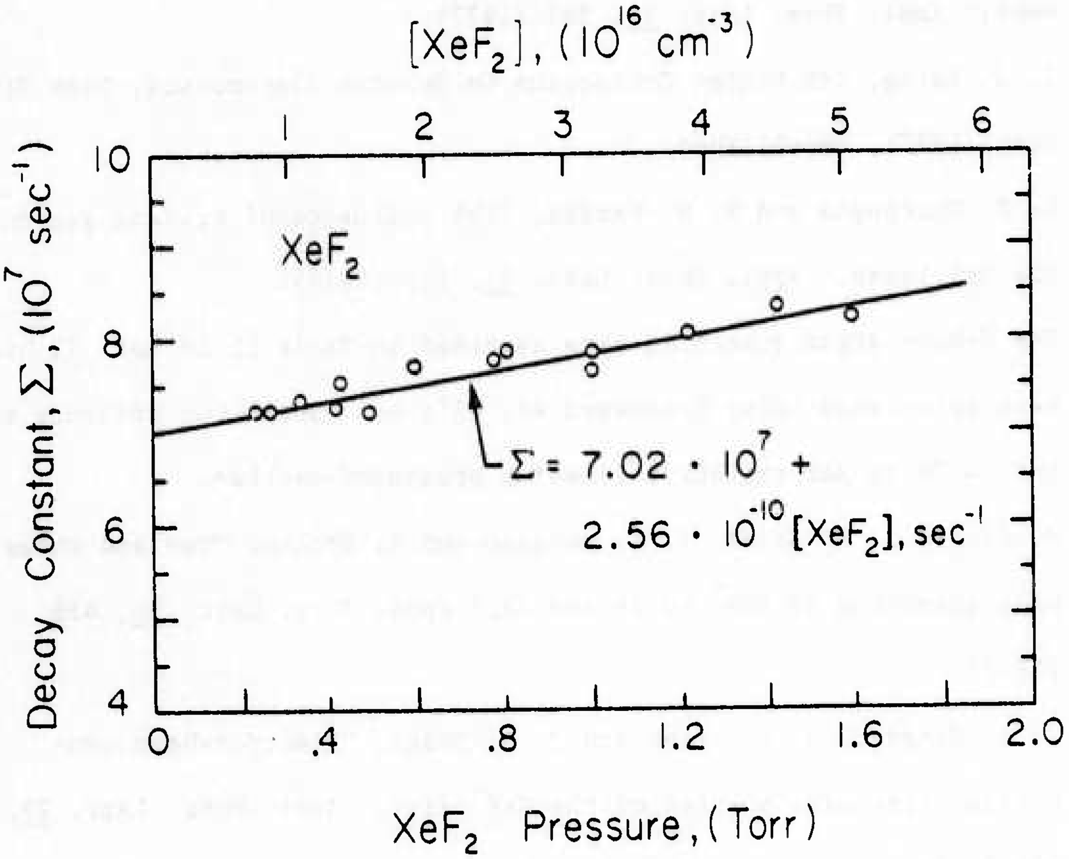

Fig. 1. Plot of decay constant, Σ, versus XeF_2 pressure. Data points are indicated by the open circles and the least squares fitting of the data is shown by the solid line.

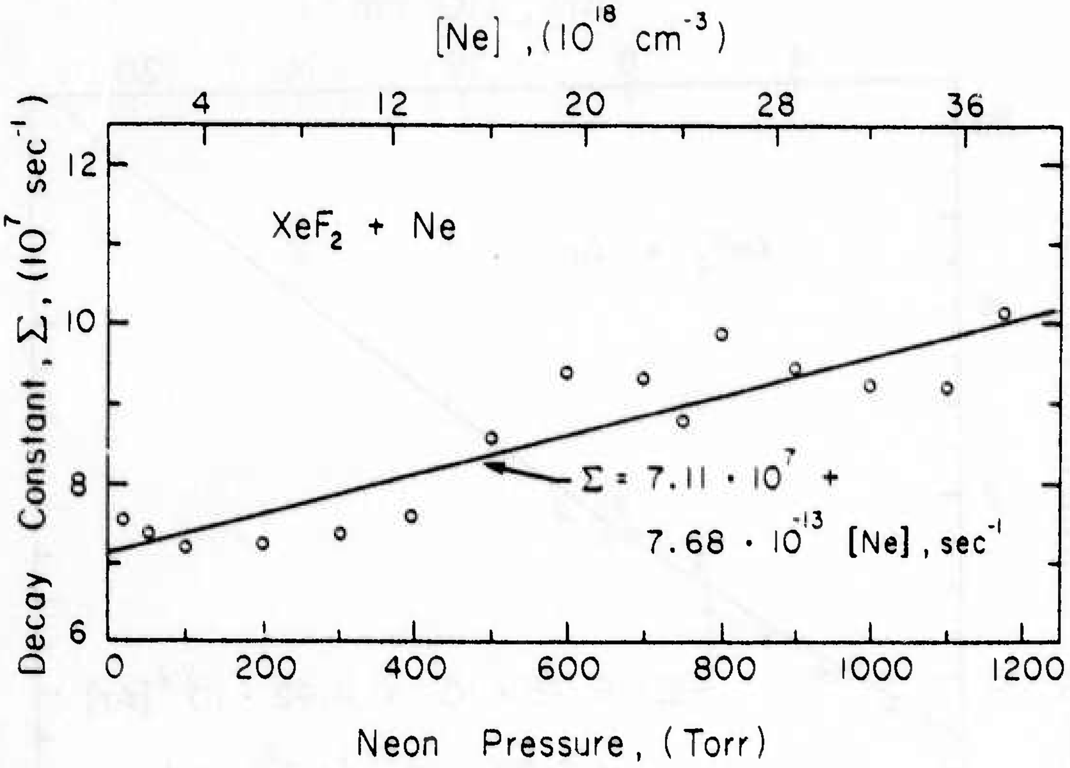

Fig. 2. Decay constant, Σ, as a function of neon pressure. The solid line again represents the least squares fitting of the data points. Uncertainty in the two-body quenching rate is reflected in the spread of the data points and the estimated error given in Table II.

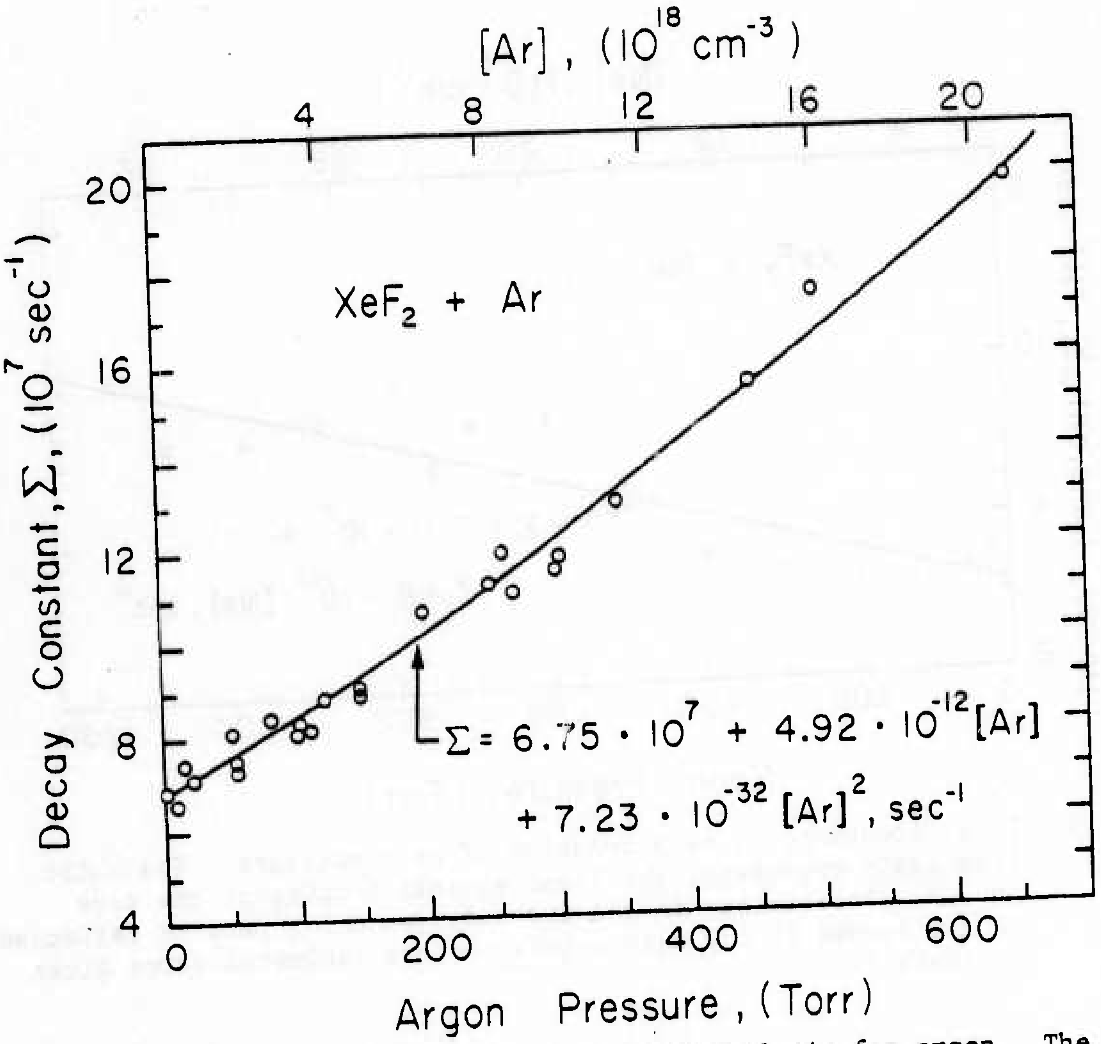

Fig. 3. Experimental data and least squares analysis for argon. The solid line represents the best fit of the data points to the quadratic relation: $\Sigma = a + bp + cp^2$. The linear and quadratic coefficients, b and c, represent the 2 and 3 body quenching rates of $XeF^*(B)$ by Ar, respectively.

Table I.

$XeF^*(B)$ radiative lifetime as measured by several investigators.

SUMMARY OF $XeF^*(B)$ RADIATIVE LIFETIMES

VALUE, (ns)	REFERENCE
16.5 ± 5.0	10
18.8 ± 1.3	4
13.5 ± 1	11
14.25 ± 0.20	This Work

Table II.

Summary of rates of deactivation of $XeF^*(B)$ by Ne, Ar and XeF_2. Uncertainties in the rates are also shown in the parentheses.

$XeF^*(B)$ QUENCHING BY Ne, Ar AND XeF_2

QUENCHER	RATE CONSTANT[a]	REFERENCE
Ne	$(7.68 \pm 1.6) \cdot 10^{-13}$	This Work
Ar	$(8 \pm 4) \cdot 10^{-13}$	14
	$(2.88 \pm 0.5) \cdot 10^{-12}$	9
	$(4.92 \pm 1.56) \cdot 10^{-12}$	This Work
2 Ar (Three body process)	$(1.5 \pm 0.5) \cdot 10^{-32}$[b]	14
	$(7.23 \pm 2.30) \cdot 10^{-32}$	This Work
XeF_2	$3.5 \cdot 10^{-10}$	4
	$1.97 \cdot 10^{-10}$	11
	$(2.56 \pm 0.32) \cdot 10^{-10}$	This Work

a. units: $cm^3 - sec^{-1}$
b. units: $cm^6 - sec^{-1}$

RADIATIVE LIFETIME OF KrF^*

The radiative lifetime of the upper level of the KrF laser at 249 nm has been measured using the pulsed photolysis technique developed for the measurement of the XeF lifetime measurements. In the lifetime experiment, the upper state of KrF was produced directly by photodissociation of KrF_2 which was synthesized in our laboratory.

The experimental apparatus used in our experiments is shown in Fig. G. Photolyzing pulses at 193 nm were produced by a discharge pumped ArF laser. This laser produced pulses with intensities of 1 Mw/cm^2 with pulse widths of less than 10 nsec. The laser radiation passed through a fused silica photolysis cell and was detected by a fast vacuum photodiode. Fluorescence pulses from KrF_2 in the cell were detected by a similar photodiode and 249 nm bandpass filter at right angles to the direction of the incident pump radiation. Pulses from the two detectors were displayed simultaneously on an oscilloscope.

KrF_2 for our experiments was contained in an evacuated pyrex cold trap, and was made to flow continuously through the photolysis apparatus by raising the temperature of the trap to about -20°C. The pressure of the KrF_2 vapor in the photolysis cell was monitored with a capacitance manometer. Continuous flow of the KrF_2 through the photolysis cell was found to reduce decomposition of the material.

Figure H shows typical pump and fluorescence pulses obtained in the KrF lifetime experiment. The 193 nm pump pulse is seen to have a halfwidth of approximately 10 nsec. More significantly the pump pulse terminates after about 18 nsec. Fluorescence data was always analyzed following the pump pulse termination so that the need for deconvolution of the fluorescence from pump pulse was obviated. As is indicated in Figure H the fluorescence following the pump pulse termination followed a simple exponential for over 2-e foldings. The lifetime of the excited state of KrF^* was therefore given by the slope of the linear decay.

In order to remove the effects of quenching of the radiating state, fluorescence data were taken for KrF_2 pressures between 0.08 and 1.2 Torr. Fluorescence decay rates were plotted as a function of pressure, and the resulting points fitted to a straight line. The zero pressure intercept of the line gave a value of 9.0 ± 0.6 nsec for the radiative lifetime of KrF^*. The slope of the line indicates that the quenching of KrF^* by KrF_2 is roughly gas-kinetic as expected. The following reprint gives a more detailed analysis of the results of the KrF^* lifetime measurement.

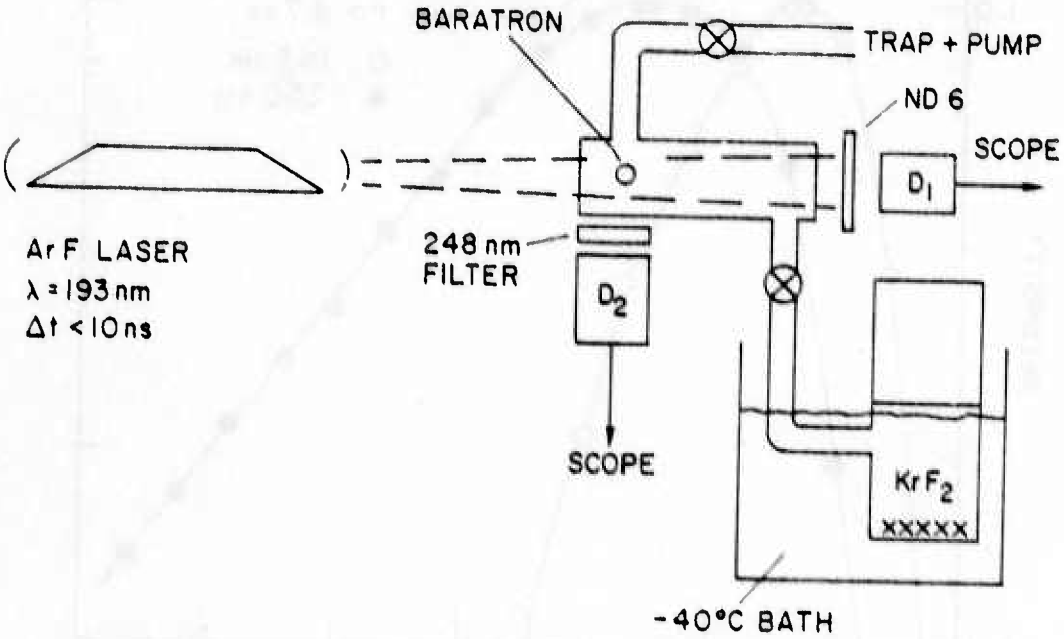

Figure 6. Experimental apparatus for KrF^* lifetime measurement.

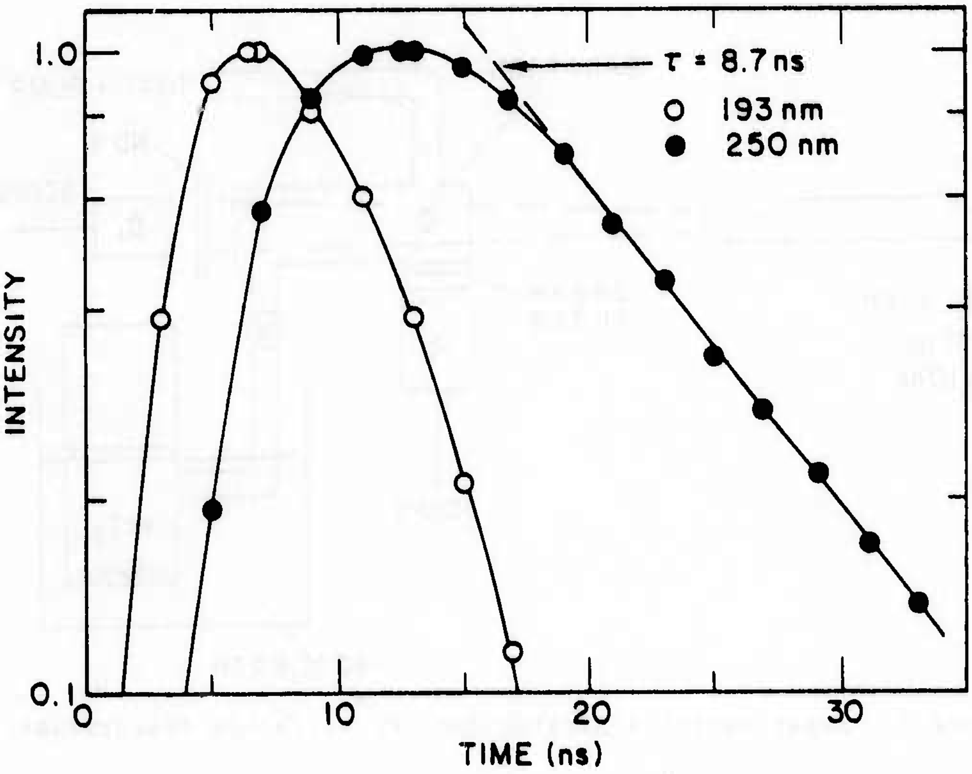

Figure H. Laser pump pulse at 193 nm and KrF^* fluorescence pulse at 250 nm.

RADIATIVE LIFETIME OF KrF*

R. Burnham and S. K. Searles
Naval Research Laboratory
Washington, D. C. 20375

The radiative lifetime of the upper laser level in krypton monofluoride which radiates at 249 nm has been measured in a pulsed photolysis experiment. The excited state of interest (KrF*) was produced through dissociative photo-excitation of krypton difluoride vapor using radiation at 193 nm from a pulsed, discharge-pumped, argon fluoride laser.[1] To the authors' knowledge, the absorption spectrum of KrF_2 in the near UV has not been observed. The results of the present experiment indicate, however, that absorption at 193 nm results in the direct dissociation of KrF_2 into KrF* + F with a high yield. Our result gives an upper limit for the dissociation energy (D_o(KrF-F)) of about 1.3 eV, since the energy of the 193 nm photon is 6.4 eV and the excited state of KrF lies at 5.1 eV. This result is consistent with an experimental value for the dissociation energy of 1.013 eV obtained by Bartlett and Sladky.[2]

Krypton difluoride for our experiments was synthesized following the general technique of Slivnik et al.[3] A solution of 0.2 moles of fluorine and 0.1 mole of krypton contained in a pyrex reactor cell was irradiated at -196°C for six hours using an unfiltered, 500 W medium-pressure mercury vapor lamp. Following photolysis, the unreacted fluorine and krypton were distilled off at -196°C and -78°C respectively. The preparation yielded approximately 100 mg of colorless crystals which had a vapor pressure of about 0.5 Torr at -78°C. Following the preparation, the reactor containing KrF_2 was connected directly to the laser photolysis apparatus which had been passivated with fluorine.

The apparatus used for the lifetime measurement was similar to that described previously.[4] Krypton difluoride vapor was made to flow continuously through the cylindrical fused quartz photolysis cell by slowly raising the temperature of the reactor from -78°C. The vapor was pumped by a small mechanical vacuum pump and liquid nitrogen trap, and the flow rate was controlled by a throttling valve located between the fluorescence cell and the pump. Continuous flow of the vapor was found to be helpful for minimizing the effects of decomposition of KrF_2 in the apparatus. The pressure in the fluorescence cell was measured adjacent to the location of the entrance window using a capacitance manometer.

Photolyzing radiation pulses at 193 nm with rise and fall times (0-100% of 10 nsec and peak intensities of 1 MW/cm^2 traversed the photolysis cell containing KrF_2 vapor and were detected with a vacuum photodiode and neutral density filter. Simultaneously, fluorescence at 249 nm was detected with a similar photodiode and a 250 nm filter with a 10 nm bandpass. The signals from the two photodiodes were displayed simultaneously on an oscilloscope. The response time of the detector and oscilloscope combination was determined by measuring their response to a 0.03 nsec. mode-locked pulse from a quadrupled YAG laser at 266 nm. The response function was roughly "bell-shaped" with rise and fall times of less than one nanosecond. A survey of fluorescence from KrF_2 upon photolysis at 193 nm was conducted using a 1/8-meter grating monochromator and photodiode. Fluorescence was observed only in a band centered at approximately 250 nm. A high-resolution spectrum of the fluorescence was not obtained.

Shapes of the 250 nm fluorescence pulses were taken directly from photographs of the oscilloscope display. Fluorescence data were analyzed for times following the termination of the photolyzing pulse from the laser. In all cases the fluorescence was found to follow a simple exponential decay over 2 e-foldings. The shapes of the fluorescence pulses were also consistent with single step dissociation into the excited state of KrF upon photolysis. The rate equation for the density of KrF^* following the termination of the photolyzing pulse was therefore taken to be:

$$\frac{d[KrF^*]}{dt} = -(1/\tau_o + k\,[M])\ \ [KrF^*]. \qquad (1)$$

In Eq. 1, τ_o is the radiative lifetime of KrF^* and k [M] is the collisional quenching rate due to the presence of KrF_2 or the products of its decomposition.

Fluorescence data were taken for pressures in the photolysis cell between 0.08 and 1.2 Torr. Fluorescence decay rates were corrected for the detector response time and plotted as a function of the pressure in the photolysis cell. The results of the experiment are shown in Figure 1. A linear least-squares fit of the data gave the lifetime for KrF^* from the zero-pressure intercept of the fitted line. The value of the radiative lifetime of KrF^* so derived was 9.0 ± 0.6 nsec. The slope of the line gave a quenching rate for KrF^* by KrF_2 (assuming negligible KrF_2 decomposition) of $3.7 \pm 1 \times 10^{-10}$ cm^3/sec.

The results of the present experiment constitute the first measurement of the radiative lifetime of KrF^*. Reasonable agreement is found between the measured lifetime and a theoretical lifetime of 7 nsec based upon the results of molecular orbital calculations on KrF by Dunning and Hay.[5] Pulsed photolysis experiments similar to those described above are being continued in order to obtain more extensive information on the radiative and collisional kinetics of the excited states of KrF.

REFERENCES

1. R. Burnham and N. Djeu, Appl. Phys. Lett. 29, 707 (1976).
2. N. Bartlett and F. O. Sladky, The Chemistry of Krypton, Xenon, and Radon, University of California Radiation Laboratory Report 19658 (June 1970).
3. J. Slivnik, A. Šmalc, K. Lutau, B. Žimva, and B. Frlec, J. Fluor. Chem. 5, 273 (1975).
4. R. Burnham and N. W. Harris, J. Chem. Phys. 66, 2742 (1977).
5. P. J. Hay and T. H. Dunning, Jr., J. Chem. Phys. 66, 1306 (1977).

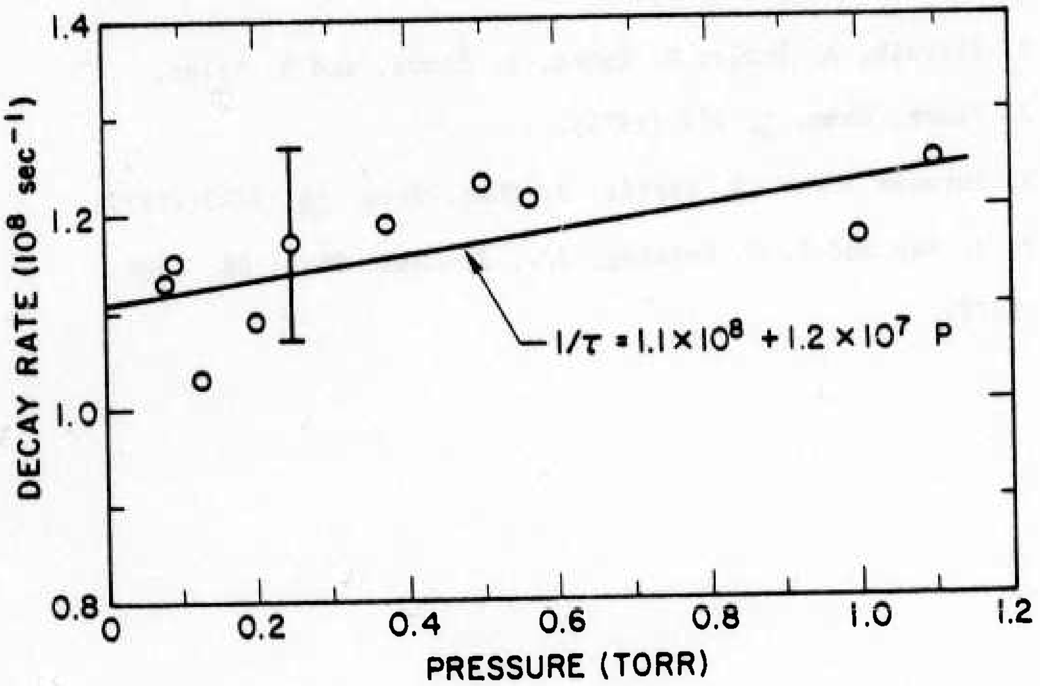

Fig. 1. Decay rate ($1/\tau$) of KrF^* fluorescence at 250 nm vs. pressure. The zero-pressure intercept of the fitted line gives a lifetime for KrF^* of 9.0 ± 0.6 nsec.

COMPUTER MODELING OF THE XENON FLUORIDE LASER

A. Introduction

During this past reporting period a laser kinetics computer code has been developed to the point where the capability now exists at NRL to model discharge-pumped gas laser systems. The energy pumped into the gas constituents through collisions with electrons accelerated by the discharge electric field is accounted for by solving the Boltzmann transport equation for the electron distribution function. The Boltzmann solver algorithm assumes a steady-state electron distribution function which is computed as a function of applied field and the fractional excitation. The effects of the following electron-molecule collisions on the distribution function are considered: momentum transfer, electronic excitation, ionization, recombination, attachment, and superelastic processes. Superelastic collisions are treated iteratively in a self consistent manner.

The Boltzmann transport equation solver has been merged with a chemical kinetic code which uses an accurate and efficient Runge-Kutta-Treanor algorithm specially suited to solving a coupled set of stiff differential equations. The rate constants for electron-molecule reactions required by the kinetics code are computed by integrating the appropriate cross sections over the electron distribution function. This Boltzmann kinetics package has been thoroughly tested by its use in modeling a variety of rare gas halide laser experiments where good agreement has been obtained.

Detailed modeling was concentrated on the e-beam sustainer pumped neon-diluent XeF laser experiment at NRL. By comparing the model with experiments a detailed energy flow kinetics chain for the XeF laser system was devised. Also, numerical studies were used to investigate the effective XeF lower laser-level deactivation rate and to elucidate laser-light absorption processes.

B. Code Development

1. Background

In the previous semiannual report,[1] the intitial development of a computer code for modeling electrically excited rare gas halide lasers was discussed. At that time a kinetics package which incorporated a convenient symbolic input format for the relevant chemical reactions and rate constants and a useful output format describing the details of the kinetics chain had been developed. Also some preliminary work had begun in modifying and testing a Boltzmann transport equation solver[2,3] in order to merge it into the kinetics package thus allowing the modeling of discharge pumped laser schemes.

2. Boltzmann Transport Equation Solver

The coupling of the Boltzmann solver to the kinetics package and the associated checkout and testing have been successfully achieved during the early part of the present reporting period. Several modidifcations of the original Boltzmann transport code were made to adapt the code to the Texas Instruments Advanced Scientific Computer (ASC) at NRL, to enable faster execution time and more efficient use of storage, to allow enough flexibility in the code for handling a variety of processes affecting the electron distribution function, and to provide for easy future modification and selected detailed output. The present configuration of the kinetics/Boltzmann code is diagrammed in Figure I.

3. Detailed Kinetics Output

The kinetics package is presently set up to handle up to 144 kinetic reactions involving up to 64 species. Although these numbers are easily increased or decreased by minor code modifications, they approximate the complexity of typical rare gas halide laser models. Even though the global laser performance code predictions (such as laser output power, pulse length, energy, and efficiency) are simple to compare with experiments, the maze of intermediate steps in the kinetics chain and in energy flow paths leading to laser output is much more difficult to unfold because of the large numbers of reactions which must be considered. Also, the rate constants for many of the intermediate formation and quenching processes are not well known. Since it is almost impossible to measure rates for every conceivable process, it is critical to determine which kinetic processes have the largest effect on laser performance and hence which rates are in need of accurate measurements and which rates require only an order of magnitude estimate.

A method for easily separating important reactions from unimportant reactions was recently added to the output routines of the kinetics code. The basic concept of this method is the printing out for various times during the pump pulse of the percentage contribution of each reaction to the formation or depletion of the species involved. Thus, those reactions which show small percentages for all species and for all times throughout the laser pulse are unimportant and can be eliminated in future runs keeping output clutter to a minimum. Conversely, the dominant reactions are clearly indicated by large percentage contributions for one or more species. This type of output allows one to construct easily and accurately energy flow diagrams (Figure J) which outline the important pumping, formation, interception, quenching, and optical extraction channels.

4. Code Verification

By examining the output from a large number of computer runs modeling lasers pumped by an e-beam only, it is reasonable to conclude that the chemical kinetics part of the rare-gas halide laser code is as accurate and as efficient as is needed for the present applications. However, certain simplifying physical assumptions of the Boltzmann solver as well as the numerical approximation methods used to solve the transport equation require validity checks to determine the volume of parameter space over which this code produces reliable results. These checks can be performed in a number of ways: (a) comparison of code predictions with experimental results; (b) comparison of code predictions and intermediate calculations with other codes which have been successfully compared with a variety of experimental lasers; and (c) "failure testing"[4] in which the code is shown to predict catastrophic results for initial conditions in which the experiment is known to be unstable (e.g., discharge arc formation) or where it it known that the physical assumptions of the model are not valid. Method (a) involves verification by comparison of a few predicted overall laser performance measurements with the real world while method (b) allows the comparison of a large number of computational details (e.g., population densities, rate constants, electron distribution functions, laser light cavity flux, etc. -- all are function of time) with codes which have been compared with many experiments.

The present version of the kinetics, Boltzmann code has been successfully verified by application of all three of the verification methods mentioned above. Comparison of predicted performances of both KrF and XeF laser systems with experiments at NRL[5,6,7] have shown agreement in laser output power and energy usually within ~ 50%. Some examples of this comparison for the XeF system are listed in Table 1. The code results also compare well in detail with computer calculations done at United Technologies, Northrup, and Air Force Weapons Laboratory. In most cases the discrepancies are explained by minor differences in cross sections and energy levels. Also the discharge part of the code has predicted arcs at high electric fields at the same values (within 20%) of E/N which produce arcs in experiments.

C. XeF Laser Modeling

The XeF laser and other rare gas halide lasers show promise of very high efficiencies and high peak powers which are critical factors for many applications. The current intense interest in the development of these lasers is concerned with attempts to increase their efficiency through investigation and understanding of processes which result in or inhibit laser oscillation. Such understanding should make possible the selection of those areas of parameter space which yield optimum laser efficiency and/or output power.

1. Kinetics Chain

The numerical modeling part of the rare gas halide laser work at NRL has been aimed at an understanding of the important upper state formation, interception, and quenching reactions and laser-light extraction. The approach has been to model typical laser systems and to study the energy flow channels from pumping (either by an electron beam alone or by a combination of an electron beam and an applied electric field) to laser energy output. An energy flow block diagram in Figure J outlines the important channels for a particular gas mixture of Ne, Xe, and NF_3 pumped by an e-beam only. The mixture, pump, and optical cavity parameters were chosen to match those in an NRL experiment[7] for purposes of comparison. In this gas mixture, the 300 keV beam electrons deposit an average of 20 keV per cm of depth of travel in the laser cavity. This deposited energy produces mainly neon ions (Ne^+), neon excited states and metastables (Ne^*), and secondary electrons. The ions and metastables then transfer their energy to the upper laser level (XeF^*) through a complex chain of reactions, all of which involve some loss of energy by downward cascade and some of which involve interception or loss of excitation or ionization energy by quenching or radiative processes. The details of the XeF^* formation processes are not well understood and the formation kinetics chain shown in Figure J is merely an approximation to the real world--our current opinion based on the best known or best estimated rates which explains the observed laser performance. More detailed measurements such as time dependent side light emission from various intermediate species are needed to tie the details of the kinetics chain to reality.

Some important processes which dominate the formation kinetics of an XeF laser under conditions modeled here are Penning ionization reactions designated generally as:

$$A^* + B \rightarrow B^+ + A + e^- .$$

This type of reaction can proceed whenever the excitation energy of A is greater than the ionization energy of B and goes fastest for reactions close to resonance. The neon metastable (Ne^*) with an energy of 16.6 eV can Penning ionize all heavier rare gases. Also excited fluoride, F^*, (which is formed by rapid NeF^* predissociation) is sufficiently energetic to Penning ionize Xe. Thus the three Penning ionization reactions:

$$Ne^* + Xe \rightarrow Xe^+ + Ne + e^-$$

$$Ne_2^* + Xe \rightarrow Xe^+ + 2\,Ne + e^-$$

$$F^* + Xe \rightarrow Xe^+ + F + e^-$$

are responsible for most of the formation of Xe^+ under the conditions of Figure J. Practically all of the XeF^* is formed from Xe^+ by the reactions:

$$Xe^+ + F^- + (M) \rightarrow XeF^* + (M)$$

$$Xe^+ + 2\,Ne \rightarrow NeXe^+ + Ne$$

$$NeXe^+ + F^- \rightarrow XeF^* + Ne.$$

A major difference between XeF and KrF lasers in Ne diluent and these same lasers in Ar diluent is that metastable neon is capable of Penning ionization of the admixture rare gas whereas Ar^* is not. Hence the formation kinetics chains in the region of parameter space treated here are quite different.

A list of reactions and rates used to model the laser system corresponding to the energy flow channels in Figure J is given in Table 2.

2. Lower Laser Level Deactivation

Xenon fluoride differs from all other rare gas monohalides in that it has a bound lower laser level. Although the ground state is very weakly bound ($\sim$ 1100 cm^{-1} from v=0 and has only a few vibrational levels, its presence can produce bottlenecking which can have a significant effect on ultimate laser light extraction. At near saturation cavity flux levels, because of rapid mixing of XeF and XeF^* due to stimulated emission and absorption, the effective stimulated lifetime of the upper laser level is increased thus making XeF^* more vulnerable to deactivation by quenching or side fluorescence emission. For every ground state XeF molecule which is quenched, a resonance reabsorption is prevented and thus a laser photon becomes available for extraction.

Most of the ground state quenching is assumed to be represented by the reaction:

$$XeF + Ne \rightarrow Xe + F + Ne .$$

Quenching by gas constituents other than Ne is comparatively negligible for the mixture discussed here. The rate of this ground state quenching process has not been measured but, if one assumes a formation chain based on reasonably well estimated rates along with a measured XeF^* lifetime[8,9] and measured quenching rates[10] then agreement between predicted and experimental laser efficiency can be obtained if a rate constant for XeF ground state quenching of 3×10^{-12} cm^3 s^{-1} is chosen. The predicted laser output efficiency is plotted as a function of the selected rate constant for XeF ground state quenching in Figure K. The circle represents the observed value of laser efficiency and corresponds to a rate constant of 3.0×10^{-12} cm^3 s^{-1}. The curve indicates how the laser performance would be affected if the rate constant were varied. For the parameters and formation kinetics discussed here, it it seen from the curve in Figure K that an efficiency of at most 3.3% could be expected if XeF ground state deactivation rate were greatly increased, for example by heating the gas.

From a simple exponential law of temperature variation of the rate constant it can be estimated that heating the gas from room temperature to 600°K would increase the deactivation rate constant by about an order of magnitude. According to the curve in Figure K, this would yield an increase in laser output power of about 50%. Of course this estimate assumes that the only effect that heating would have on the kinetics would be to increase the lower laser level deactivation rate. In actuality, gas heating may also have a significant effect on the formation and quenching of the upper laser level and its overall effect on laser performance is presently difficult to judge.

It should also be noted that the XeF ground state quenching rate of 3×10^{-12} cm^3 s^{-1} is really the effective average rate of depopulation by any or all of several collisionally induced processes from only those vibrational levels of the XeF(X) state which are lower levels for the actual lasing lines--mainly 351.1 nm and 353.1 nm. It is only these vibrational levels which contribute to the bottlenecking.

3. Absorption

Earlier experiments[7] have shown that when neon is used in place of argon as the diluent gas in an XeF laser a substantial improvement in output power and efficiency is realized. This improved laser performance was found to be due to reduced transient absorption at the laser wavelength in the neon diluent case vs. the argon diluent case. Since transient absorption can significantly limit laser performance, it is imperative to determine which species are responsible for laser-light absorption and to understand the processes by which these species are formed or depleted.

A study[11,12] of such absorption processes was conducted by comparing predicted transient densities of suspected absorbers with experimentally measured absorptions. Some results of this work for an XeF laser in neon diluent are summarized in the plots of Figure L. The open circles connected by the solid lines in the upper portion of Figure L represent absorptions measured[7] by passing probe laser radiation through a 100 cm path length of various e-beam excited gas mixtures as indicated on the horizontal axis. In the lower portion of Figure L, on a relative normalized scale, are plotted computed population densities of selected candidate absorbers. The horizontal location of the data points corresponds to the gas mixture for which the modeling was done while the vertical axis represents the predicted relative absorption, or relative number density for the species indicated. The number density, N, and absorption, α, are related linearly by $\alpha = N\sigma$ where σ is the photoabsorption cross section. The vertical scale is normalized somewhat arbitrarily so that the peak predicted relative absorption for each species plotted is equal to 1.25% per cm which is the highest observed total absorption shown in the upper portion of the figure. All of the theoretical and experimental data points in Figure L and correspond to a total gas pressure of 5 atm.

The identity of the transient species responsible for the observed absorption is determined as follows. When 0.1% Xe is added to pure Ne, the measured absorption is seen to drop by about an order of magnitude. The only transient species which show a comparable predicted reduction between the pure Ne and Ne + 0.1% Xe cases are Ne_2^* and Ne_2^+. All other species show either no drop in concentration at all or an increase. Hence Ne_2^* or Ne_2^+ or both are indicated to be the main XeF laser light absorbing species in e-beam excited pure neon. Similarly, the absorption is seen to increase by about a factor of ten when the Xe concentration is raised from 0.1% to 1.0%. The model computes that the main absorbers for the pure neon case, Ne_2^* and Ne_2^+ (dashed lines), actually decrease substantially with increasing Xe admixture and hence these species do not contribute significantly to absorption. However, the predicted contributions of Xe_2^+ and Xe_2^* (solid lines) to the total absorption do follow the observed increase with increasing Xe concentration and, again, no other species show a similar (or any) rise. Also, a much smaller absorption is measured in the laser mix case ($Ne/Xe/NF_3$ = 99.76/0.18/0.06) than in the Ne + 1.0% Xe case and the only species that show any drop in concentration are Xe_2^* and Xe_2^+. Hence the ionized and neutral dimers of xenon are indicated to be the main absorbers of laser light in the XeF laser modeled here.

If the computed absolute Xe_2^+ density for the laser mix is multiplied by its calculated XeF laser wavelength photoabsorption cross section[13] then the predicted absolute absorption for this species is obtained. This value is indicated by the "X" in the upper part of Figure L and agrees (within expected error limits) with the observed absorption. Since the assumption of an unusually high photoabsorption cross section for Xe_2^* would be required for this species to be responsible for the measured laser mix absorption, it is concluded that Xe_2^+ is the predominant transient absorber in a xenon fluoride laser with neon diluent.

References

1. NRL Memorandum Report 3580 Sept. 1977.

2. The initial version of the Boltzmann code was obtained from Maj. T. H. Johnson of Air Force Weapons Laboratory. It is based on the

article: J. J. Lowke, A. V. Phelps, and B. W. Irwin, J. Appl. Phys. 44, 4664 (1973).

3. A. Hunter and T. H. Johnson, Private comm. 1977.
4. T. H. Johnson, J. Comp. Phys. 21, 245 (1976).
5. L. F. Champagne, J. G. Eden, N. W. Harris, N. Djeu, and S. K. Searles, Appl. Phys. Lett. 30, 160 (1977).
6. L. F. Champagne, Fourth Colloquium on Electronic Transition Lasers, Munich, Germany, (June 1977).
7. L. F. Champagne and N. W. Harris, Appl. Phys. Lett. 31, 513 (1977).
8. R. Burnham and N. W. Harris, J. Chem. Phys. 66, 2742 (1977).
9. J. G. Eden and R. W. Waynant, Optics Letters 2, 13-15 (January 1978).
10. J. G. Eden and R. W. Waynant, to be published in J. Chem. Phys. (1978).
11. L. J. Palumbo and L. F. Champagne, Fifth Conf. on Chemical and Molecular Lasers, postdeadline paper, St. Louis (April 1977).
12. L. J. Palumbo, T. G. Finn, and L. F. Champagne, Thirtieth Annual Gaseous Electronics Conf., Palo Alto (October 1977).
13. W. Wadt, Fifth Conf. on Chemical and Molecular Lasers, St. Louis (April 1977).

TABLE 1

COMPARISON OF PREDICTED AND OBSERVED LASER PERFORMANCE

A. Parameters

Gas mixture: $Ne/Xe/NF_3 = 99.76/0.18/0.06$

Total Pressure: 5 atm

E-beam energy deposition per pulse: 158 J/ℓ

E-beam current density: 7 A/cm^2

Pump pulse duration: 1 μsec

Laser cavity mirror reflectivity product: 50%

Laser cavity length: 100 cm

B. Comparison of Performance

Quantity	Units	Experiment[a]	Model
Laser energy output per pulse	J/ℓ	2.8	3.7
Laser output power density at peak	MW/cm^2	0.28	0.39
Intrinsic energy efficiency	%	1.8	2.3
Total laser light absorption at peak	$\% \ cm^{-1}$	0.07	0.10

[a] L. F. Champagne and N. W. Harris, Appl. Phys. Lett. 31, 513 (1977).

TABLE 2.

REACTIONS AND RATE CONSTANTS FOR MODELING E-BEAM PUMPED XENON FLUORIDE LASER IN NEON DILUENT

Reaction	Rate Constant,[a] cross section, or lifetime	Notes or Reference
(a) e-beam ($\vec{e}$) pumping		
* $\mathrm{Ne} + \vec{e} \longrightarrow \mathrm{Ne}^{+} + e^{-} + \vec{e}$	4.31(-18) cm^2	b,c
* $\mathrm{Ne} + \vec{e} \longrightarrow \mathrm{Ne}^{*} + \vec{e}$	1.23 (-18) cm^2	b,c
$\mathrm{Xe} + \vec{e} \longrightarrow \mathrm{Xe}^{+} + e^{-} + \vec{e}$	3.14 (-17) cm^2	b,c
$\mathrm{Xe} + \vec{e} \longrightarrow \mathrm{Xe}^{*} + \vec{e}$	8.99 (-18) cm^2	b,c
(b) electron attachment		
* $\mathrm{F}_2 + e^{-} \longrightarrow \mathrm{F}^{-} + \mathrm{F}$	1.0 (-9)	d,e
* $\mathrm{NF}_3 + e^{-} \longrightarrow \mathrm{F}^{-} + \mathrm{NF}_2$	1.0 (-9)	d
$\mathrm{F} + e^{-} + \mathrm{M} \longrightarrow \mathrm{F}^{-} + \mathrm{M}$	1.5 (-31)	f
(c) Neutral kinetics		
* $\mathrm{F} + \mathrm{F} + \mathrm{M} \longrightarrow \mathrm{F}_2 + \mathrm{M}$	6.0 (-31)	e
* $\mathrm{NF}_2 + \mathrm{F} + \mathrm{M} \longrightarrow \mathrm{NF}_3 + \mathrm{M}$	6.0 (-31)	f
* $\mathrm{Ne}^{*} + 2\,\mathrm{Ne} \longrightarrow \mathrm{Ne}_2^{*} + \mathrm{Ne}$	6.0 (-33)	f
$\mathrm{Ne}^{*} + \mathrm{F}_2 \longrightarrow \mathrm{NeF}^{*} + \mathrm{F}$	6.0 (-10)	f
$\mathrm{Ne}^{*} + \mathrm{NF}_3 \longrightarrow \mathrm{NeF}^{*} + \mathrm{NF}_2$	7.0 (-11)	f
* $\mathrm{Xe}^{*} + \mathrm{Xe} + \mathrm{Ne} \longrightarrow \mathrm{Xe}_2^{*} + \mathrm{Ne}$	1.6 (-32)	g
* $\mathrm{Xe}^{*} + 2\,\mathrm{Ne} \longrightarrow \mathrm{NeXe}^{*} + \mathrm{Ne}$	5.0 (-34)	f
$\mathrm{Xe}^{*} + 2\,\mathrm{Xe} \longrightarrow \mathrm{Xe}_2^{*} + \mathrm{Xe}$	5.0 (-32)	h
$\mathrm{Ne}_2^{*} + \mathrm{F}_2 \longrightarrow \mathrm{NeF}^{*} + \mathrm{Ne} + \mathrm{F}$	1.0 (-9)	i

Reaction	Rate Constant,[a] cross section, or lifetime	Notes or Reference
(c) Neutral kinetics (continued)		
$Ne_2^{*} + NF_3 \longrightarrow NeF^{*} + Ne + NF_2$	7.0 (-11)	i
${}^{*}NeXe^{*} + Xe \longrightarrow Xe_2^{*} + Ne$	1.0 (-10)	i
${}^{*}NeF^{*} \longrightarrow F^{*} + Ne$	2.0 (+9)	j,k
$NeF^{*} + F_2 \longrightarrow Ne + F + F_2$	5.0 (-10)	i
$NeF^{*} + NF_3 \longrightarrow Ne + F + NF_3$	5.0 (-11)	f
$NeF^{*} + Xe \longrightarrow Xe^{*} + F + Ne$	5.0 (-10)	f
$NeXeF^{*} + F_2 \longrightarrow Ne + Xe + F + F_2$	5.0 (-10)	i
$NeXeF^{*} + NF_3 \longrightarrow Ne + Xe + F + NF_3$	5.0 (-11)	i
${}^{*}NeXeF^{*} + Xe \longrightarrow Ne + Xe + F + Xe$	1.0 (-10)	i
$F^{*} + F_2 \longrightarrow F + F_2$	3.5 (-10)	j
${}^{*}F^{*} + NF_3 \longrightarrow F + NF_3$	3.8 (-10)	f
${}^{**}F + 2\ Ne \longrightarrow NeF^{*} + Ne$	5.0 (-34)	j
(d) Penning Ionization		
${}^{*}Ne^{*} + Xe \longrightarrow Xe^{+} + e^{-} + Ne$	5.0 (-10)	f
${}^{*}Ne^{*} + Xe \longrightarrow NeXe^{+} + e^{-}$	1.0 (-10)	f
$Ne^{*} + Ne^{*} \longrightarrow Ne^{+} + e^{-} + Ne$	5.0 (-10)	f
${}^{*}Ne_2^{*} + Xe \longrightarrow Xe^{+} + e^{-} + 2\ Ne$	5.0 (-10)	f
${}^{*}Ne_2^{*} + Xe \longrightarrow NeXe^{+} + e^{-} + Ne$	1.0 (-10)	f
${}^{*}F^{*} + Xe \longrightarrow Xe^{+} + e^{-} + F$	1.3 (-10)	j
(e) Dimer and trimer formation		
${}^{*}Ne^{+} + 2\ Ne \longrightarrow Ne_2^{+} + Ne$	4.4 (-32)	l
${}^{*}Ne^{+} + Ne + Xe \longrightarrow XeNe^{+} + Ne$	1.0 (-31)	l

Reaction	Rate Constant,[a] cross section, or lifetime	Notes or Reference
(e) Dimer and trimer formation (continued)		
$\mathrm{Xe^+ + 2\,Xe \longrightarrow Xe_2^+ + Xe}$	2.0 (-31)	1
$\mathrm{Xe^+ + Xe + Ne \longrightarrow Xe_2^+ + Ne}$	1.0 (-31)	1
$\mathrm{^*Xe^+ + 2\,Ne \longrightarrow NeXe^+ + Ne}$	1.0 (-31)	1
$\mathrm{^*Xe_2^+ + Xe + Ne \longrightarrow Xe_3^+ + Ne}$	6.0 (-32)	f
$\mathrm{Xe_3^+ + Xe \longrightarrow Xe_2^+ + 2\,Xe}$	1.7 (-13)	1
(f) Charge Transfer		
$\mathrm{Ne^+ + Xe \longrightarrow Xe^+ + Ne}$	1.0 (-13)	1
$\mathrm{Ne_2^+ + Xe \longrightarrow Xe^+ + 2\,Ne}$	5.0 (-14)	m
$\mathrm{Ne_2^+ + Xe \longrightarrow NeXe^+ + Ne}$	5.0 (-14)	1
$\mathrm{^*XeNe^+ \longrightarrow NeXe^+}$	1.0 (+8) sec - 1	f
$\mathrm{XeNe^+ + Ne \longrightarrow Ne_2^+ + Xe}$	5.0 (-14)	i
$\mathrm{XeNe^+ + Xe \longrightarrow Xe_2^+ + Ne}$	5.0 (-14)	i
$\mathrm{^*NeXe^+ + Xe \longrightarrow Xe_2^+ + Ne}$	2.0 (-10)	1
$\mathrm{Ne_3^+ + Xe \longrightarrow Xe^+ + 3\,Ne}$	5.0 (-14)	i
$\mathrm{^*Ne_2^+ + NF_3 \longrightarrow NF_3^+ + 2\,Ne}$	5.0 (-10)	j
(g) Dissociative Recombination		
$\mathrm{^*Ne_2^+ + e^- \longrightarrow Ne^* + Ne}$	2.5 (-8)	n
$\mathrm{^*Xe_2^+ + e^- \longrightarrow Xe^* + Xe}$	1.3 (-7)	n
$\mathrm{^*XeNe^+ + e^- \longrightarrow Ne^* + Xe}$	6.0 (-8)	f
$\mathrm{^*NeXe^+ + e^- \longrightarrow Xe^* + Ne}$	6.0 (-8)	f
$\mathrm{^*Ne_3^+ + e^- \longrightarrow Ne^* + 2\,Ne}$	3.0 (-8)	f
$\mathrm{^*Xe_3^+ + e^- \longrightarrow Xe^* + 2\,Xe}$	5.0 (-6)	f

Reaction	Rate Constant,[a] cross section, or lifetime	Notes or Reference
${}^{*}NF_3^{+} + e^{-} \longrightarrow F^{*} + NF_2$	5.0 (-8)	j
(h) Ion-ion recombination		
${}^{*}Ne^{+} + F^{-} \longrightarrow NeF^{*}$	1.0 (-6)	m
${}^{*}Ne_2^{+} + F^{-} \longrightarrow NeF^{*} + Ne$	1.0 (-6)	f
${}^{*}XeNe^{+} + F^{-} \longrightarrow NeF^{*} + Xe$	1.0 (-6)	i
${}^{*}NeXe^{+} + F^{-} \longrightarrow NeXeF^{*}$	1.0 (-6)	f
${}^{*}Ne_3^{+} + F^{-} \longrightarrow NeF^{*} + 2\,Ne$	1.0 (-6)	f
(i) Radiation		
${}^{*}Ne_2^{*} \longrightarrow 2\,Ne + h\nu_1$	10 ns	f
${}^{*}Xe_2^{*} \longrightarrow 2\,Xe + h\nu_2$	33 ns	o
${}^{*}NeXe^{*} \longrightarrow Ne + Xe + h\nu_3$	200 ns	i
${}^{*}NeF^{*} \longrightarrow Ne + F + H\nu_4$	2.5 ns	j
${}^{*}NeXeF^{*} \longrightarrow Ne + Xe + F + h\nu_5$	20 ns	i
(j) Upper Laser Level Formation (neutral channel)		
${}^{*}Xe^{*} + F_2 \longrightarrow XeF^{*} + F$	7.5 (-10)	p
${}^{*}Xe^{*} + NF_3 \longrightarrow XeF^{*} + NF_2$	9.0 (-11)	p
$Xe_2^{*} + F_2 \longrightarrow XeF^{*} + Xe + F$	7.5 (-10)	f
${}^{*}Xe_2^{*} + NF_3 \longrightarrow XeF^{*} + Xe + NF_2$	9.0 (-11)	f
$NeXe^{*} + F_2 \longrightarrow XeF^{*} + Ne + F$	7.5 (-10)	f
${}^{*}NeXe^{*} + NF_3 \longrightarrow XeF^{*} + Ne + NF_2$	9.0 (-11)	f
(k) Upper Laser Level Formation (ion channel)		
${}^{*}Xe^{+} + F^{-} \longrightarrow XeF^{*}$	1.0 (-6)	m

Reaction	Rate Constant,[a] cross section, or lifetime	Notes or Reference
${}^{*}Xe_2^{+} + F^{-} \longrightarrow XeF^{*} + Xe$	1.0 (-6)	m
${}^{*}NeXe^{+} + F^{-} \longrightarrow XeF^{*} + Ne$	1.0 (-6)	f
$Xe_3^{+} + F^{-} \longrightarrow XeF^{*} + 2\ Xe$	1.0 (-6)	f
(1) Upper Laser Level Quenching		
$XeF^{*} + F_2 \longrightarrow Xe + F + F_2$	3.8 (-10)	q
$XeF^{*} + NF_3 \longrightarrow Xe + F + NF_3$	2.8 (-11)	q
${}^{*}XeF^{*} + Ne \longrightarrow NeXeF^{*}$	7.7 (-13)	q
$XeF^{*} + Xe \longrightarrow 2Xe + F$	3.3 (-11)	q
$XeF^{*} + Xe + Ne \longrightarrow 2Xe + F + Ne$	2.0 (-31)	f
$XeF^{*} + 2\ Xe \longrightarrow 3\ Xe + F$	2.4 (-29)	q
(m) Laser Radiation and Oscillation		
${}^{*}XeF^{*} \longrightarrow XeF + h\nu_f$	14.25 ns	r, s
$XeF^{*} \longrightarrow XeF + h\nu_\ell$	14.25 ns/Ω	s
${}^{*}XeF^{*} + h\nu_\ell \longrightarrow XeF + 2\ h\nu_\ell$	14 Å^2	t
${}^{*}XeF + h\nu_\ell \longrightarrow XeF^{*}$	14 Å^2	t
${}^{*}h\nu_\ell \longrightarrow h\nu_o$	9.6 ns	u
${}^{*}XeF + Ne \longrightarrow Xe + F + Ne$	3.0 (-12)	v
$Xe + F + Ne \longrightarrow XeF + Ne$	2.3 (-33)	w
(n) Absorption of Laser Radiation (λ = 351 nm)		
$F_2 + h\nu_\ell \longrightarrow 2\ F$	6.6 (-5) Å^2	x
${}^{*}F^{-} + h\nu_\ell \longrightarrow F + e^{-}$	0.02 Å^2	y

Reaction	Rate Constant,[a] cross section, or lifetime	Notes or Reference
*$Ne_2^+ + h\nu_\ell \longrightarrow Ne^+ + Ne$	0.005 Å^2	z
$Ne_3^+ + h\nu_\ell \longrightarrow Ne^+ + 2\ Ne$	0.005 Å^2	f
*$Xe_2^+ + h\nu_\ell \longrightarrow Xe^+ + Xe$	0.24 Å^2	z

Notes on Table 2

* Reactions preceded by an asterisk contribute (in the model) more than 5% to the formation rate or depletion rate of at least one species. This contribution is computed at the peak of the pump pulse when a quasi-equilibrium state is obtained.

a. Units of rate constants are $cm^{+3}\ s^{-1}$ or $cm^{+6}\ s^{-1}$ for two-and three-body reactions respectively. Cross sections are in cm^2 and lifetimes in ns. Unless otherwise noted, the rate constant is listed. Number in parentheses is exponent to the base 10.

b. Cross section in cm^2 listed.

c. e-beam pumping cross sections are derived from electron energy deposition calculations carried out with a computer code developed by D. B. Brown at NRL. These effective cross sections are a function of e-beam energy (300 KeV), total gas pressure (5 atm), gas mixture ($Ne/Xe/NF_3$ = 99.76/0.18/0.06), and laser geometry.

d. NF_3 and F_2 attachment rate for electrons of a few eV is guessed to be about the same.

e. W. L. Nighan, et al., U. T. Report No. R77-922617-2, United Technologies Research Corp., East Hartford, Conn. 06108 (1977).

f. Guessed by analogy.

g. H. H. Nakano, et al., SRI Report No. MP 76-99, Stanford Research Institute, Menlo Park, Calif. (December 1976).

h. C. A. Brau, to be published.

i. Guessed.

j. D. L. Huestis, private communication (1977).

k. Predissociation rate constant in units of s^{-1}.

l. A. V. Phelps, JILA Data Memo No. 1., Joint Institute for Laboratory Astrophysics, Boulder, Colo. (May 1977).

m. M. A. Biondi and J. N. Bardsley, private communication (1977).

n. C. A. Brau, to be published.

o. D. C. Lorentz, et al. SRI Report No. MP 73-2, Stanford Research Institute, Menlo Park, Calif. (1973).

p. J. Velazco, et al., J. Chem. Phys. 65, 3475 (1976).

q. J. G. Eden and R. W. Waynant, to be published in J. Chem Phys. (1978).

r. J. G. Eden and R. W. Waynant, to be published in Optics Letters 2, (January 1978).

s. The laser cavity solid angle, Ω, was chosen to be $4\pi \times 10^{-6}$ sterradians for the runs discussed here.

$h\nu_f$ represents side fluorescence photons while $h\nu_\ell$ represents intracavity photons traveling nearly parallel to the laser axis.

t. Stimulated emission cross section, σ_{SE} is listed.

u. Cavity lifetime, τ_c, in the constant gain approximation is given $\tau_c^{-1} = -(c/2\ell_c)\,\ell n\,(R_1R_2)$ for a cavity length, ℓ_c, of 100 cm and reflectivity product, R_1R_2, of 50%. Photons transmitted by the output mirror are designated by $h\nu_o$.

v. This rate was varied to fit the experiment, see text.

w. S. C. Lin, unpublished notes (May 1977).

x. R. K. Steunenberg and R. C. Vogel, J. Am. Chem. Soc. 76, 101 (1955).

y. A. Mandl, Phys. Rev. A 3, 251 (1971).

z. W. Wadt, Fifth Conf. on Chemical and Molecular Lasers, St. Louis (April, 1977).

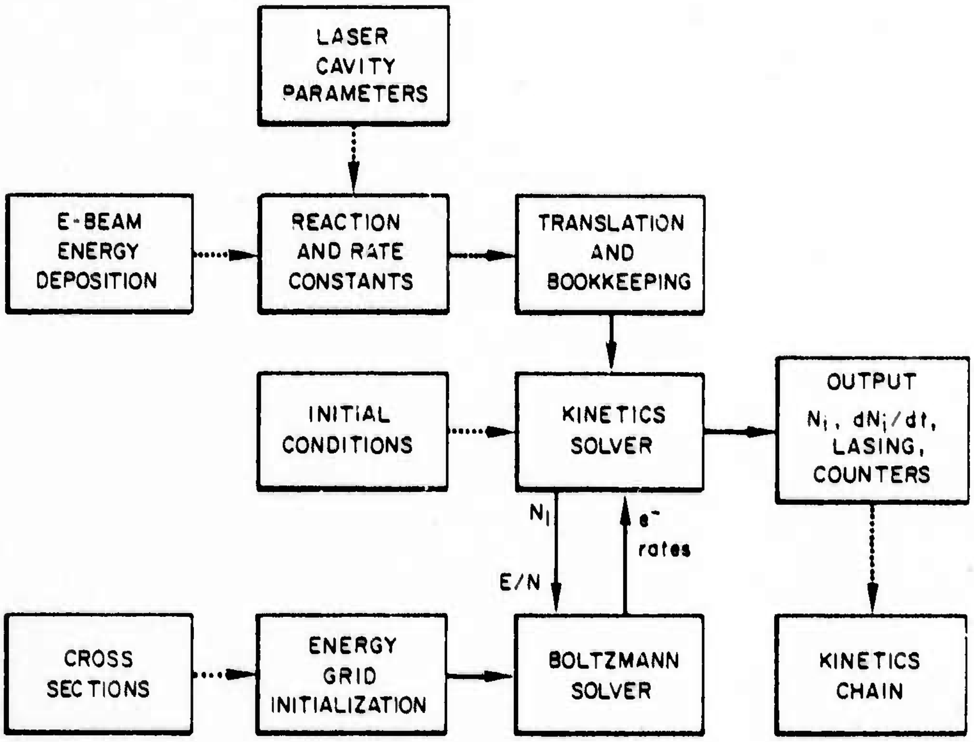

Figure I. Block diagram of present version of the kinetics code for modeling rare gas halide laser systems. Dashed arrows designate information provided by the user while solid arrows designate internal communications from one part of the code to another.

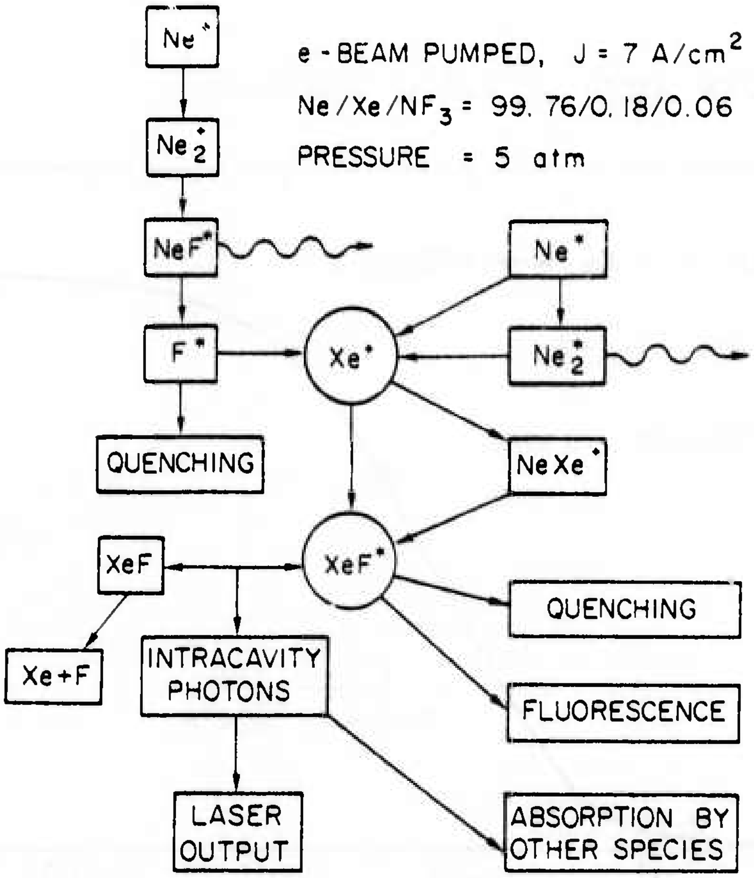

Figure J. Energy flow diagram for an e-beam pumped XeF laser in neon diluent showing the dominant pathways from initial e-beam excitation to laser output. Wavy arrows designate loss channels for excited species through fluorescence radiation.

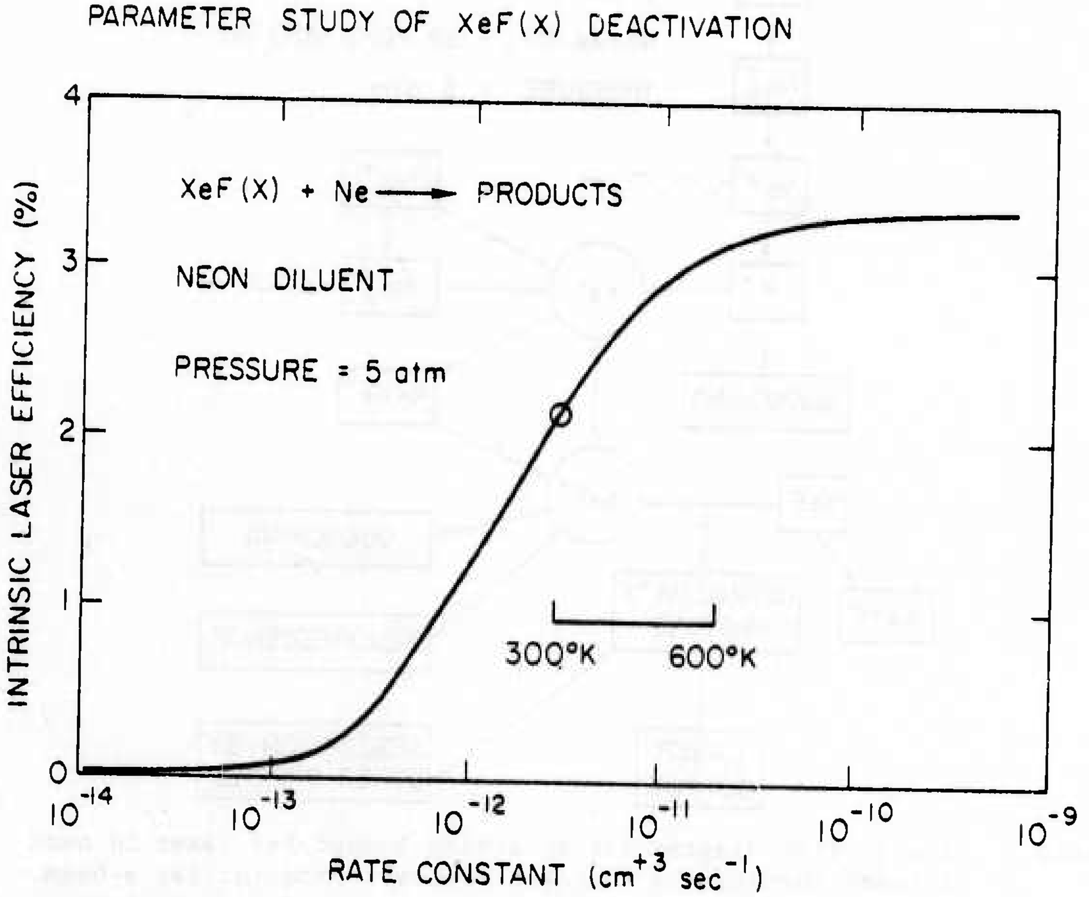

Figure K. Effect of the value assumed for the XeF(X) deactivation rate constant on the predicted intrinsic laser output efficiency. The open circle and the temperature scale are discussed in the text.

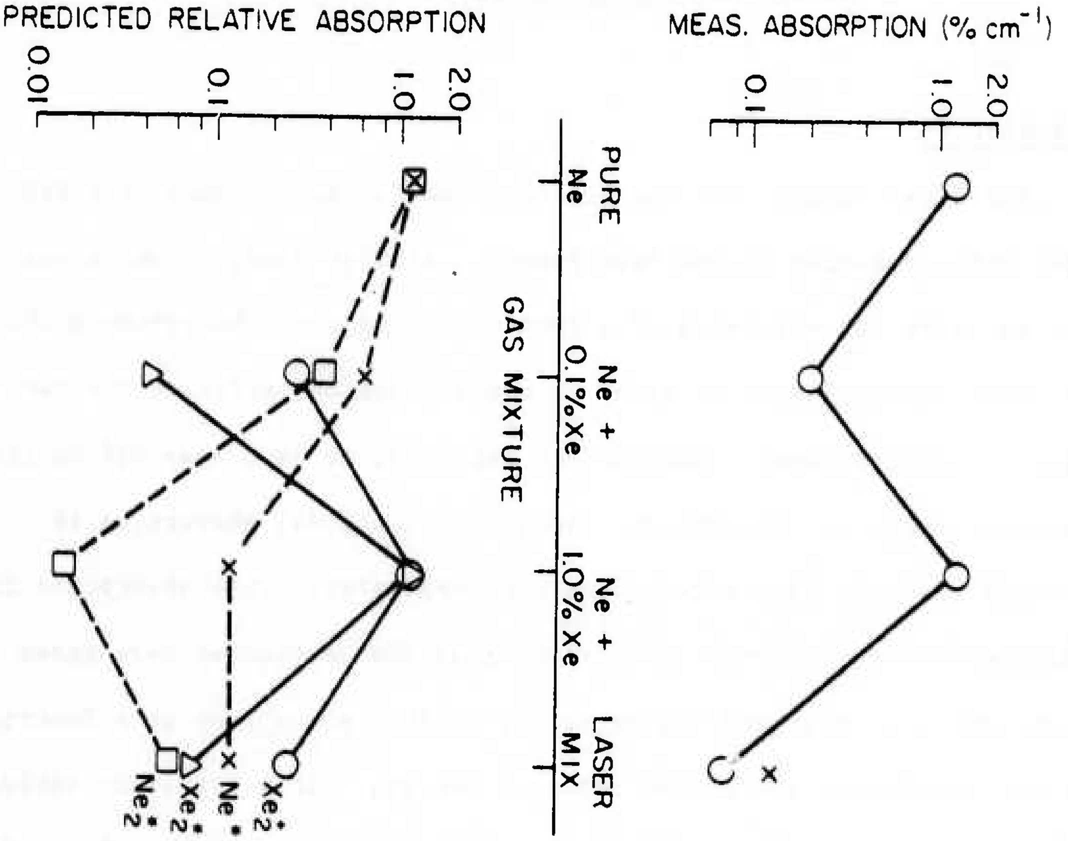

Figure L. Measured transient absorptions of the XeF laser wavelength in four different e-beam pumped gas mixtures compared with computed relative densities of selected transient species for these same mixtures. The laser mix ratio is Ne/Xe/NF_3 = 99.76/0.18/0.06. The total pressure in all cases is 5 atm. Pumping was done by a 300 keV e-beam with 7 A/cm^2 incident to the active laser volume.

LONG PULSE RARE GAS HALIDE LASER
(Experimental)

Introduction

The final results for the electron beam pumped (E-beam only XeF laser were presented in the last report. At that time, it was necessary to infer the existence of a substantial optical absorption within the laser medium itself in order to explain the operation of the XeF laser in argon diluent. During this reporting we have measured on line gain and background absorption. Substantial optical absorption is observed when the rare gases alone are irradiated. This absorption is attributed to the excited state species of the particular rare gases which are irradiated and the magnitude of this absorption is a function of both wavelength and energy input to the gas. This transient optical absorption is reduced when the laser constituents are added. The influence of the diluent gas on the XeF laser is discussed in Section A.

We observe that for the electron beam pumped XeF laser the optical absorption within the laser medium is eliminated when neon is used as the diluent. In addition, with neon, the threshold pumping current which is required to obtain stimulated emission is significantly lower. This results in improved output power and efficiency. These findings indicated that improved operation could be achieved for the electron beam controlled (with sustainer) XeF laser in neon diluent.

Unlike the electron beam pumped laser, an electron beam controlled XeF laser is less constrained by limitations such as foil heating and the basic inefficiencies of electron guns. For these reasons, it may be the system of choice in scaling to higher average powers. The preliminary results for the electron beam controlled XeF laser in neon diluent are contained in Section (B). Since absorption in pure neon is observed to be less than that in pure argon over a large region of the UV spectrum (249 nm to 363 nm) neon was substituted for argon as the diluent in the electron beam pumped KrF laser. The preliminary results for the electron beam pumped KrF laser are discussed in Section (C).

THE INFLUENCE OF DILUENT GAS ON THE XeF LASER

L. F. Champagne and N. W. Harris
Naval Research Laboratory
Washington, D. C. 20375

Substitution of neon for argon as the diluent gas in electron-beam-pumped XeF lasers allows increased optical extraction energies of 2.8 $J\ell^{-1}$ and efficiencies of 1.8%. The improved performance in neon diluent is due to a reduction of the optical absorption in the laser medium which occurs at the laser wavelength. This optical absorption is shown to be present when the rare gases alone are irradiated.

Applied Physics Letters, Vol. 31, No. 8, 15 October 1977

In a recent paper[1] we reported the long-pulse operation of an electron-beam-pumped XeF laser in argon diluent. Analysis of the laser performance indicated that the output power was limited by transient absorption processes which occur at the laser wavelength during the excitation pulse. This transient absorption, in rare-gas halide lasers, which occurs in both e-beam-controlled discharges, has been observed elsewhere at several selected wavelengths from 249 to 450 nm.[2-7]

In this paper, we report detailed measurements of the extent of these absorption processes and of the XeF laser gain and performance in both argon and neon diluents with e-beam pumping. Experimental results indicate that transient absorption is due to processes which occur in the pure rare gases and that the effect of these processes can be reduced or eliminated in the presence of the laser constituents. In argon, the laser gain is offset by absorption losses which are more severe at higher input energies. However, in neon diluent, the absorption losses are lower and are observed to be independent of input energy. The replacement of the argon diluent by neon increases the electrical efficiency (energy extracted/energy deposited) of the XeF laser at the maximum output power from 0.5 to 1.8% and the volumetric output from 0.8 to 2.8 J/ℓ.

The experimental apparatus, which was described previously,[1,6] is a 1-m laser chamber equipped with 2.2-cm-diam Brewster-angle windows. Electron-beam pulses of 1 μsec width and variable intensity up to 8 A/cm^2 were delivered to the gas. A pulsed ion laser similar to that described by Simmons and Witte[8] was used to probe the discharge. An argon ion line at 364 nm and a neon ion line at 338 nm[9] were used to measure the loss on either side of line center. A prism was placed at the output of the probe laser to select the required probe wavelength. On-line gain and loss is measured using a discharge-pumped XeF laser[10] as well as an argon ion line at 351.1 nm. The gain measured by the XeF laser is 30% greater than that measured by the argon ion laser. This higher value for the gain is thought to be more representative of the gain on line center for the e-beam-pumped XeF laser and is reported below.

The probe pulse is monitored by SF photodiodes before and after the laser chamber. A long optical path length between the chamber and the output diode is used to reduce the fluorescence signal to less than 10% of the laser signal.

Figure 1 is a plot of gain and absorption for the XeF laser as a function of energy deposited in the gas by the electron beam as calculated by the method used in Ref. 11. Absorption is measured in both the pure rare gas and the optimum laser mixture. For the argon diluent gas at maximum output power, the optimum operating pressure is 2.5 atm and the optimum concentration is $Ar:Xe:NF_3::99.5:0.36:0.12$. Since the stopping power of neon is about one-half that of argon, the measurements in neon were performed at 5 atm, in order to keep the energy deposited in the gas by the electron beam equal for the two diluents.

There is no significant difference in the measured gain at the laser wavelength for the two diluents. Also, comparable absorption losses are measured at the laser wavelength when either pure argon or neon is irradiated. This absorption is observed to increase with energy input to the gas and is always greater than the absorption in the laser gas mixture. Absorption levels measured on either side of line center were the same within experimental error for both the argon and neon laser mixtures. With the addition of the laser gas constituents, the loss is reduced but while it is essentially eliminated in the neon diluent there is still a significant loss in the argon diluent. These data indicate the existence of collisional processes which either remove an absorbing species or prevent its formation.

Figure 2 plots the optical absorption in both argon and neon as a function of xenon concentration. All measurements are taken at the laser wavelength. With small additions of xenon to argon and neon a reduction in the optical absorption is observed which is significantly larger in the neon case. In argon the decrease in absorption is attributed to charge transfer to xenon which reduced the formation of the absorbing species (presumed to be Ar_2^+).[6] In neon, Penning ionization reactions are introduced and appear to provide an additional channel by which a precursor to or actual absorbing species is removed. The possible reactions are

$$Ne^*(Ne^*_2) + Xe \rightarrow Ne(Ne_2) + Xe^* + e. \qquad (1)$$

For both argon and neon, as the concentration of xenon increases the optical absorption increases, indicating that a new absorbing species involving xenon is being introduced. As the concentration is increased the reaction

$$Xe^* + Xe + M \rightarrow Xe_2^+ + M \qquad (2)$$

leads to the formation of Xe_2^+ whose cross section for absorption at the laser wavelength is known to be very large.[12] This strong correlation between xenon concentration and Xe_2^* absorption sets an upper limit to the amount of xenon which can be used in the XeF laser.

Figure 3 shows the variation in output power as a function of mirror coupling for both argon and neon diluent. Other conditions are as for Fig. 1 with the energy input kept constant at 158 J/ℓ. With the gain and loss data described above, the saturation intensity was calculated using the method of Ref. 1. This gives a saturation intensity of 9.32 MW/cm^2 for argon diluent and 0.37 MW/cm^2 for neon diluent. These values agree within the experimental uncertainties, thus providing additional indication that the difference in laser performance between the diluents can be attributed to changes in the loss processes rather than to the gain processes.

The most striking difference between the two diluents is seen in Fig. 4 where efficiency is shown as a function of pressure. The efficiency attained with neon rises with pressure up to the limit of the apparatus (5 atm), whereas the efficiency using argon falls. For the argon diluent the output mirror coupling was optimized at each pressure to take account of the change in absorption with pressure. The absorption in neon is small and constant and hence the optimum coupling did not change with pressure. When neon is used as the diluent, the gas composition is not kept constant but is optimized at each operating pressure. It was found that the maximum output power was obtained with constant number densities of 6 x 10^{16}/cm^3 for NF_3 and 1.8 x 10^{17}/cm^3 for Xe. The output power was much more sensitive to the number density of NF_3 and Xe for the neon diluent than for the argon diluent. The maximum output energy from this laser using argon diluent was 0.31 J at a pressure of 2.5 atm which corresponds to an efficiency of 0.5%. Using neon diluent the maximum energy measured was 1.08 J with an efficiency of 1.8% at a pressure of 5 atm. The active volume is 0.38.1.

We have demonstrated much improved efficiency (1.8%) and optical energy extraction (2.8 $J\ell^{-1}$) by substituting neon for argon as the diluent in the XeF laser. The improvement is shown to be due to a reduction in the optical absorption in the medium. The magnitude of this optical absorption is dependent on which rare gases are used and on their relative concentrations. Work presently in progress includes identifying the details of the loss mechanism and investigating the effect of diluent gas on an electron-beam-controlled discharge XeF laser.

The authors are grateful for the many helpful discussions with N. Djeu, T. Finn, and L. Palumbo, and for the technical assistance rendered by D. M. Shores and R. DeLoatch.

References

1. L. F. Champagne, J. G. Eden, N. W. Harris, N. Djeu, and S. K. Searles, Appl. Phys. Lett. 30, 160 (1977).
2. R. O. Hunter, C. Houton, and J. Oldnettel, Third Summer Colloquium on Electronic Transition Lasers, Snowmass, Colo. 1976 (unpublished).
3. E. Zamir, D. L. Heustis, D. C. Lorents, and H. H. Nakano, Ref. 2.
4. H. T. Powell and J. R. Murray, Lawrence Livermore Laboratories Laser Program Annual Report --1974, 1975 (unpublished).
5. J. A. Mangano and J. H. Jacob (private communication).
6. R. O. Hunter (private communication).
7. L. F. Champagne, J. G. Eden, N. W. Harris, and S. K. Searles, Ref. 2.
8. W. W. Simmons and R. S. Witte, IEEE J. Quantum Electron. QE-6, 648 (1970).

9. W. B. Bridges and A. N. Chester, Appl. Opt. 4, 573 (1965).

10. R. Burnham and N. Djeu, Appl. Phys. Lett. 29, 707 (1976).

11. S. K. Searles and G. A. Hart, Appl. Phys. Lett. 28, 384 (1976).

12. W. Wadt (private communication).

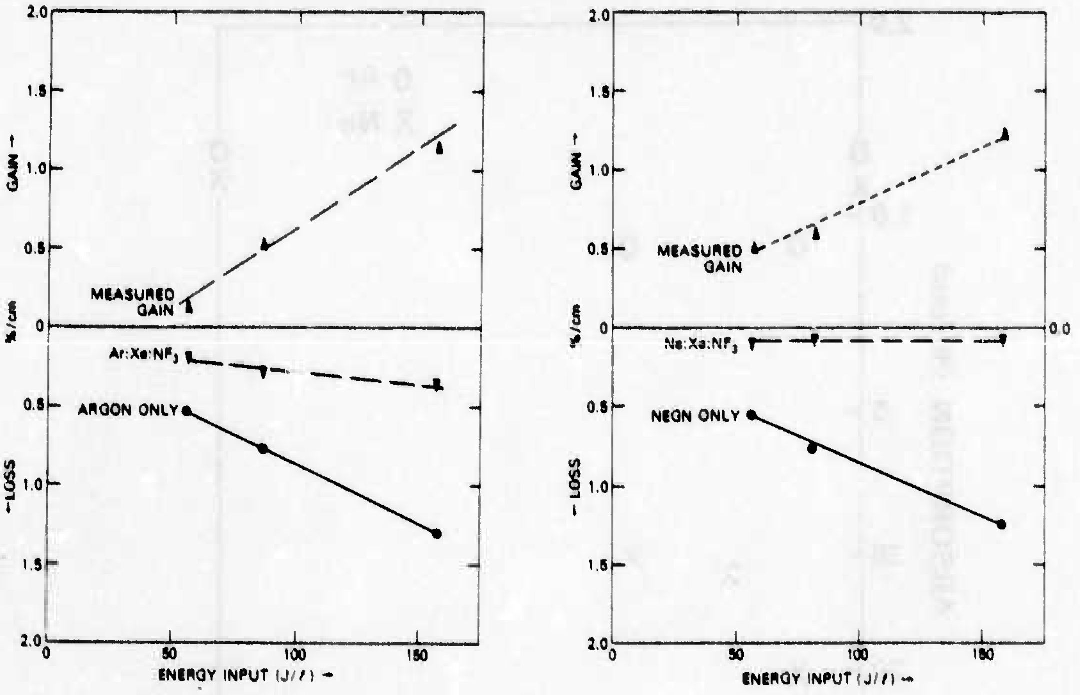

Fig. 1. Measured gain at 351.1 nm and loss at 338 and 364 nm in XeF laser mixtures as a function of deposited energy for argon diluent and neon diluent.

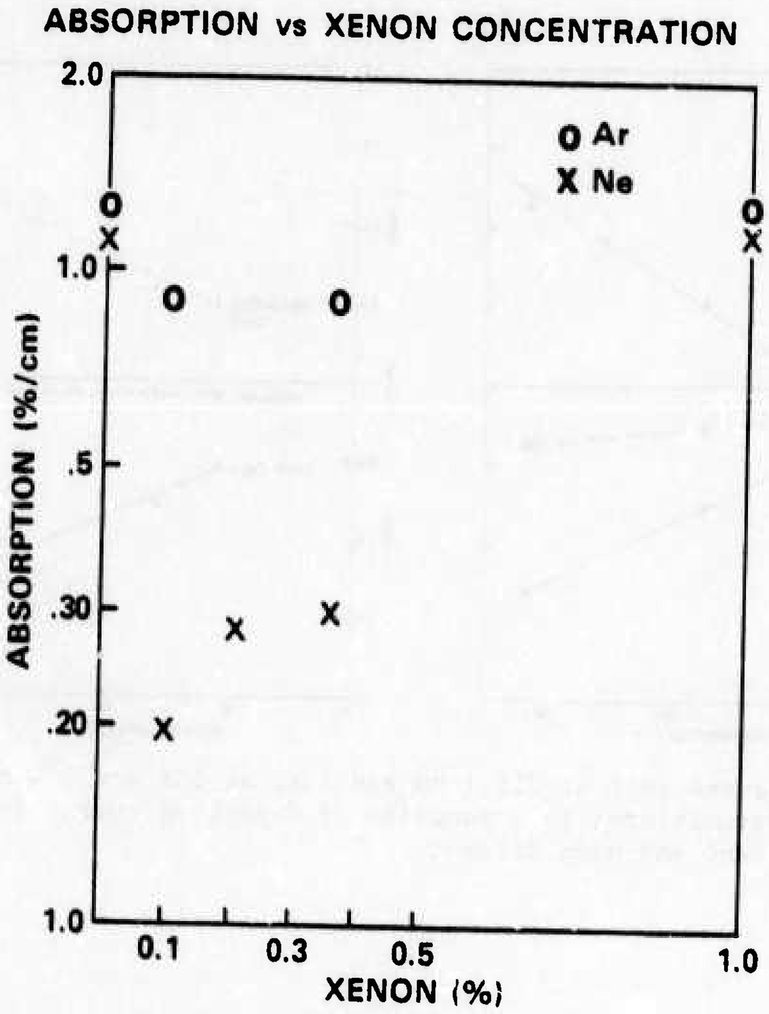

Fig. 2. Measured absorption at 351.1 nm in both argon and neon as a function of xenon concentration.

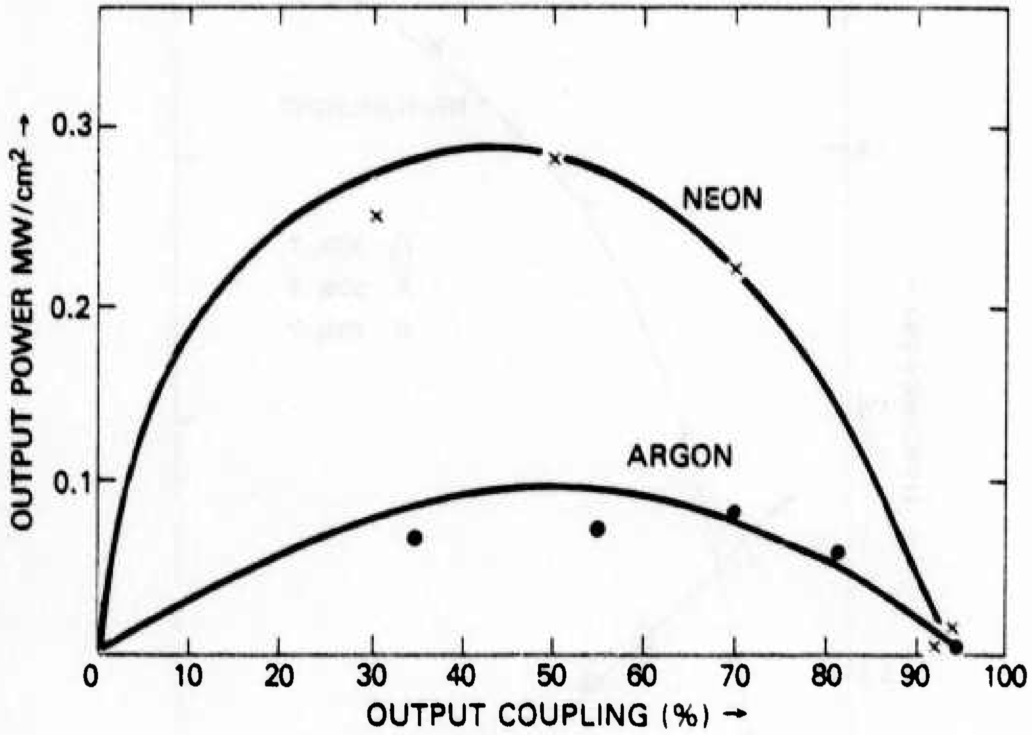

Fig. 3. XeF laser output power as a function of output coupling for neon and argon diluents.

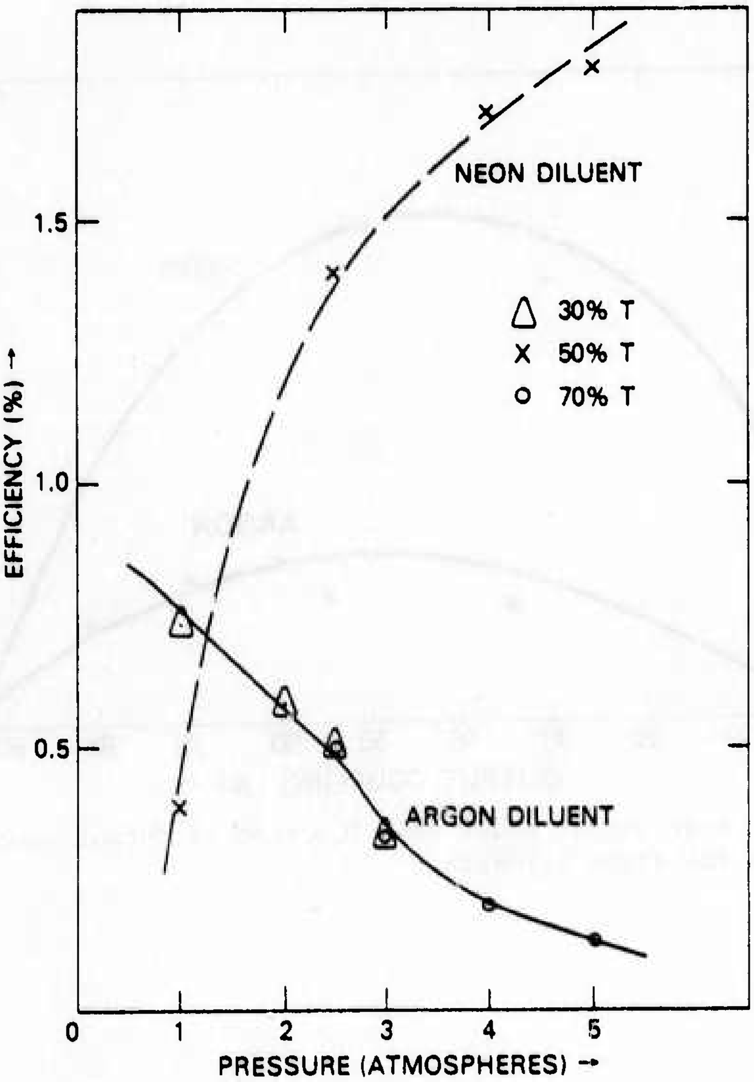

Fig. 4. Efficiency of XeF laser as a function of total pressure for neon and argon diluents.

ELECTRON BEAM CONTROLLED, NEON STABLILIZED XeF LASER

L. F. Champagne
Naval Research Laboratory
Washington, D. C. 20375

To be published in Proceedings of the Colloquium on High Power Lasers and Applications, "Laser 77" Congress, Munich, Germany, 20-22 June 1977.

High power and efficiency has been demonstrated for the long pulse electron beam pumped rare gas halide lasers [1-5]. However, in order to scale these laser systems limitations such as foil heating and inefficiencies of electron guns must be overcome. The electron beam controlled XeF laser is less constrained by these limitations and for this reason may be the system of choice in going to high average powers. In this paper we will discuss the operation of the electron beam controlled XeF laser and compare its performance with that of the electron beam pumped laser.

Much of what has been learned about the electron beam pumped XeF laser applies to the electron beam controlled system. The threshold pumping currents required for stimulated emission are significantly lower when neon is used as the diluent in place of argon. This substitution of neon for argon also improves the operation of the laser by reducing the optical absorption in the laser medium. In addition, the electron beam controlled discharge exhibits improved discharge stability when neon is used as the diluent due to its lower ionization efficiency. In an applied electric field energies 4 times that deposited by the e-beam alone increase laser output by a factor of 3.5. However, to date the efficiency for the e-beam controlled system is slightly lower than for the directly pumped e-beam system.

The experimental apparatus, which has been described in more detail previously [1], consists of a 1 meter laser chamber with a 2.2 cm optical aperture. A pulsed rare gas ion laser similar to that described by Simmons and Witte [6] probes the discharge. An argon ion line at 364 nm and a neon ion line at 338 nm are used to measure absorption on either side of line center. On line gain and loss is measured with a discharge pumped XeF laser [7]. The probe pulse is monitored with S-5 photodiodes placed before and after the laser chamber.

Figure 1 is a plot of gain and absorption for the XeF laser as a function of energy deposited into the gas by the electron beam. The energy deposited into the gas is calculated by the method used in Ref. [1]. Absorption is measured in both the pure rare gas and the optimum laser mixture. For the argon diluent laser mixture at maximum output power, the optimum operating pressure is 2.5 atmospheres and the optimum concentration is $Ar:Xe:NF_3$::99.5:0.12. Since the stopping power of neon is about one-half that of argon, all measurements in neon were performed at 5 atmospheres, in order to keep the energy deposited into the gas by the electron beam equal for the two diluents. The neon diluent composition at 5 atmospheres is $Ne:Xe:NF_3$::99.76:0.18:0.06.

There is no significant difference in the measured gain at the laser wavelength for the two diluents. Also, comparable absorption losses are measured at the wavelength when either pure argon or neon is irradiated and this absorption is observed to increase with energy input to the gas. Absorption levels measured on either side of line center are the same within experimental error for both argon and xenon laser mixtures. The major differences are that the absorption is less in the laser gas mixture than in the pure rare gases and that the absorption in neon diluent is significantly less than in argon diluent. These data indicate that a species formed from the rare gas only causes the absorption and that collisional processes between the rare gas and the laser constituents either remove an absorbing species or prevent its formation.

Figure 2 plots the optical absorption in both argon and neon as a function of xenon concentration. Absorption levels are measured at the laser wavelength. With small additions of xenon to argon and neon a reduction in the optical absorption is observed which is significantly larger in the neon case. In argon the decrease in absorption is attributed to charge transfer which reduces the formation of the absorbing species (presumed to be Ar_2^+) [8]. In neon, Penning ionization provides an additional channel by which a precursor to or an actual absorbing species is removed. The possible reactions are

$$Ne^* \, (Ne_2^*) + Xe \rightarrow Ne \, (Ne_2) + Xe^+ + e. \qquad (1)$$

For both argon and neon as the concentration of xenon increases the optical absorption increases indicating that a new absorbing species involving xenon is being introduced. As the concentration is increased the reaction

$$Xe^+ + Xe + M \rightarrow Xe_2^+ + M, \qquad (2)$$

leads to the formation of Xe_2^+ whose cross section for absorption at the laser wavelength is known to be very large [9]. This strong correlation between xenon concentration and Xe_2^+ absorption sets an upper limit to the amount of xenon which can be used in the XeF laser.

Figure 3 is a plot of output power and efficiency as a function of applied electric field for the electron beam controlled laser. The operating pressure is 3 atmospheres and data is plotted for one microsecond optical pulses. In this experiment, the Ne/Xe ratio is kept constant and the amount of NF_3 is varied.

As the concentration of NF_3 is increased, the maximum value of the applied electric field for which a one microsecond optical pulse can be maintained also increases. However, the output power and laser enhancement decreases. At higher applied electric fields, the sustained discharge cannot be maintained for one microsecond. In the presence of an electric field the energy extracted is 1.8 $J\text{-}l^{-1}$ which is 3.5 times as much energy as that for e-beam pumping alone. In order to obtain this laser enhancement the energy input to the gas was increased by a factor of five which results in a reduced overall efficiency of the laser system. Most efficient operation and best energy extraction for the e-beam controlled laser occurs for that concentration which yields the best energy extraction and efficiency for pure e-beam pumping. At 3 atmospheres twice as much energy can be obtained from the controlled system as from the electron beam pumped laser under optimum conditions.

Table 1 lists the operating characteristics of the electron beam controlled XeF laser when operating at 3 atmospheres. Of note here is that most of the energy is delivered by the sustainer.

Higher average powers can be obtained at slightly less efficiency under electron beam controlled operation. Significant laser enhancements can be achieved from the neon diluent electron beam controlled XeF laser. When neon is used as the diluent in place of argon threshold pumping currents are lower and optical absorption at the laser wavelength is significantly reduced.

Table 1 Electron beam controlled XeF laser

Operating Pressure	3.0 ATM
Composition	NF_3:Xe:Ne 0.06:0.18:99.76
Optimum Transmission	50%
Output Energy	1.8 $J\text{-}\ell^{-1}$
Efficiency	0.8%
Measured Gain	1.85%-cm^{-1} [4 ATM]
Laser Enhancement	3.5:1
Energy Deposited by the Fun [E_g]	46 $J\text{-}\ell^{-1}$
Energy Deposited by the Sustainer [E_s]	184 $J\text{-}\ell^{-1}$
$\frac{E_g + E_s}{E_g}$	5
Current Density Due to the Electron Beam [Jb]	6 AMPS-cm^{-2}
Current Density Due to the Sustainer [Js]	120 AMPS-cm^{-2}
Js:Jb	20:1

References

1. L. F. Champagne, J. G. Eden, N. W. Harris, N.Djeu and S. K. Searles, Appl. Phys. Lett. 30, 160 (1977).
2. R. O. Hunter, C. Houton, J. Oldnettel, postdeadline paper, Third Summer Colloquium on Electronic Transition Lasers, Snowmass, CO, September 1976.
3. L. F. Champagne and N. W. Harris, Appl. Phys. Lett. (to be published).
4. L. F. Champagne and N. W. Harris, 1977 IEEE/OSA Conference on Laser Engineering and Applications, Washington, D. C., June 1977.
5. J. H. Jacob, J. A. Mangano, and M. Rokni, 1977 IEEE/OSA Conference on Laser Engineering and Applications, Washington, D. C., June 1977.
6. W. W. Simmons and R. S. Witte, IEEE J. Quantum Electronics, QE-6, 648, (October 1970).
7. R. Burnham and N. Djeu, Appl. Phys. Lett. 29, 707 (1976).
8. R. O. Hunter, private communication.
9. W. Wadt, private communication.

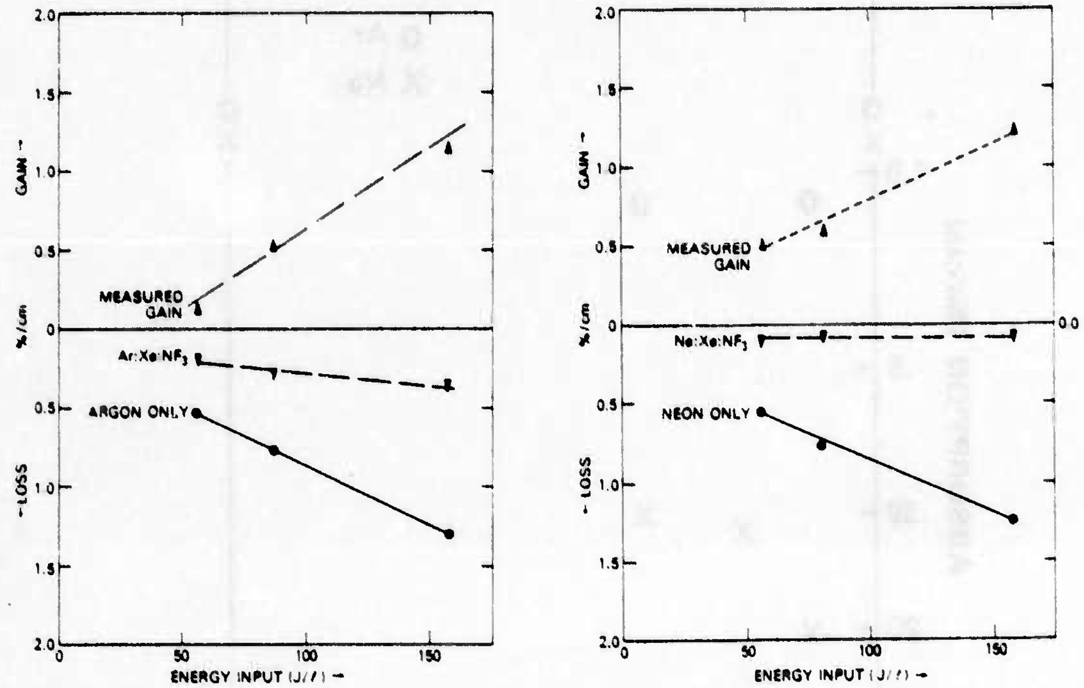

Fig. 1. Measured gain at 351.1 nm and loss at 338 nm and 364 nm in XeF laser mixtures as a function of deposited energy for argon diluent and neon diluent.

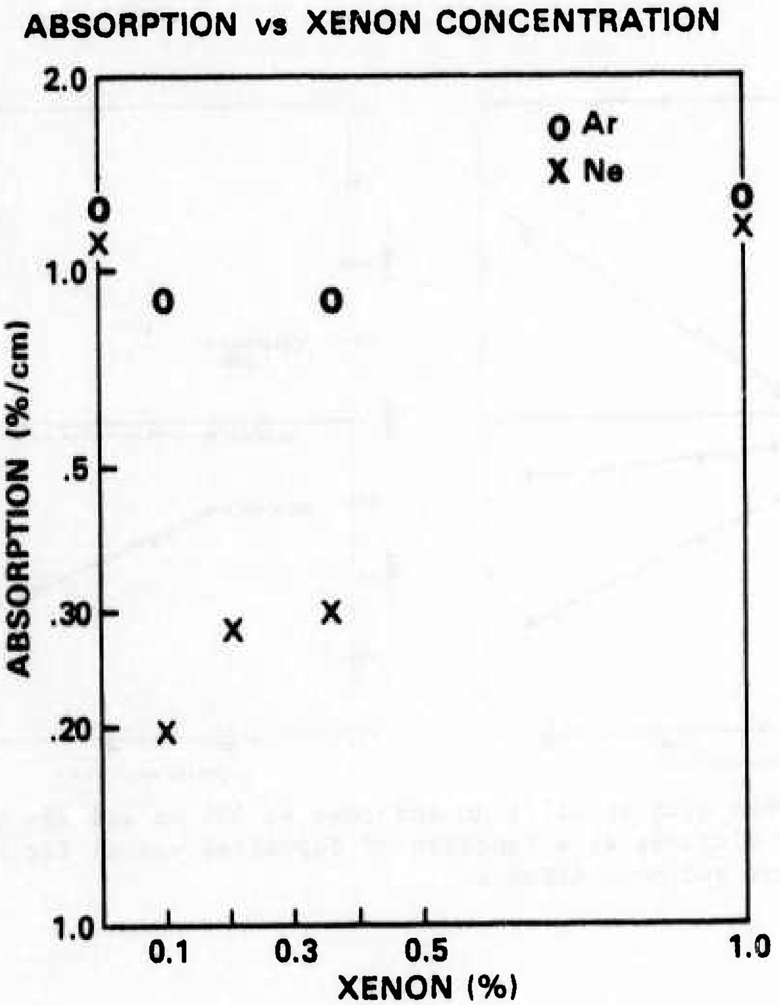

Fig. 2. Measured absorption at 351.1 nm in both argon and neon as a function of xenon concentration.

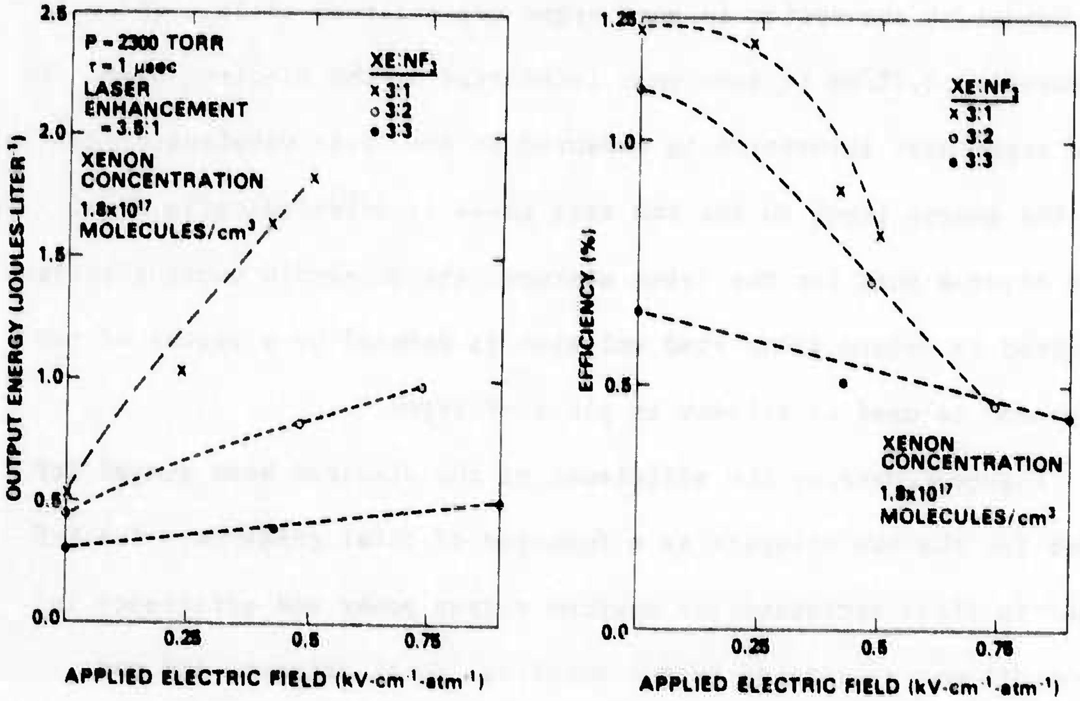

Fig. 3. XeF laser output energy and efficiency as a function of applied electric field.

C. Electron Beam Pumped KrF Laser in Neon Diluent

When neon is used in place of argon as the diluent for the electron beam pumped KrF laser we observe increased extraction efficiency and comparable output energy for optical pulse lengths in the range from 0.5 to 15 μsec. In preliminary experiments with the pure rare gases the transient absorption in pure argon was observed to be 1.2%/cm as compared to 0.7%/cm in neon when irradiated by the electron beam. In this experiment absorption is measured at the laser wavelength (249 nm) and the energy input to the two rare gases is experimentally equal. We also observe that for the laser mixture, the threshold pumping current required to obtain stimulated emission is reduced by a factor of two when neon is used as diluent in place of argon.

Figure M compares the efficiency of the electron beam pumped KrF laser for the two diluents as a function of total pressure. The KrF laser is first optimized for maximum output power and efficiency in argon diluent by varying output coupling, total pressure and gas composition. Then the laser is operated with neon as the diluent. Under these conditions when the total pressure is increased from two to three atmospheres in neon while keeping the concentration of krypton and fluorine constant, comparable energy can be extracted from the laser but less energy is being absorbed by the gas. The optimum output coupling is the same for both diluents (T = .31). A difference between the argon and neon is that the neon metastable atom @ 16.6 ev is sufficiently energetic to ionize krypton (14.1 ev). At 11.6 ev the argon metastable is not sufficiently energetic to ionize krypton. The possible reactions are:

$Ne^{*}(Ne_2^{*}) + Kr \rightarrow Kr^{+} + Ne(Ne_2) + e^{-}$.

This is a new channel for forming a precursor to the excited state species together with a reduction in optical absorption could account for the improved efficiency (~ 25%) of the KrF laser.

Table 1 compares the operation of the electron beam pumped KrF laser for the two diluents.

Table 1

Pressure	2 atm	3 atm
Composition	$Ar:Kr:F_2$ 95.85:4.0:0.15	$Ne:Kr:F_2$ 97.2:2.7:0.1
Optical Pulselength	0.5 μsec	0.5
Optimum Transmission	T = .31	T = .31
Extracted Energy	$4.2\ J\text{-}\ell^{-1}$	$4.2\ J\text{-}\ell^{-1}$
Efficiency	6.0%	$56\ J\text{-}\ell^{-1}$
Input Energy	$70\ J\text{-}\ell^{-1}$	7.5%
Small Signal Gain		$1.1\%\ \text{-}\ cm^{-1}$
Saturation Intensity		$\sim 2.7\ MW\ \text{-}\ cm^{-2}$
Transient Absorption		$\sim 0.05\%\ \text{-}\ cm^{-1}$

Small signal gain is measured using a discharge pumped KrF laser to probe the electron beam controlled discharge. By using the observed small signal gain and output power from the laser for various output coupling it is possible to estimate the saturation intensity and transient absorption to first order by making a two parameter fit to the modified Rigrod equation for high gain lasers with transient absorption.

$$\frac{I}{I_{sat}} = (1-A)\,\frac{1-\sqrt{r}}{1-(1-A)^2\sqrt{r}}\left[g_{oL} + \ln\left((1-A)^2\sqrt{r}\right)\right].$$

where g_{oL} = one pass gain

$1-(1-A)^2$ = one pass loss

I_{sat} = saturation intensity

r = mirror reflectivity

The improved efficiency for the KrF laser in neon diluent (~ 25%) is observed for optical pulse lengths ranging from 0.5 to 1.5 microseconds (Figure N) but occurs only over a narrow pressure range.

Since we have reduced the amount of energy input to the gas by the electron beam which is required to obtain maximum output power we expect that with the addition of a controlled discharge, laser enhancement (L.E.) for the electron beam controlled KrF laser should also be improved.

Laser enhancement is related to the discharge enhancement by

$$\text{L.E.} \propto \frac{E_s + E_g}{E_g},$$

where E_s is the energy input to the gas by the sustainer and E_g is the energy input to the gas by the gun.

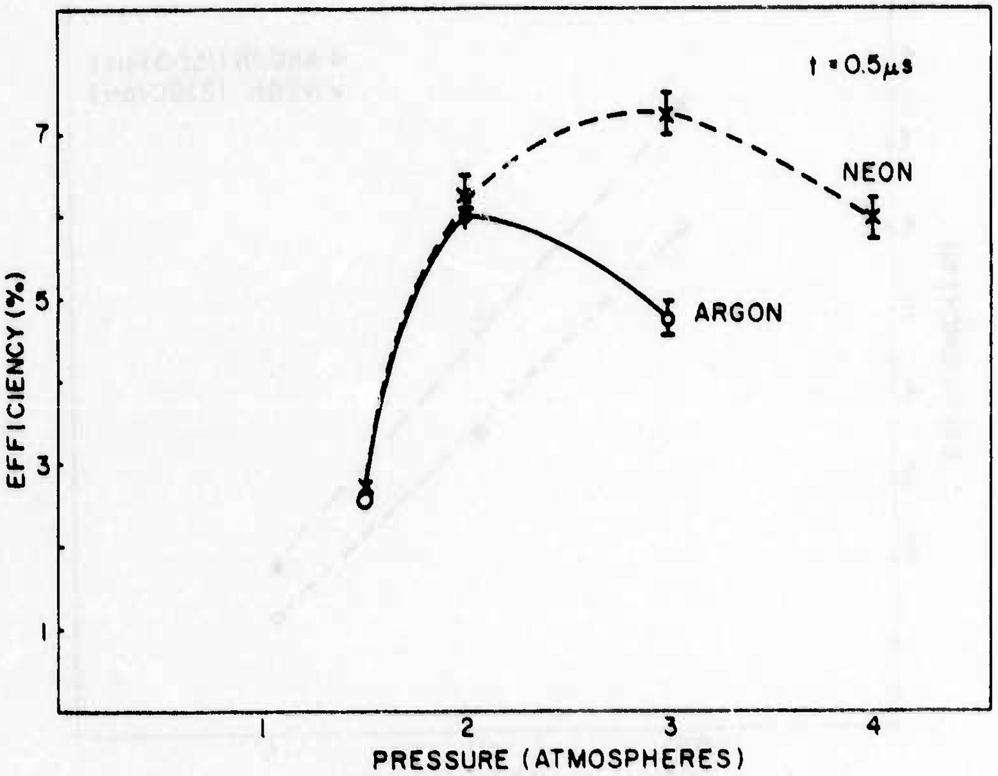

Figure M. Efficiency of the KrF laser as a function of pressure for neon and argon diluents.

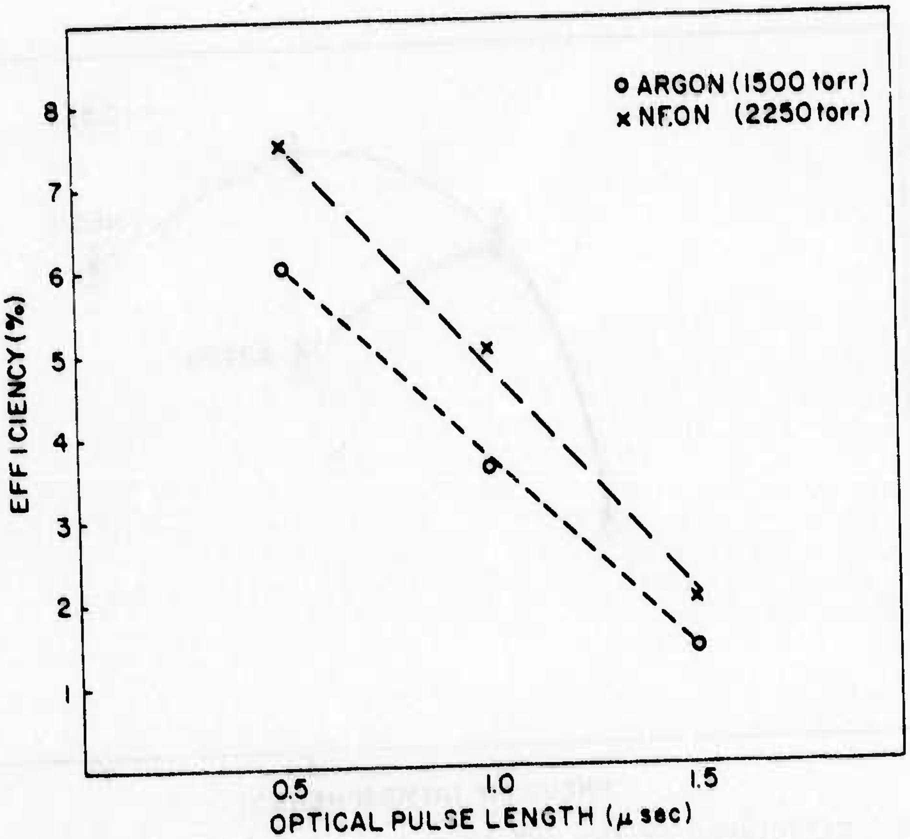

Figure N. Efficiency of the KrF laser as a function of optical pulse length for neon and argon diluents.

ELECTRON ENERGY DEPOSITION IN THE RARE GASES

Summary:

A one dimensional code which includes scattering was used to calculate energy deposition in He, Ne, Ar, Kr, and Xe for incident electron energies of 150 - 400 keV.

Background:

Electron beam devices are used to excite laser gases. Energy deposition calculations can be utilized to determine laser efficiency and to determine the mechanism for laser emission. Energy deposition calculations are also an essential consideration in the design of large scale lasers with a high overall efficiency. In a large scale laser it is desirable to absorb a major fraction of the beam energy without a significant gradient in the deposition uniformity. The growing interest in electron beam pumped lasers and electron beam-sustainer pumped lasers motivated the writing of this section as a follow-on to Reference (1). Reference one described the features of Transport Electron Program (TEP) developed by D. B. Brown, in detail. A limited set of deposition data was also given.

Objective:

The purpose of this section is to provide a more complete set of easy-to-use deposition tables for pure rare gases. A sample calculation for a typical laser case is presented.

Calculations:

TEP treats the movement of a high energy electron from a vacuum into a target with a finite thickness and with infinite dimensions in the directions perpendicular to incident electron direction. The target thickness is divided into 41 slabs. In the work reported here the slab thickness was chosen to be a convenient pressure-distance product. Table 1 shows the slab thickness as well as the other input data required to execute TEP. In Table 1, Z is the atomic number, A is the atomic mass, and V_k and V_L are the energies (in keV) of the k and L X-ray absorption edges respectively. The TEP output is displayed in Table 2 as a function of rare gas and incident electron energy. The data is presented as the number of Siloelectron watts of energy deposited in each of the 41 slabs.

Figures O-Q show plots of the computed output data. The energy sum over all 41 slabs is less than the incident electron energy because there is a finite probability that an electron will be backscattered out of the target. In He the backscattering is small while in Xe it is a significant fraction of the incident electron energy. The heading, "electron remaining," indicates the fraction of the incident electrons which remain in the target. At an incident electron energy of 200 keV in He, 1.3% of the electrons are backscattered and carry 4.0 keV out of the target. In Xe 41.8% of the electrons are backscattered and carry 61.5 keV out of the target.

Use of the data in Table 2:

In an electron beam device, a thin foil entrance window is used to separate the high pressure rare gas from the vacuum region. The energy absorption by the foil can be and should be taken into consideration. A specific example will now be cited to demonstrate the use of the TEP calculations. The example problem is to determine the energy deposited in 2000 torr Argon by a 1 kJ, 300 keV e-beam with a 10 x 100 cm cross section. The entrance window is 0.00254 cm titanium. The pulse duration is one μsec. First, the titanium foil has a mass thickness of 0.01143 g/cm^2 from its density of 4.5 g/cm.^{3} From Table 1 the mass thickness of 1,000 torr-cm of Argon is 0.176/41 divided by 2 or .00215 g/cm^2. Thus 0.00254 cm Ti is approximately equivalent to (0.01143/.00215) x 1000 or 5320 torr - cm of Ar because of their closeness in atomic number. For Ar, Fig. P reveals that the deposition rate has risen to 9.4 eV/torr - cm at 5320 torr equivalent Ar. The deposition into the first centimeter of the Ar gas at the given pressure of 2000 torr is 2000 x 9.4 = 18.8 keV or 6.3% of the total beam energy per unit area which is 1 J/cm^2 assuming a parallel beam. Therefore 63 mJ are dropped into first one cm^3 next to the foil. In the second cm^3 the energy has peaked at 68 mJ and in the tenth the energy has dropped to 37 mJ. Similarly 5.47 of the beam energy or 54 mJ is loaded into the foil. A repeat of these calculations at 200 and 400 keV would show a trade-off between the desired deposition uniformity and the unwarranted deposition in the foil.

The TEP code can be used to select an e-beam device for an experiment or to compare laser efficiency values from one device to another by normalizing laser pulse energy to deposited energy rather than to stored energy in the capacitor bank. The TEP code can be used to calculate the production of excited states. Division of the energy by the W value which the energy required to form one ion pair by a high energy electron yields the ion production rate. For the example of 2000 torr

Ar, $W_{Ar} = 26$ eV and 1.51×10^{16} ions and electrons are made in the 1 μsec long pulse in the first cm^3 behind the foil. The ion production rate is needed to model an e-beam excited laser.

Some words of caution are required about the interpretation of the TEP output. The TEP output is one dimensional. In the example it was assumed that scattering did not increase the beam cross sectional area. In fact scattering will increase the beam area depending on the target Z and the beam shape. For example a thin beam in Ar will have about a 90° field angle divergence. The energy deposited near the foil will be close to the calculated value but 10 cm away the calculated value will be too high.

It is hoped that this discussion will be helpful to laser researchers interested in improving their understanding of e-beam deposition without having to run their own complex and time-consuming codes.

References

1. DARPA-NRL Laser Program, NRL Memorandum Report 3084, July 1975.

Table 1

Transport Electron Program Input Data

Z	A	V_k(keV)	V_L(keV)	Mass thickness per 41 slabs (g/cm^2) @ 25^{o}C	Slab thickness (torr-cm at 25^{o}C)
He 2	4.0026	0.024587	0.001*	0.282	32,000
Ne 10	20.179	0.8669	0.045	0.178	4,000
Ar 18	39.948	3.20290	0.32	0.176	2,000
Kr 36	83.80	14.3256	1.921	0.184	1,000
Xe 54	131.30	34.561	5.452	0.289	1,000

*Artifical value for the computer.

Table 2

Energy Deposition as a Function of Rare Gas and Incident Electron Energy

```
Helium

   200 keV  electron energy
   32,000   torr-cm slab thickness
   0.987    electron remaining

 Slab                keV

 (1) .2193E+02 (2) .2770E+02 (3) .3124E+02 (4) .3115E+02 (5) .2745E+02
 (6) .2151E+02 (7) .1506E+02 (8) .9491E+01 (9) .5412E+01 (10).2807E+01
 (11).1332E+01 (12).5806E+00 (13).2335E+00 (14).8697E-01 (15).3010E-01
 (16).9710E-02 (17).2927E-02 (18).8268E-03 (19).2192E-03 (20).5469E-04
 (21).1286E-04 (22).2852E-05 (23).5983E-06 (24).1188E-06 (25).2235E-07
 (26).3989E-08 (27).6762E-09 (28).1090E-09 (29).1670E-10 (30).2438E-11
 (31).3390E-12 (32).4493E-13 (33).5681E-14 (34).6854E-15 (35).7894E-16
 (36).8684E-17 (37).9127E-18 (38).9168E-19 (39).8802E-20 (40).8080E-21
 (41).7090E-22
```

```
Helium

   250 keV electron energy
   32,000  torr-cm slab thickness
   0.989   electron remaining

 Slab                keV

 (1) .1818E+02 (2) .2218E+02 (3) .2602E+02 (4) .2887E+02 (5) .2996E+02
 (6) .2888E+02 (7) .2578E+02 (8) .2127E+02 (9) .1623E+02 (10).1145E+02
 (11).7480E+01 (12).4538E+01 (13).2561E+01 (14).1347E+01 (15).6621E+00
 (16).3046E+00 (17).1315E+00 (18).5331E-01 (19).2035E-01 (20).7324E-02
 (21).2489E-02 (22).7994E-03 (23).2431E-03 (24).7007E-04 (25).1916E-04
 (26).4975E-05 (27).1228E-05 (28).2884E-06 (29).6446E-07 (30).1373E-07
 (31).2787E-08 (32).5396E-09 (33).9971E-10 (34).1759E-10 (35).2964E-11
 (36).4771E-12 (37).7340E-13 (38).1080E-13 (39).1518E-14 (40).2042E-15
 (41).2624E-16
```

Helium

```
  300 keV   electron energy
  32,000 torr-cm slab thickness
  0.990  electron remaining

Slab                 keV

(1) .1604E+02 (2) .1872E+02 (3) .2157E+02 (4) .2437E+02 (5) .2672E+02
(6) .2822E+02 (7) .2853E+02 (8) .2747E+02 (9) .2508E+02 (10).2165E+02
(11).1763E+02 (12).1353E+02 (13).9780E+01 (14).6657E+01 (15).4268E+01
(16).2579E+01 (17).1470E+01 (18).7915E+00 (19).4026E+00 (20).1937E+00
(21).8827E-01 (22).3812E-01 (23).1562E-01 (24).6075E-02 (25).2246E-02
(26).7894E-03 (27).2641E-03 (28).8417E-04 (29).2556E-04 (30).7402E-05
(31).2045E-05 (32).5393E-06 (33).1358E-06 (34).3267E-07 (35).7509E-08
(36).1650E-08 (37).3467E-09 (38).6968E-10 (39).1339E-10 (40).2463E-11
(41).4324E-12
```

Helium

```
  400 keV  electron energy
  32,000   torr-cm slab thickness
  0.991    electron remaining

Slab                  keV

(1) .1384E+02 (2) .1531E+02 (3) .1671E+02 (4) .1834E+02 (5) .2004E+02
(6) .2172E+02 (7) .2330E+02 (8) .2467E+02 (9) .2572E+02 (10) 2631E+02
(11).2635E+02 (12).2576E+02 (13).2450E+02 (14).2260E+02 (15).2016E+02
(16).1734E+02 (17).1436E+02 (18).1142E+02 (19).8715E+01 (20).6371E+01
(21).4458E+01 (22).2984E+01 (23).1911E+01 (24).1170E+01 (25).6847E+00
(26).3831E+00 (27).2050E+00 (28).1049E+00 (29).5133E-01 (30).2403E-01
(31).1076E-01 (32).4613E-02 (33).1892E-02 (34).7431E-03 (35).2794E-03
(36).1006E-03 (37).3468E-04 (38).1145E-04 (39).3621E-05 (40).1097E-05
(41).3156E-06
```

Neon

200 keV electron energy
4,000 torr-cm slab thickness
0.880 electron remaining

```
Slab                keV

(1) .1664E+02 (2) .2121E+02 (3) .2342E+02 (4) .2365E+02 (5) .2226E+02
(6) .1974E+02 (7) .1653E+02 (8) .1309E+02 (9) .9800E+01 (10).6933E+01
(11).4634E+01 (12).2928E+01 (13).1749E+01 (14).9888E+00 (15).5293E+00
(16).2686E+00 (17).1293E+00 (18).5915E-01 (19).2572E-01 (20).1065E-01
(21).4200E-02 (22).1580E-02 (23).5675E-03 (24).1948E-03 (25).6393E-04
(26).2009E-04 (27).6046E-05 (28).1744E-05 (29).4829E-06 (30).1283E-06
(31).3276E-07 (32).8039E-08 (33).1897E-08 (34).4308E-09 (35).9419E-10
(36).1983E-10 (37).4025E-11 (38).7874E-12 (39).1485E-12 (40).2704E-13
(41).4702E-14
```

Neon

250 keV electron energy
4,000 torr-cm slab thickness
0.889 electron remaining

```
Slab                keV

(1) .6138E+01 (2) .7588E+01 (3) .8366E+01 (4) .9352E+01 (5) .1009E+02
(6) .1068E+02 (7) .1111E+02 (8) .1140E+02 (9) .1154E+02 (10).1157E+02
(11).1149E+02 (12).1131E+02 (13).1105E+02 (14).1070E+02 (15).1027E+02
(16).9768E+01 (17).9202E+01 (18).8577E+01 (19).7903E+01 (20).7193E+01
(21).6458E+01 (22).5715E+01 (23).4978E+01 (24).4264E+01 (25).3586E+01
(26).2959E+01 (27).2392E+01 (28).1893E+01 (29).1465E+01 (30).1107E+01
(31).8171E+00 (32).5882E+00 (33).4128E+00 (34).2822E+00 (35).1879E+00
(36).1218E+00 (37).7680E-01 (38).4709E-01 (39).2800E-01 (40).1590E-01
(41).7806E-02
```

Neon

300 keV electron energy
4,000 torr-cm slab thickness
0.888 electron remaining

```
Slab               keV

(1) .1225E+02 (2) .1524E+02 (3) .1739E+02 (4) .1907E+02 (5) .2012E+02
(6) .2060E+02 (7) .2058E+02 (8) .2013E+02 (9) .1931E+02 (10).1817E+02
(11).1676E+02 (12).1514E+02 (13).1337E+02 (14).1153E+02 (15).9694E+01
(16).7929E+01 (17).6303E+01 (18).4862E+01 (19).3635E+01 (20).2631E+01
(21).1843E+01 (22).1248E+01 (23).8168E+00 (24).5163E+00 (25).3152E+00
(26).1857E+00 (27).1057E+00 (28).5805E-01 (29).3079E-01 (30).1576E-01
(31).7792E-02 (32).3720E-02 (33).1715E-02 (34).7641E-03 (35).3289E-03
(36).1368E-03 (37).5498E-04 (38).2137E-04 (39).8027E-05 (40).2909E-05
(41).9685E-06
```

Neon

400 keV electron energy
4,000 torr-cm slab thickness
0.895 electron remaining

```
Slab               keV

(1) .1021E+02 (2) .1251E+02 (3) .1368E+02 (4) .1525E+02 (5) .1642E+02
(6) .1735E+02 (7) .1804E+02 (8) .1849E+02 (9) .1870E+02 (10).1872E+02
(11).1856E+02 (12).1825E+02 (13).1780E+02 (14).1721E+02 (15).1650E+02
(16).1568E+02 (17).1476E+02 (18).1374E+02 (19).1266E+02 (20).1151E+02
(21).1034E+02 (22).9147E+01 (23).7970E+01 (24).6830E+01 (25).5749E+01
(26).4748E+01 (27).3843E+01 (28).3045E+01 (29).2360E+01 (30).1787E+01
(31).1321E+01 (32).9529E+00 (33).6701E+00 (34).4592E+00 (35).3064E+00
(36).1991E+00 (37).1258E+00 (38).7734E-01 (39).4611E-01 (40).2624E-01
(41).1292E-01
```

Argon

150 keV electron energy
1,000 torr-cm slab thickness
0.782 electron remaining

```
Slab                keV

(1) .1036E+02 (2) .1263E+02 (3) .1379E+02 (4) .1388E+02 (5) .1330E+02
(6) .1227E+02 (7) .1095E+02 (8) .9467E+01 (9) .7913E+01 (10).6389E+01
(11).4976E+01 (12).3735E+01 (13).2699E+01 (14).1876E+01 (15).1254E+01
(16).8056E+00 (17).4977E+00 (18).2956E+00 (19).1689E+00 (20).9280E-01
(21).4908E-01 (22).2499E-01 (23).1226E-01 (24).5793E-02 (25).2640E-02
(26).1161E-02 (27).4926E-03 (28).2019E-03 (29).7995E-04 (30).3061E-04
(31).1133E-04 (32).4061E-05 (33).1409E-05 (34).4733E-06 (35).1541E-06
(36).4864E-07 (37).1489E-07 (38).4423E-08 (39).1275E-08 (40).3561E-09
(41).9187E-10
```

Argon

200 keV electron energy
2,000 torr-cm slab thickness
0.782 electron remaining

```
Slab                keV

(1) .1855E+02 (2) .2215E+02 (3) .2315E+02 (4) .2212E+02 (5) .1991E+02
(6) .1705E+02 (7) .1393E+02 (8) .1085E+02 (9) .8061E+01 (10).5703E+01
(11).3842E+01 (12).2465E+01 (13).1506E+01 (14).8764E+00 (15).4864E+00
(16).2575E+00 (17).1302E+00 (18).6292E-01 (19).2908E-01 (20).1287E-01
(21).5458E-02 (22).2220E-02 (23).8669E-03 (24).3252E-03 (25).1173E-03
(26).4072E-04 (27).1361E-04 (28).4386E-05 (29).1363E-05 (30).4086E-06
(31).1183E-06 (32).3310E-07 (33).8953E-08 (34).2343E-08 (35).5933E-09
(36).1455E-09 (37).3457E-10 (38).7962E-11 (39).1778E-11 (40).3850E-12
(41).7863E-13
```

```
Argon

  250 keV electron energy
  2,000 torr-cm slab thickness
  0.787 electron remaining

Slab                keV

(1) .1571E+02 (2) .1906E+02 (3) .2102E+02 (4) .2147E+02 (5) .2094E+02
(6) .1975E+02 (7) .1810E+02 (8) .1617E+02 (9) .1405E+02 (10).1188E+02
(11).9749E+01 (12).7757E+01 (13).5976E+01 (14).4454E+01 (15).3208E+01
(16).2231E+01 (17).1498E+01 (18).9709E+00 (19).6071E+00 (20).3663E+00
(21).2132E+00 (22).1198E+00 (23).6499E-01 (24).3404E-01 (25).1722E-01
(26).8420E-02 (27).3979E-02 (28).1818E-02 (29).8039E-03 (30).3440E-03
(31).1425E-03 (32).5718E-04 (33).2223E-04 (34).8379E-05 (35).3062E-05
(36).1086E-05 (37).3736E-06 (38).1248E-06 (39).4049E-07 (40).1271E-07
(41).3638E-08
```

```
Argon

  300 keV electron energy
  2,000 torr-cm slab thickness
  0.792 electron remaining

Slab                keV

(1) .1365E+02 (2) .1667E+02 (3) .1879E+02 (4) .1992E+02 (5) .2023E+02
(6) .1995E+02 (7) .1925E+02 (8) .1826E+02 (9) .1706E+02 (10).1568E+02
(11).1418E+02 (12).1260E+02 (13).1099E+02 (14).9393E+01 (15).7864E+01
(16).6439E+01 (17).5150E+01 (18).4020E+01 (19).3059E+01 (20).2268E+01
(21).1637E+01 (22).1150E+01 (23).7859E+00 (24).5221E+00 (25).3372E+00
(26).2116E+00 (27).1291E+00 (28).7651E-01 (29).4407E-01 (30).2467E-01
(31).1342E-01 (32).7098E-02 (33).3649E-02 (34).1824E-02 (35).8867E-03
(36).4192E-03 (37).1928E-03 (38).8628E-04 (39).3753E-04 (40).1569E-04
(41).5713E-05
```

```
Argon

  400 keV electron energy
  2,000 torr-cm slab thickness
  0.802 electron remaining

Slab                keV

(1) .1067E+02 (2) .1381E+02 (3) .1507E+02 (4) .1677E+02 (5) .1770E+02
(6) .1830E+02 (7) .1855E+02 (8) .1849E+02 (9) .1822E+02 (10).17[illegible]0E+02
(11).1725E+02 (12).1661E+02 (13).1589E+02 (14).1509E+02 (15).1423E+02
(16).1332E+02 (17).1237E+02 (18).1138E+02 (19).1038E+02 (20).9373E+01
(21).8371E+01 (22).7391E+01 (23).6446E+01 (24).5548E+01 (25).4710E+01
(26).3940E+01 (27).3246E+01 (28).2632E+01 (29).2099E+01 (30).1645E+01
(31).1266E+01 (32).9570E+00 (33).7099E+00 (34).5165E+00 (35).3685E+00
(36).2577E+00 (37).1764E+00 (38).1178E+00 (39).7598E-01 (40).4570E-01
(41).2221E-01
```

```
Krypton

  200 keV electron energy
  1,000 torr-cm slab thickness
  0.652 electron remaining

Slab                keV

(1) .1971E+02 (2) .2344E+02 (3) .2317E+02 (4) .2082E+02 (5) .1754E+02
(6) .1398E+02 (7) .1058E+02 (8) .7603E+01 (9) .5188E+01 (10).3364E+01
(11).2073E+01 (12).1215E+01 (13).6783E+00 (14).3608E+00 (15).1831E+00
(16).8880E-01 (17).4117E-01 (18).1828E-01 (19).7776E-02 (20).3175E-02
(21).1245E-02 (22).4693E-03 (23).1703E-03 (24).5953E-04 (25).2007E-04
(26).6527E-05 (27).2051E-05 (28).6228E-06 (29).1829E-06 (30).5202E-07
(31).1433E-07 (32).3825E-08 (33).9906E-09 (34).2489E-09 (35).6075E-10
(36).1440E-10 (37).3319E-11 (38).7438E-12 (39).1622E-12 (40).3438E-13
(41).6835E-14
```

```
Krypton

  300 keV electron energy
  1,000 torr-cm slab thickness
  0.659 electron remaining

Slab                keV

(1) .1492E+02 (2) .1906E+02 (3) .2064E+02 (4) .2105E+02 (5) .2053E+02
(6) .1946E+02 (7) .1803E+02 (8) .1637E+02 (9) .1457E+02 (10).1273E+02
(11).1090E+02 (12).9139E+01 (13).7498E+01 (14).6016E+01 (15).4715E+01
(16).3609E+01 (17).2695E+01 (18).1963E+01 (19).1395E+01 (20).9658E+00
(21).6519E+00 (22).4289E+00 (23).2750E+00 (24).1718E+00 (25).1046E+00
(26).6212E-01 (27).3595E+00 (28).2029E-01 (29).1117E-01 (30).5995E-02
(31).3140E-02 (32).1605E-02 (33).8010E-03 (34).3902E-03 (35).1857E-03
(36).8629E-04 (37).3918E-04 (38).1738E-04 (39).7513E-05 (40).3118E-05
(41).1110E-05
```

```
Krypton

  400 keV electron energy
  1,000 torr-cm slab thickness
  0.670 electron remaining

Slab                keV

(1) .1202E+02 (2) .1626E+02 (3) .1775E+02 (4) .1902E+02 (5) .1950E+02
(6) .1950E+02 (7) .1915E+02 (8) .1855E+02 (9) .1778E+02 (10).1686E+02
(11).1585E+02 (12).1477E+02 (13).1364E+02 (14).1248E+02 (15).1132E+02
(16).1015E+02 (17).9016E+01 (18).7917E+01 (19).6872E+01 (20).5892E+01
(21).4989E+01 (22).4170E+01 (23).3438E+01 (24).2796E+01 (25).2241E+01
(26).1771E+01 (27).1379E+01 (28).1057E+01 (29).7986E+00 (30).5939E+00
(31).4349E+00 (32).3134E+00 (33).2223E+00 (34).1552E+00 (35).1066E+00
(36).7197E-01 (37).4768E-01 (38).3086E-01 (39).1923E-01 (40).1110E-01
(41).4974E-02
```

Xenon

200 keV electron energy
1,000 torr-cm slab thickness
0.582 electron remaining

```
Slab                 keV

(1) .3092E+02 (2) .3227E+02 (3) .2669E+02 (4) .1947E+02 (5) .1287E+02
(6) .7786E+01 (7) .4343E+01 (8) .2245E+01 (9) .1080E+01 (10).4861E+00
(11).2052E+00 (12).8153E-01 (13).3058E-01 (14).1086E-01 (15).3659E-02
(16).1172E-02 (17).3579E-03 (18).1043E-03 (19).2907E-04 (20).7761E-05
(21).1987E-05 (22).4887E-06 (23).1156E-06 (24).2632E-07 (25).5778E-08
(26).1224E-08 (27).2503E-09 (28).4950E-10 (29).9471E-11 (30).1755E-11
(31).3150E-12 (32).5485E-13 (33).9267E-14 (34).1520E-14 (35).2424E-15
(36).3757E-16 (37).5665E-17 (39).8313E-18 (40).1188E-18 (41).1654E-19
(41).2209E-20
```

Xenon

300 keV electron energy
1,000 torr-cm slab thickness
0.577 electron remaining

```
Slab                 keV

(1) .2536E+02 (2) .2981E+02 (3) .2943E+02 (4) .2690E+02 (5) .2331E+02
(6) .1933E+02 (7) .1537E+02 (8) .1174E+02 (9) .8610E+01 (10).6063E+01
(11).4101E+01 (12).2665E+01 (13).1664E+01 (14).9988E+00 (15).5767E+00
(16).3204E+00 (17).1715E+00 (18).8844E-01 (19).4398E-01 (20).2111E-01
(21).9785E-02 (22).4383E-02 (23).1899E-02 (24).7960E-03 (25).3232E-03
(26).1271E-03 (27).4850E-04 (28).1795E-04 (29).6451E-05 (30).2252E-05
(31).7640E-06 (32).2521E-06 (33).8092E-07 (34).2529E-07 (35).7696E-08
(36).2282E-08 (37).6597E-09 (38).1860E-09 (39).5113E-10 (40).1368E-10
(41).3370E-11
```

Xenon

400 keV electron energy
1,000 torr-cm slab thickness
0.584 electron remaining

```
Slab               keV

(1) .2174E+02 (2) .2720E+02 (3) .2837E+02 (4) .2802E+02 (5) .2658E+02
(6) .2455E+02 (7) .2214E+02 (8) .1955E+02 (9) .1689E+02 (10).1429E+02
(11).1183E+02 (12).9584E+01 (13).7588E+01 (14).5870E+01 (15).4435E+01
(16).3270E+01 (17).2353E+01 (18).1652E+01 (19).1131E+01 (20).7554E+00
(21).4918E+00 (22).3122E+00 (23).1933E+00 (24).1167E+00 (25).6871E-01
(26).3946E-01 (27).2211E-01 (28).1209E-01 (29).6453E-02 (30).3362E-02
(31).1710E-02 (32).8499E-03 (33).4126E-03 (34).1957E-03 (35).9075E-04
(36).4114E-04 (37).1824E-04 (38).7908E-05 (39).3346E-05 (40).1362E-05
(41).4785E-06
```

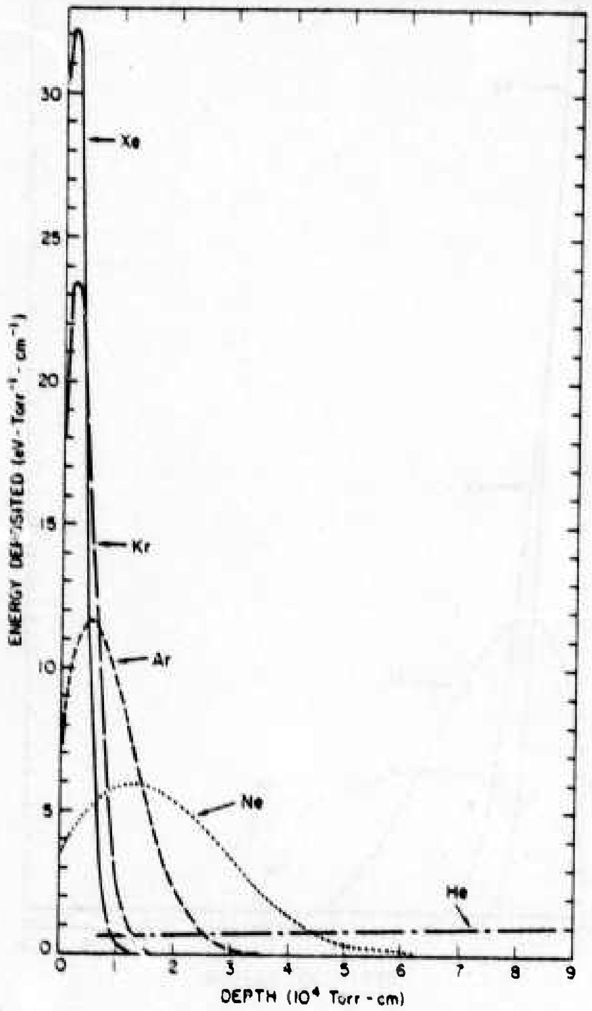

Figure 0. Calculated deposited energy as a function of depth for a 200 keV incident electron.

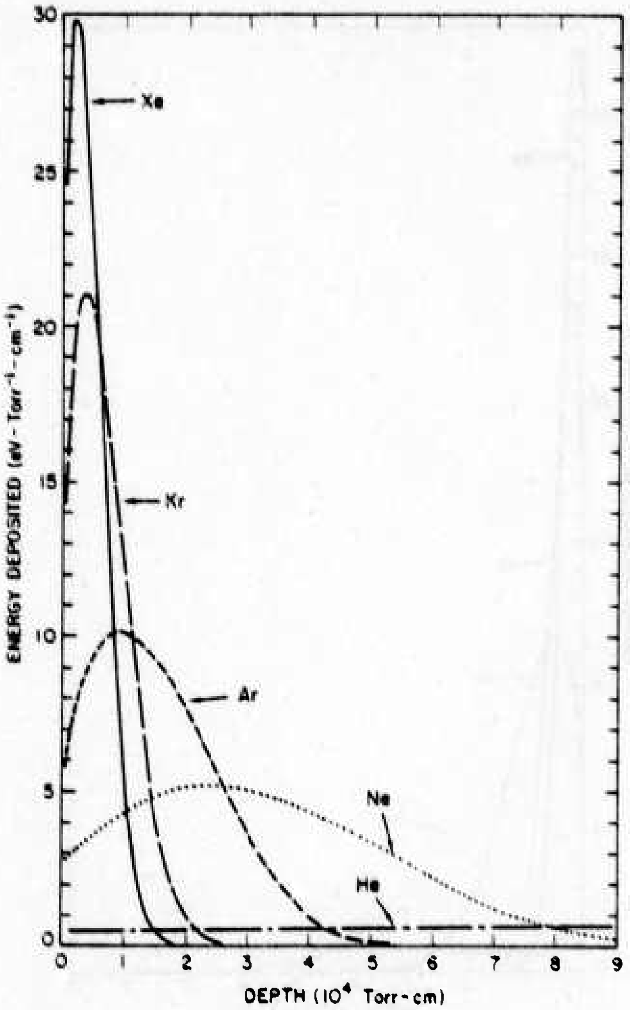

Figure P. Calculated deposited energy as a function of depth for a 300 keV incident electron.

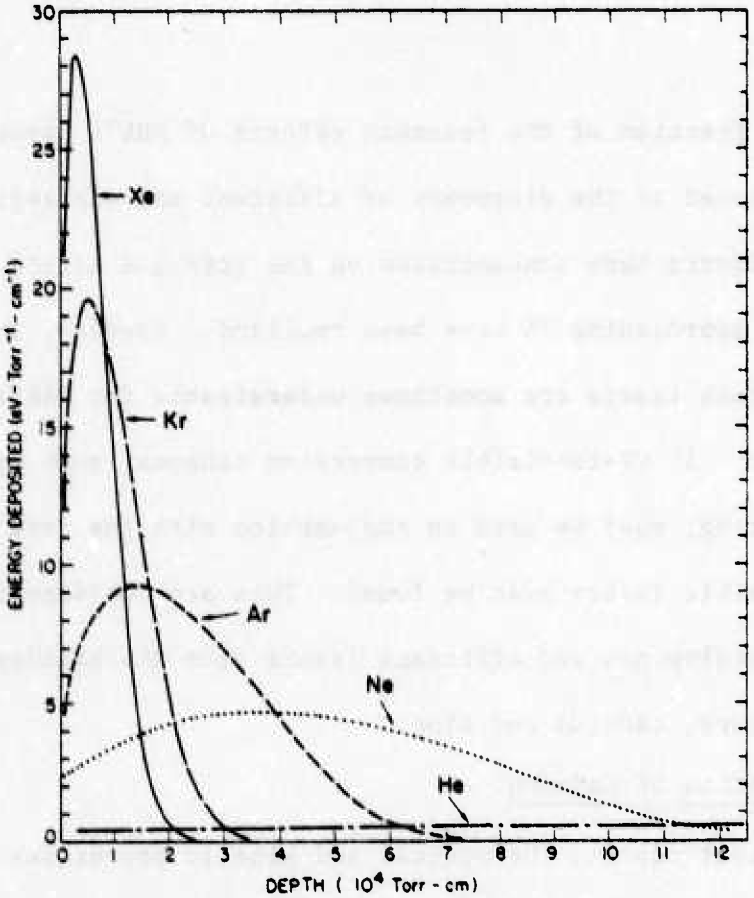

Figure Q. Calculated deposited energy as a function of depth for 400 keV incident electron.

METAL HALIDE LASER STUDIES ON HIGH-CURRENT 50 ns GUN

Introduction

A large fraction of the research efforts of NRL's Laser Physics Branch is devoted to the discovery of efficient and energetic lasers. Our recent efforts have concentrated on the rare gas halide lasers where efficiencies approaching 7% have been realized. However, the UV wavelengths of these lasers are sometimes undersirable for DARPA applications and so either: 1) UV-to-visible conversion schemes, such as stimulated Raman Scattering, must be used in conjunction with the rare gas halides or 2) new visible lasers must be found. This section describes our efforts to develop new and efficient lasers from the halides of the IIB metals: mercury, cadmium and zinc.

E-beam Excitation of Cadmium

In our last report, the optical and kinetic properties of the recently observed HgCl laser were discussed. At that time, it was pointed out that since the e-beam pumped HgCl laser depends on ion-ion recombination for formation of the $HgCl^*(B)$ state, the efficiency is low. However, with cadmium, the strong possibility for neutral rare gas metastable to excited cadmium transfer exists. In particular:

$$Xe^M + Cd \rightarrow Cd^* + Xe \qquad (1)$$

where Xe^M represents a xenon metastable from the ^3P manifold. Figure R illustrates the advantage of Cd over Hg in this respect. The Cd 7^3D

levels are in close coincidence (50 cm^{-1}) with the ^3P, state of Xe and the $5^3P_{0,1,2}$ levels of Cd lie within the Xe_2^* molecular manifold of states. This is in contrast to Hg where no suitable energy matchup exists.

Consequently, in the last six months, the heated cell that was built for the NRL high current 50 ns gun has been further modified to accommodate the higher temperatures (500-600°C) required to obtain 1-5 torr of Cd. The major improvement in cell performance came from installing re-entrant quartz windows. This eliminates the need for externally heating the windows with heating tapes and improves the homogeneity of the metal vapor-rare gas mixture. Secondly, the interior of the laser cell was coated with chrome to avoid reaction of the cadmium with the stainless steel walls. Also, more heating rods were installed (see last report, p. 64) to improve the uniformity of the cell's temperature. Temperature cycling of the e-beam foil remains a problem, however, and so the cell was re-machined to accept larger bolts to more fully compress the aluminum gaskets. We also plan in the near future to attempt toweld the foil to the cell body which would eliminate a major obstacle to the reliable high temperature operation of the cell.

Since the completion of these modifications, several electron beam pumping experiments with cadmium have been conducted. When 2000 torr Ar/250 torr Xe/cadmium mixtures at ~ 400°C are irradiated with the electron beam, strong Cd atomic emission on the $5^3D \rightarrow 5^3P$ series at ~ 350 nm and the $6^3S \rightarrow 5^3P$ series at ~ 500 nm is observed. This behavior is consistent with $Xe_2^* \rightarrow$ Cd (5^3D or 6^3P) energy transfer and subsequent Cd^* radiative transfer. Although the $Cd^* 5^3D$ levels are not shown in Fig. R, they also lie in close proximity to the Xe_2^* vibrational levels.

Therefore, the proposed $Xe^* \rightarrow Cd^*$ excitation scheme appears to be suitable for the production of $Cd^*(5^3P)$ atoms.

Subsequent to these experiments, attempts to observe CdX^* fluorescence (X = Cl, Br, I) were made using $Ar/XCl/Cd/CCl_4$ or HI mixtures. These attempts were unsuccessful, however, suggesting that at the high temperatures used in these experiments, reaction of Cd with the halogen donor to form CdX_2 occurred rapidly and certainly before the e-beam could be fired. Therefore, we plan to convert in the near future to a flowing system whereby the halogen donor and rare gases would be premixed and passed over hot Cd and immediately admitted to the laser cell.

Optical Pumping of CDX^* by Photodissociation of CDX_2

In the literature there seems to be some uncertainty as to the region of the spectrum where the lowest lying states of the CdX^* molecules (X=I, Br and Cl) can be expected to fluoresce. This, of course, is of importance to DARPA since it is essential that the proposed laser wavelengths coincide with an atmospheric window. To answer this question, quartz absorption tubes of 10-15 cm length and ~ 2.5 cm o.d. were constructed and filled with several mg of either CdI_2 or $CdCl_2$ and 100 torr helium. The cells were then placed in an oven, heated to ~ 400°C and irradiated with 193 nm emission from a discharge-pumped ArF laser. For CdI_2, above 350°C intense, deep red fluorescence with peak fluorescence at $\lambda \sim 650$ nm was observed. Although superradiant laser emission was not observed, it is felt that optically pumped oscillation could be obtained with the installation of an optical cavity. This has not been done since much higher laser efficiencies will be obtained with electrical pumping and so future work will be concentrated in this area. In conclusion, the electron beam heated cell has been modified to successfully contain homogeneous mixtures at Ar/Xe/Cd at temperatures in the 400°C range. Irradiation of these mixtures has produced strong Cd^* emission, in agreement with the proposed $Xe^M \rightarrow Cd^*$ excitation scheme. A flowing gas system is being constructed to permit $CdX^*(B)$ state fluorescence and laser studies. ArF laser excitation of CdI_2 and $CdCl_2$ has shown that the B → X bands of both CdI^* and $CdCl^*$ emit most strongly in the 640 - 670 nm range.

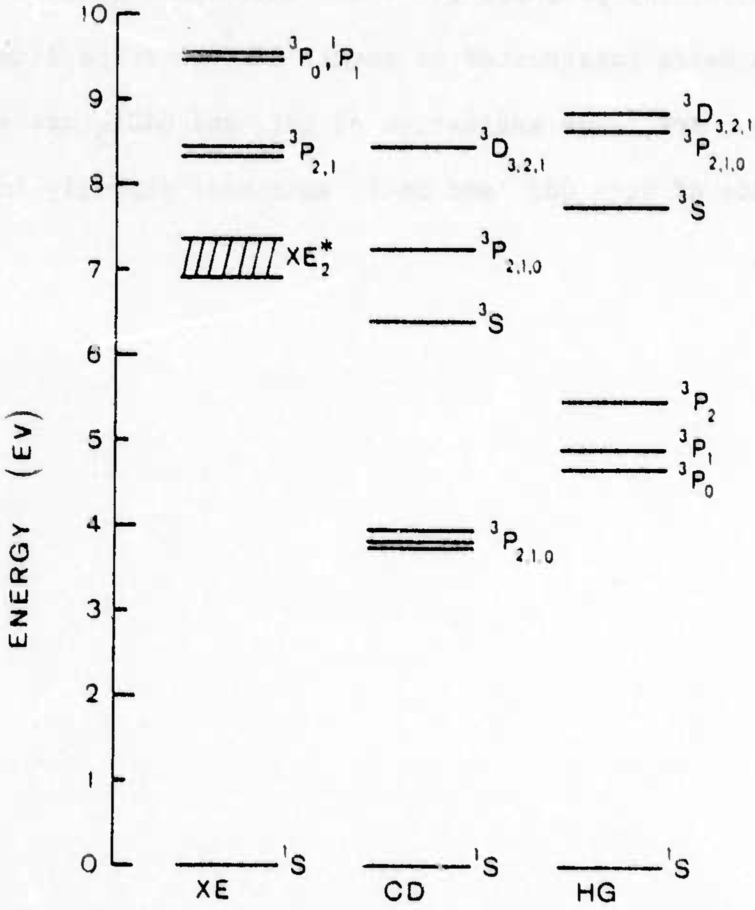

Fig. R. Partial schematic energy level diagrams for xenon, mercury and cadmium.

QUENCHING OF Ba(^{1}D)

In a previous NRL experiment, high densities of Ba 6s6p (^{1}P) atoms were observed in a Ba + N_2O flame. It was conjectured that laser action could be achieved between the 6s6p (^{1}P) and the 6s5d (^{1}D) levels of Ba if the metastable (^{1}D) level could be quenched quickly enough. The radiative lifetime of the (^{1}D) has not been reported, but should be longer than one second. During this reporting period experiments have been conducted to measure the quenching rates of Ba(^{1}D) by N_2, CO, H_2 D_2, and CH_4,

The approach to this experiment is a technique using two collinear beams of light; one to prepare the Ba atoms in the metastable state by optical pumping to a high lying state and allowing radiative relaxation to the metastable state, and the other to probe the metastable state population by absorption. In this experiment the 6p5d (^{1}P) level (see Fig. S) was chosen to be the upper state for both the pump and probe transitions. Since the pump radiation is provided by a pulsed laser and the probe beam is CW, the quenching lifetime is determined by the decay of the probe beam absorption after each pulse.

The apparatus used to provide Ba atoms is a vacuum flow system shown schematically in Fig. T. An alumina crucible containing the barium metal is resistively heated by a tungsten wire "basket" to temperatures near 1250 K, and the resulting barium vapor is entrained in flowing argon introduced beneath the crucible. Typical Ar pressures and flow rates are around 5 torr and a few cm/sec respectively. The quenching gas was either mixed with the Ar carrier gas or introduced separately about 2 cm downstream from the crucible. A commercial CW dye laser was used as a probe beam at 582.6 nm (see Fig. S) with single mode operation. For the pump beam, a source tunable to 350.1 nm was required.

At the time, no suitable tunable laser system in the right wavelength range was known. A program was initiated to investigate various dyes selected on the basis of absorption and emission spectra for use as a dye laser pumped with a KrF discharge laser. The dyes 1, 3, 5 -Triphenylbenzene, 1, 1' - Binaphthyl, and p-terphenyl were tested, and only the latter lased (p-terphanyl had been previously shown to lase using a flashlamp[1]). Subsequently two articles appeared in the literature reporting p-terphenyl as a dye laser with a KrF laser optical pump.[2,3] The tuning range of the dye was limited when a conventional dye laser cavity was used, and a prism-beam-expander cavity design[4] was employed to give the required tuning range and adequate resolution. A schematic of the cavity is shown in Fig. U. Despite the inherent high loss of the cavity due to reflection from the prism face, the measured tuning range was from 356.3 to 331.0 and from 328.0 to 324.0 nm, and there was sufficient energy at 350.1 nm to obtain stimulated radiation in the Ba vapor from the $6p5d\,^1P$ to $6s5d\,^1D$ transition (582.6 nm).

So far, measurements have been made on the quenching rates of N_2 and CO. These are: 1.19×10^{-11} cm^3/sec, and 10.6×10^{-11} cm^3/sec respectively with a standard deviation of ± 12%. Preliminary work on

H_2, D_2, and CH_4 has been done, but more data is required to accurately determine their quenching rates. CO_2 was also tried as a quenching gas, but was so reactive that no absorption signal could be obtained, even when very small amounts of the gas were introduced. Except for the rare gases, all the gases observed so far are reactive with Ba vapor and this puts the upper limit on the amount of gas which can be added before the signal becomes too small to be measurable. As was expected the quenching rate of Argon which is used as a carrier gas, is too small to be measured since self-quenching and impurities determine the longest lifetime observed when only Argon is flowing.

Figure V presents the data obtained on quenching by N_2 and CO. The inverse of the metastable state lifetime is plotted against the partial pressure of the quenching gas. Data points are fitted to straight-line graphs, and quenching rates are proportional to the slopes of the lines. In terms of the original motivation, it seems that N_2 may be a good candidate for a quenching gas to bring about lasing between the 6s6p (^1P) and the 6s5d(^1D) levels. Approximately one torr of N_2 would give the (^1D) level a 1 μsec lifetime which is comparable to the radiative lifetime between the 6s6p (^1P) and (^1D) levels. While CO has a much faster quenching rate, it is also much more reactive and might lower the gain below threshold. Both gases may be tried in the chemical laser experiment, the value of this work is to indicate how much quenching gas should be required.

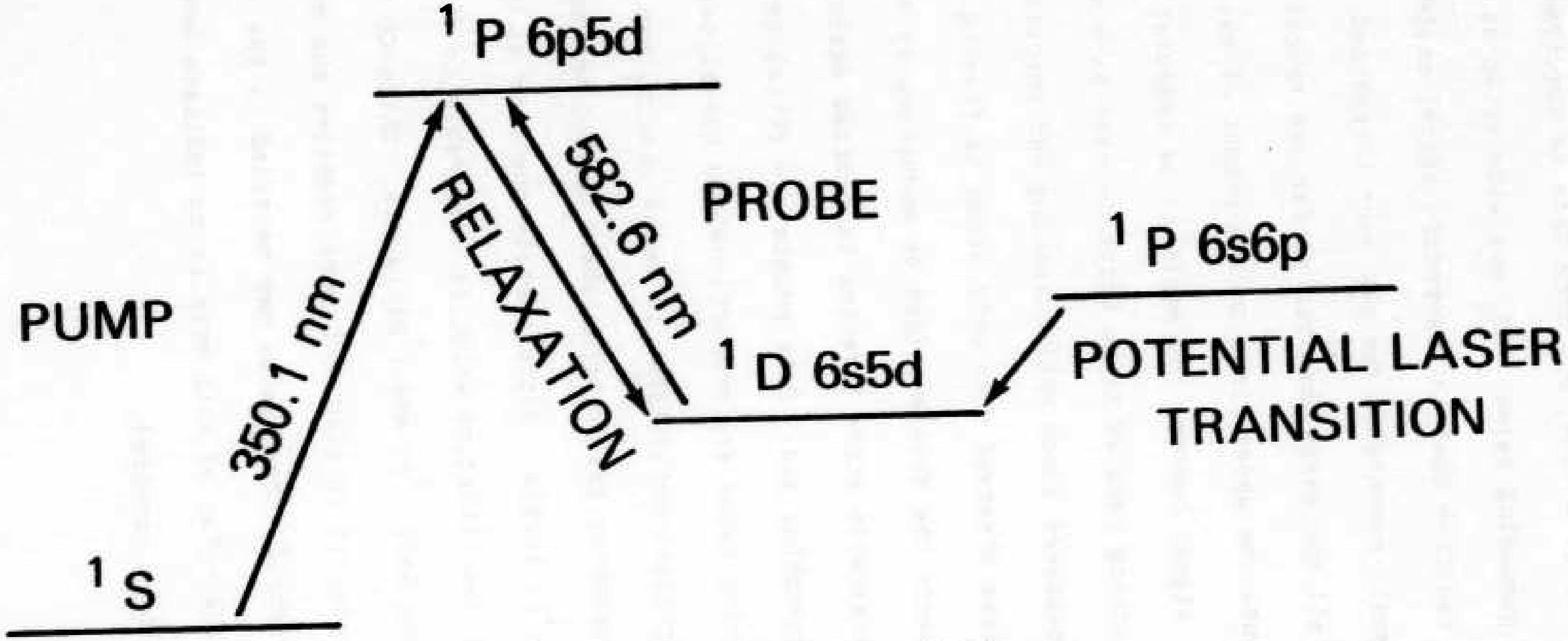

Figure 5. Barium Energy Level Diagram.

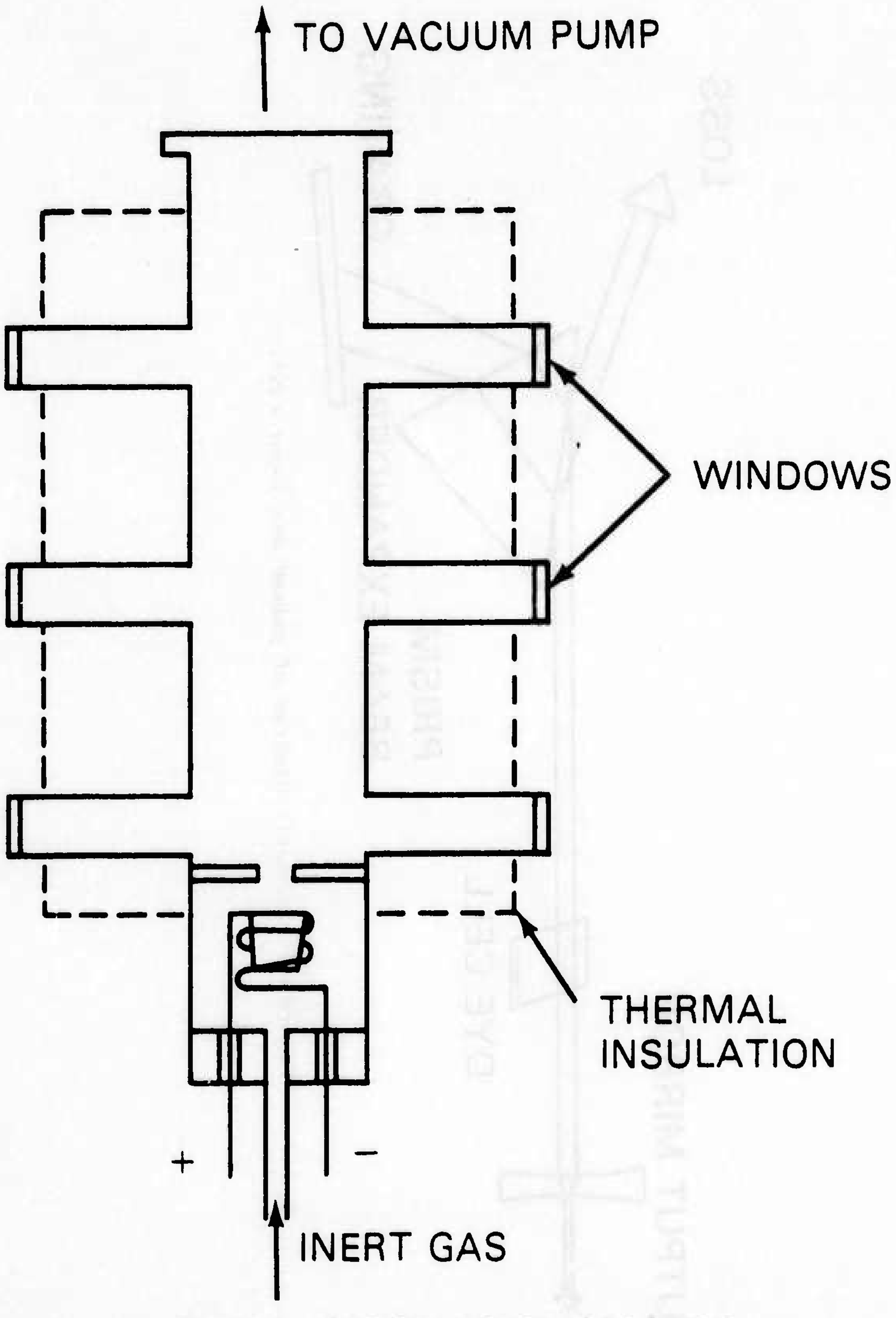

Figure T. Schematic diagram of Ba furnace.

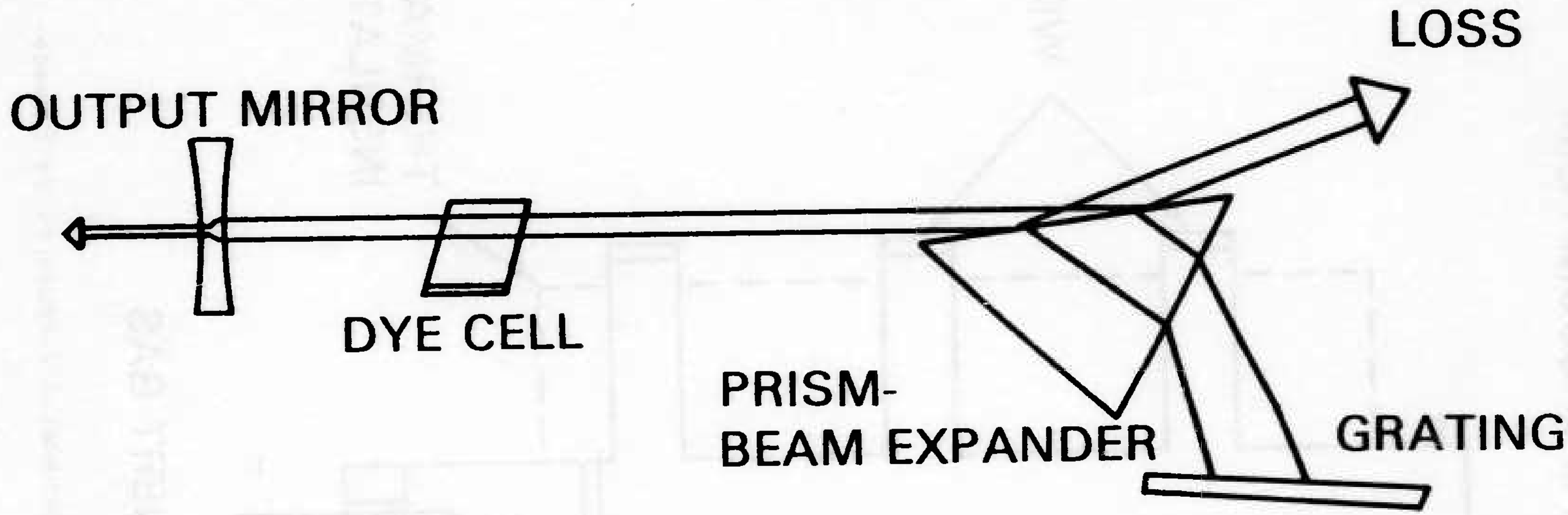

Figure U. Schematic diagram of pulsed dye laser cavity.

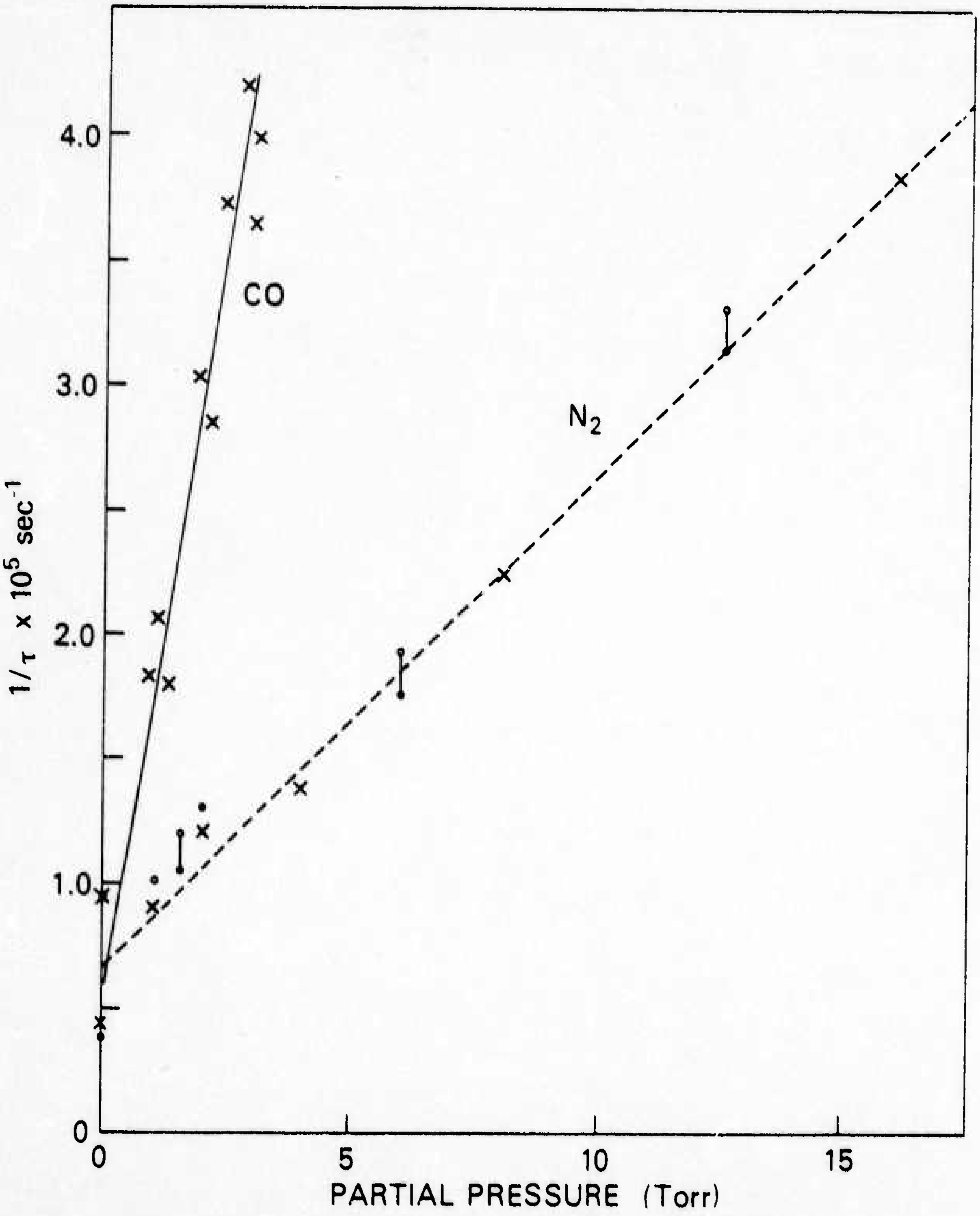

Figure V. Plot of Ba Quenching vs. partial pressures of CO and N_2.